NASA Technical Memorandum X-74038

INTERNAL PERFORMANCE PREDICTIONS FOR LANGLEY SCRAMJET ENGINE MODULE

S. Z. Pinckney

JANUARY 1978

National Aeronautics and Space Administration

Langley Research Center
Hampton, Virginia 23665

INTERNAL PERFORMANCE PREDICTIONS FOR LANGLEY SCRAMJET ENGINE MODULE

S. Z. Pinckney

Langley Research Center

SUMMARY

A one-dimensional theoretical method for the prediction of the internal performance of a scramjet engine is presented. Using this method, the evaluation of the effects of vehicle forebody flow parameters and characteristics on predicted thrust for the Langley scramjet engine indicate the engine capture mass flow, and thus thrust is strongly influenced by changes in vehicle forebody characteristics. Evaluation of the effects of changes in the engine internal parameters on thrust indicate that changes in engine flow parameters, such as additive drag, fuel equivalence ratio, nozzle length or nozzle exit area and combustor pressure integral cause significant changes in internal thrust. Theoretical internal performance predictions, in terms of thrust coefficient and specific impulse, are presented for free-stream Mach numbers of 5, 6, and 7, free-stream dynamic pressure of 23,940 N/m^2, forebody angles of 4.6^0 to 14.6^0 and a fuel equivalence ratio of 1.0.

INTRODUCTION

Vehicle design considerations in hypersonic flow (reference 1) show that the reliable prediction of a scramjet engine's performance is an absolute requirement. This becomes evident upon consideration of the fact that the net thrust is the difference between two large and nearly equal forces, the nozzle thrust and the inlet ram drag. Misdirection or location (relative to vehicle center of gravity) of the large nozzle thrust vector can result in exorbitant vehicle trim drag penalties (reference 1) while intelligent engine vehicle integration to control the thrust vector location and orientation can result in significant gains in lift (references 2 and 3). In order to further study the problems inherent in hypersonic vehicle engine integration, the need exists for engine performance computations covering a range of Mach numbers and angles of attack. As any initial hypersonic flight experiments will probably be conducted on a small scale experimental vehicle, emphasis should be placed on providing hypersonic engine performance results which would be applicable to this case.

To meet this need, the Langley scramjet modular engine (figure 1) discussed in references 4 through 8 was chosen for analysis of its performance characteristics. The modular engine concept lends itself to integration with the

vehicle airframe. This engine was designed with modest contraction ratios and fixed geometry. Three swept-back fuel injection struts are used to enhance the inlet flow compression and reduce the combustor length by providing multiple injection planes. The engine configuration is rectangular in cross-sectional shape, has swept sidewall planar surfaces, has an opening upstream of the cowl leading edge through which flow spillage occurs for starting and normal operation, and has the external cowl surface at a small angle (1 1/2°) with the local flow to keep external cowl drag minimal. Vehicle-engine integration is assumed to be such that large portions of the vehicle afterbody are used as part of the engine exhaust nozzle.

There are several computerized methods available (references 9 through 11) to calculate the performance of hydrogen-fueled, supersonic combustion ramjet engines based on real-gas, equilibrium thermodynamic properties. For the present analysis, the method chosen was originally developed by Griffin Y. Anderson of Langley Research Center, with the idea that the program structure is such that future modifications could easily be made to fit the problem under consideration. The cycle process and performance parameters are based on assuming one-dimensional fluid flow and real gas equilibrium thermodynamic properties in conjunction with the control volume concept. The thermodynamic property data was taken from reference 12 and modified so that the enthalpy base matches that of reference 13. The original computerized method has been modified so as to account individually and separately for heat (due to surface heat transfer) and friction losses of the flow before entering the engine and of the engine flow as it passes through the inlet, combustor, and nozzle. Other modifications to the analysis allow for inclusion of the effects of flow spillage through the bottom of the inlet and of injected fuel temperature. Shock kinetic energy efficiencies are used to account for nonviscous losses of the engine capture flow in the forebody, inlet and nozzle portions of the engine cycle analysis. The method and the modifications are discussed.

A cycle and performance analysis has been performed for an engine module of a size believed to be representative of that for an experimental hypersonic vehicle. These computations were made for free-stream Mach numbers of 5, 6, and 7, for altitudes corresponding to a free-stream dynamic pressure of ~ 23,940 N/m^2 (~ 500 lb/ft^2), and for boundary layer corrected forebody surface angles of 4.6°, 7.1°, 9.6°, 12.1°, and 14.6°. It was also necessary to make estimates of friction and heat losses, nozzle plume drag and size, inlet spillage, additive drag, drag due to lift, and inlet contraction ratios. The procedures utilized to obtain these estimates are discussed and the results are presented along with the performance results.

SYMBOLS

A	area (m^2)
$A_{1,j}$	the area at station "1" that the mass flow W_D (no spillage) would occupy with the station "1" velocity and density which includes boundary layer losses (m^2)

B_p	combustor wall pressure integral parameter defined by equation (47)
C_A	engine force coefficient (A_A/q_oA_c)
C_B	engine force coefficient (A_B/q_oA_c)
C_E	nozzle plume drag coefficient (D_E/q_oA_c)
C_F	friction coefficient
C_I	inlet additive drag coefficient (D_A/q_oA_c)
D_E	nozzle plume drag (N)
D_A	inlet additive drag (N)
E	defined by equation (16)
F	defined by equation (15)
$F(p,p_s)$	defined as equal to p (N/m^2)
ΔF	friction losses (N)
g	acceleration due to gravity (m/sec^2)
h	enthalpy (J/Kg)
$(h_t)_{fuel}$	heating value of fuel (J/Kg)
H	engine height (m)
ΔH	engine component heat loss (J/sec)
$(\Delta H)_{fuel}$	heat added to fuel through regenerative engine cooling
I_{Sp}	specific impulse (sec)
K	ratio of specific heats
M	Mach number
p	pressure (N/m^2)
Pr	Prandtl number
q	dynamic pressure (N/m^2)
R_θ	Reynolds number based on momentum thickness

S	entropy (J/^{o}K)
T	temperature (^{o}K)
ΔT	increment of temperature (^{o}K)
V	velocity (m/sec)
W	mass flow (kg/sec)
β	mass averaged nozzle exit flow direction relative to vehicle forebody surface
ζ	parameter defined by equation (7)
η_{comb}	combustion efficiency
η_K	shock kinetic energy efficiency (adiabatic)
Λ_A	component in the flight direction of the engine force parallel to vehicle forebody surface (N)
Λ_B	component in the flight direction of the engine force normal to vehicle forebody surface (N)
Λ_I	absolute pressure force on the capture flow stream tube over the inlet spillage flow area and normal to forebody surface and defined by equation(3)(N)
Λ_p	absolute pressure force on the lower surface of the plume normal to forebody surface
ξ	parameter defined by equation (9)
ρ	density (kg/m^3)
σ	parameter defined by equation (8)
τ	engine thrust (N)
ϕ	fuel equivalence ratio
χ	parameter defined by equation (6)
ω	vehicle forebody angle with free-stream (deg.)
Ω	momentum pA + WV, (N)

Subscripts

A	parameters include no boundary layer losses

AV	average of parameter over engine component being considered
c	cowl
CE	value of parameters at entrance of engine component being considered
CO	engine component being considered such as vehicle forebody, inlet, combustor, and nozzle
comb	combustor engine component
f	vehicle forebody engine component
fuel	fuel
G	guessed value during iteration for solution
HS	parameter value as computed for heat sink engine of reference 18
I	inlet engine component
inv.	inviscid value outside boundary layer
$M_0 = 6$	value of parameter at freestream Mach number of 6.0
N	nozzle engine component
PE	Langley scramjet engine module of present paper. Capture area is 0.1672 m^2
S	isentropic expansion of flow at an engine station to pressure of the immediate upstream engine station
t	stagnation value
W	wall value
0	free-stream station
1	engine inlet entrance station
2	engine inlet throat station
3	engine combustor exit station
4	engine nozzle exit station

Superscripts

' prime quantities include no shock losses for engine component in consideration

ENGINE PERFORMANCE ANALYSIS

The present method of solution for a scramjet consists of combining a one-dimensional fluid flow model and real gas equilibrium thermodynamics with the control volume concept. The control volume assumed relative to the engine inlet entrance station and the one dimensional fluid flow model chosen are illustrated in figure 2. The engine capture mass flow passes from the free stream through the vehicle bow shock, along the forebody surface, through the inlet (spilling flow through the bottom of the inlet), through the combustor and out through the nozzle exit. The changes in the engine flow parameters through the engine are computed one dimensionally. Calculations are done separately for the vehicle forebody flow field, inlet, combustor, and nozzle and approximately account for the shock losses, friction losses, and heat losses along with flow spillage through the bottom of the engine.

The resultant force (or thrust) in the flight direction exerted on a vehicle by the engine is the integral of the absolute pressure forces in this direction on the surfaces washed by the capture flow of the engine. Therefore, utilizing the control volume concept and the one-dimensional flow model (figure 2) the engine's resultant thrust is predicted by the computation of the engine force $\Lambda_A/\cos\omega$ in a direction parallel to the vehicle forebody surface and the engine force $\Lambda_B/\sin\omega$ on the capture flow stream tube in a direction normal to the vehicle forebody surface and vectorally resolving both forces to the flight direction. The vectoral relationship between the engine forces $\Lambda_A/\cos\omega$ and $\Lambda_B/\sin\omega$ with resultant thrust in the flight direction is shown in figure 2. The force $\Lambda_A/\cos\omega$ is equal to the integral of the absolute pressure forces on the surface washed by the flow and in a direction parallel to the forebody surface. The force $\Lambda_A/\cos\omega$ is also equal to the nozzle exit flow momentum, minus the momentum of the capture flow at the inlet entrance station, the plume drag, and the additive drag summed in a direction parallel to the vehicle forebody. The force $\Lambda_B/\sin\omega$ is equal to the integral of the absolute pressure forces on the surfaces washed (excluding the vehicle forebody surface) by the capture flow and in a direction normal to the vehicle forebody surface. The force $\Lambda_B/\sin\omega$ is also equal to the pressure force (Λ_I) on the capture flow stream tube over the spillage area of the inlet, the pressure force (Λ_p) over the plume lower surface area and the nozzle exit flow momentum summed in a direction normal to the vehicle forebody surface. The forces Λ_B have to be evaluated as they have a component in the drag direction (figure 2) which

must be included in the net thrust determination. The resultant engine thrust, in coefficient form and in the vehicle flight direction, is given by,

$$\frac{\tau}{q_o A_c} = C_A + C_B \qquad 1(a)$$

The coefficient relative to the force Λ_A is given by,

$$C_A = \frac{\Lambda_A}{q_o A_c} \qquad 1(b)$$

and the force Λ_A is given by,

$$\Lambda_A = \{\overbrace{(p_4 + \rho_4 V_4^2)A_4}^{\text{Nozzle Exit Momentum}} \text{ Cosine } \beta - \overbrace{(p_1 + \rho_1 V_1^2)A_1}^{\text{Inlet Entrance Momentum}} - \overbrace{q_o A_c (C_I + C_E)}^{\text{Stream Tube Pressure Forces}}\} \text{ Cos } \omega \qquad 1(c)$$

The coefficient relative to the force Λ_B is given by,

$$C_B = \frac{\Lambda_B}{q_o A_c} \qquad 1(d)$$

and the force Λ_B is given by,

$$\Lambda_B = \{\overbrace{\Lambda_I + \Lambda_p}^{\text{Stream Tube Pressure Forces}} + \overbrace{(p_4 A_4 + W_4 V_4)}^{\text{Nozzle Exit Momentum}} \sin \beta\} \sin \omega \qquad 1(e)$$

Another measure of the scramjet engine internal performance is given by specific impulse. The specific impulse is the thrust in flight direction divided by the fuel flow per second and is given by,

$$I_{sp} = \frac{\tau}{W_{fuel} g} \qquad (2)$$

In order to compute the thrust coefficient or specific impulse, the engine's corresponding one-dimensional internal flow has to be computed based on assumed or computed values for the nozzle exit area A_4, the additive drag coefficient C_I, the plume drag coefficient C_E, the plume force Λ_p normal to the forebody surface, the fuel flow W_{fuel}, and the engine's inlet mass flow spillage and aerodynamic

contraction ratio A_1/A_2. The nozzle exit area, the additive drag coefficient, the plume drag coefficient, the plume force normal to the forebody surface, and the engine inlet mass flow spillage and aerodynamic contraction ratio must be determined experimentally or approximated theoretically. The parameters chosen as input to the analysis are listed in Table I. The methods used to obtain these input parameters are discussed in the following sections.

The calculations for the engine capture flow are made separately and in the following order: free stream, vehicle forebody flow field, inlet, combustor, and nozzle. In general, the vehicle forebody flow field and inlet calculations consist of making constant pressure momentum balance computations separately across the vehicle forebody flow field and inlet assuming the pressures to be, respectively, p_0 and p_1. In so doing, the capture flow is penalized as to friction and heat losses. Following the constant pressure computation the engine capture flow is penalized as to shock losses using the concept of shock kinetic energy efficiency. Then in the vehicle forebody flow calculation the flow is compressed to pressure "p_1", the pressure of the inviscid flow downstream of the forebody shock. In the inlet flow calculation the flow is compressed to the inlet aerodynamic throat area "A_2". The flow calculation across the combustor consists of setting up a control volume on the combustor as shown in figure 3, and generating a one-dimensional momentum and heat balance for the control volume. The resulting set of equations are solved for the combustor exit flow conditions. The one-dimensional flow computations for the nozzle consist of isentropically expanding the flow from the combustor exit to the nozzle exit area A_4. The nozzle exit flow conditions thus obtained are then penalized as to friction and heat losses in the nozzle. A more detailed development of the theoretical one-dimensional flow method utilized is presented in the Appendix.

ENGINE PERFORMANCE

Prediction of the performance of a scramjet engine requires knowledge of several parameters whose values are strongly engine design or vehicle-engine integration oriented. In fact, for some engines and vehicles, the determination of the values of these parameters can be reliably done only by experimental means or at least by a combination of theoretical and experimental means. This is particularly true when dealing with the Langley scramjet module and its integration with a vehicle. For example, schedules (as a function of inlet entrance or vehicle forebody inviscid Mach number) of the module spillage flow $\frac{W_0 - W_1}{W_0}$, additive drag ($C_{}$ inlet pressure force A_I normal to the forebody surface, and inlet aerodynamic contraction ratio (A_2/A_1), are determined experimentally or through a combination of experiment and theory. In the present analysis, theoretical approximations are obtained for the nozzle exit area

(A_4/A_1), plume drag (C_E), plume force A_p normal to forebody surface, and heat and friction losses of the vehicle forebody, the inlet, the combustor and the nozzle. The nozzle plume shape, nozzle exit area, nozzle exit flow direction, plume force A_p, and plume drag are strongly dependent on the vehicle afterbody shape (nozzle top surface) in relation to the engine. The methods used to generate the additional engine parameters needed to make performance computations are discussed and the resulting engine parameters presented in figures 4 through 20. A list of these engine parameters is presented in Table I. Theoretical performance computations, using these parameters, were made for free-stream Mach numbers 5, 6, and 7, free-stream dynamic pressure 23,940 N/m^2 and vehicle forebody surface angles of 4.6^o, 7.1^o, 9.6^o, 12.1^o and 14.6^o relative to the free stream. These predictions are discussed and the results presented in figures 21 through 23. The sensitivity of predicted engine force A_A (parallel to vehicle forebody surface) to the engine parameters of figures 4 through 20 is also discussed and the results presented graphically in figures 24 through 29.

Engine Parameters

Pressure ratio across vehicle forebody shock and the inviscid Mach number.- The pressure ratio p_1/p_0 across the vehicle forebody shock, the vehicle forebody's inviscid Mach number and the inviscid kinetic energy efficiency $(\eta_K)_f$ across the shock are assumed to be those computed for conical flow corresponding to cone angles equal to the vehicle forebody surface angle "ω" relative to the free stream plus 0.4^o to account for boundary layer on the surface. The resulting theoretical pressure ratios, inviscid Mach numbers and inviscid shock kinetic energy efficiencies are presented in figure 4 for free-stream Mach numbers 5, 6, and 7. This assumption for the inviscid forebody flow is a result of experimental testing of representative vehicle forebody shapes as well as comparison of theoretically predicted surface pressures (reference 14) with cone surface pressures.

Inlet mass flow spillage.- The mass flow captured as a function of the mass flow that could be captured without inlet spillage was determined experimentally. These experimental results are presented in figure 5 in terms of spillage flow ratio $\frac{W_o - W_1}{W_o}$ for an inlet entrance (or vehicle forebody) inviscid Mach number range $(M_{1,\ Inv.})$ of 2.3 to 6.0. In general, the procedure used to obtain these results consists of obtaining static and pitot pressure surveys of the flow downstream of the struts and integrating the mass flow per unit area generated from these surveys over the survey area while correcting for local flow direction. A detailed discussion of the method used for the Mach number 6.0 data is presented in reference 4 while a more general discussion of all the data is presented in reference 6. For the present calculations it

was also assumed that $\frac{A_c - A_1}{A_c}$ is equal to $\frac{W_o - W_1}{W_o}$. The cowl area A_c is the area obtained by the projection of the inlet leading edges on a plane normal to the forebody flow. This assumption results in the computation of W_o (eq. 21 of Appendix) as based on the mass flow captured W_1 as computed from the one-dimensional flow at station 1 (eq. 20 of Appendix). This assumes the one-dimensional flow computed for station 1 extends all across the cowl area. The W_o is therefore smaller than would be obtained if nonviscous flow conditions were assumed across the spillage flow area $(A_c - A_1)$.

Inlet aerodynamic contraction ratio.- The inlet aerodynamic contraction ratio was determined experimentally (reference 6) and the results are presented in figure 6 for an inlet entrance (or vehicle forebody) inviscid Mach number range of 2.3 to 6.0. This Mach number schedule is based on experimental values for mass weighted average throat Mach number and total pressure along with the assumption of adiabatic flow.

Inlet normal force and additive drag.- The inlet normal force A_I is the absolute pressure force on the capture stream tube over the spillage area and is assumed to be approximated by,

$$A_I = 2.4\ H^2\ p_1 \tag{3}$$

The parameter H is the engine height. The relation thus assumed for A_I is based on the assumption that the lower surface of the inlet stream tube exposed to the external flow and located between the inlet entrance station and the cowl leading edge is acted on by the forebody flow field static pressure p_1 over the exposed stream tube surface area.

The additive drag is determined using a combination of experimental and theoretical results. Experimental values for engine capture flow (modified values of reference 6 between $(M_1)_{Inv.}$ values of 2.3 to 6.0) are used to determine approximately where the dividing stream line (between capture and spillage flow) is located at the inlet entrance station (station "1") to the cowl lip. This dividing streamline is determined by matching pressure and flow direction along the stream tube surface dividing the internal and external flow. This method approximates the down turning of the flow and the pressure in each of the shock bays open to the external flow. This procedure is applied through the inlet along the dividing stream line to a point just foreward of the cowl lip. The strong shock located in the vicinity of the cowl lip and detached shock waves (for the lower Mach numbers) make it necessary to assume a relatively arbitrary fairing from the dividing stream line, already defined, to the cowl lip. The absolute static pressures along this stream line are then approximated by the experimentally measured inlet sidewall and strut static pressures. The additive drag as approximated by this procedure is presented in figure 7 in

terms of additive drag coefficient ($C_I = D_A/q_0 A_c$) for free-stream Mach numbers of 5, 6, and 7.

Nozzle plume drag, normal force Λ_p, exit area and exit flow direction.- The internal nozzle flow and external plume are computed theoretically using a technique known as floating shock fitting developed by Moretti in reference 15 and discussed further by Salas in reference 16. The computerized version of the method used in the present nozzle-plume computations was developed by Salas for two-dimensional and axisymmetric flows. The two-dimensional version is used in the present computations. The internal nozzle flow properties, external plume shape and flow properties including local flow directions, and pressure distribution along the lower surface of the external plume are generated using the nozzle vehicle afterbody relationship presented in figure 8. The nozzle-plume computations are for a perfect gas with a specific heat ratio of 1.25 and initial conditions at the nozzle entrance are obtained using the method of the present paper to generate one-dimensional flow parameters at the nozzle entrance. The plume drag is then calculated by integrating the absolute pressure forces on the lower surface of the plume in a direction parallel to the vehicle forebody surface. The results of these computations in terms of plume drag coefficient (C_E) are presented in figure 9 in terms of $D_E/q_0 A_c$. The nozzle force Λ_p normal to the vehicle forebody surface is obtained by integrating the absolute pressure forces on the lower surface of the plume in a direction normal to the forebody surface. The results of these computations are presented in figure 10 in terms of $\Lambda_p/q_0 A_c$. The nozzle exit area is obtained from the plume shape at the trailing edge of the vehicle afterbody surface and in a plane normal to the average nozzle flow direction. The results of these computations in terms of area ratio (A_4/A_1) are presented in figures 11(a) and 11(b). The average nozzle exit flow direction (β) is obtained by mass weighting the local flow directions across the nozzle exit plane and the results of these computations are presented in figure 12.

Friction and heat losses of engine capture flow.- The friction losses are computed assuming the form of Reynolds analogy put forth in equation (2) of the Appendix. Therefore, before friction losses can be computed, an approximation of the heat loss must be obtained.

Heat-transfer computations were made for the vehicle forebody region ahead of the engine and the results are presented in figure 13. These theoretical heat-transfer values for the forebody were computed using the method of reference 17, assuming flat plate flow and transition beginning at $R_\theta = 1000$. The assumption of flat plate flow for these computations was made as it is believed that this assumption will produce a thicker boundary layer than that for a corresponding conical flow assumption and therefore would be the pessimistic case.

Heat-transfer computations for the internal surfaces of the engine are reported for a smaller scale heat sink version in reference 18. These

computations were made for $M_o = 7.0$, $M_1 = 6.0$, and $\phi = 1.0$ and produced the following heat loss values for the inlet, combustor, and nozzle.

$$(\Delta H_I)_{HS} = 3.26 \times 10^4 \text{ Joules}$$

$$(\Delta H_{comb})_{HS} = 1.687 \times 10^5 \text{ Joules} \qquad (4)$$

$$(\Delta H_N)_{HS} = 5.60 \times 10^4 \text{ Joules}$$

The above heat-transfer values obtained for the heat sink engine (subscript HS) of reference 18 are scaled up to the present engine (subscript PE) for a free-stream Mach number of 6.0 using the following approximating relationship (modified from reference 17) between the engine component heat-transfers of the two engines.

$$(\Delta H_{CO})_{PE} = \left[\frac{(\rho V)_{PE}}{(\rho V)_{HS}}\right]_{CE} \times \frac{(A_C)_{PE}}{(A_C)_{HS}} \times \left[\frac{q_{HS}}{q_{P.E.}}\right]_{CE}^{\frac{1}{7}} \times \left(\frac{(A_C)_{HS}}{(A_C)_{PE}}\right)^{\frac{1}{7}}$$

$$\times \frac{(h_{t,o} - h_w)_{PE}}{(h_{t,o} - h_w)_{HS}} \left(\Delta H_{CO}\right)_{HS} \qquad (5)$$

This relationship for scaling of the heat load assumes the friction coefficient is inversely proportional to $(q_o A_c)^{1/7}$ instead of the more correct expression of being inversely proportional to $(q_o A_c^{1/2})^{1/7}$. In the scaling of the heat transfers to very large engines it becomes important that the more correct expression be used. The engine component (subscript CO) heat-transfer results obtained using this computational procedure are presented in figure 14 for $M_o = 6.0$; the nozzle heat transfers presented do not include the heat transfer to the vehicle afterbody portion of the nozzle. Results were obtained for the free-stream Mach numbers 5 and 7 using the theoretical curves for engine cooling presented in figure 23 of reference 7 to generate values for the ratio of engine component heat-transfer to the engine component heat-transfer at $M_o = 6.0$. The results of these computations are presented in figure 15 in terms of $\Delta H/\Delta H_{M_o = 6.0}$ for a free-stream Mach number range from 4.0 to 8.0. The engine component heat-transfers calculated (for $M_o = 5, 7$) using the curves of figures 14 and 15 are presented in figure 16; again the nozzle value does not include the heat-transfers for the vehicle afterbody portion of the nozzle.

Remaining engine parameters.- Values for the remaining parameters needed in order to make engine performance computations are assumed keeping in mind any reasonable physical limits or known vehicle restrictions. These include fuel equivalence ratio (ϕ), combustion efficiency (η_{comb}), enthalpy level of the hydrogen fuel, and combustor wall pressure integral factor (given in reference 19 and discussed in the Appendix).

For an operational type hypersonic vehicle it would be desirable to achieve cruise at a fuel equivalence ratio less than 1.0 so as to have acceleration capabilities up to $\phi = 1.0$. Engine size is a problem for an experimental vehicle and it becomes more important to keep engine size down as much as possible by designing for cruise at $\phi = 1.0$ and accelerate using fuel equivalence ratios greater than 1.0. Therefore, the major portion of the engine performance computations of the present paper were made for a fuel equivalence ratio of 1.0 (and M_o = 5, 6, and 7) with representative engine performance computations for fuel equivalence ratios of 0.5 and 1.5 (and $M_o = 6$).

The value assumed for the combustion efficiency (η_{comb}) is 0.95 which is believed to be a realistic assumption for fuel equivalence ratios of 1.0. For fuel equivalence ratios greater than or less than 1.0, the combustion efficiency increases but to what degree it is not known. Therefore, the arbitrary assumption of 1.0 for the combustion efficiency was made for the engine performance computations at fuel equivalence ratios of 0.5 and 1.5.

The enthalpy level of the fuel is assumed to be 1.415×10^3 Joules/kg which corresponds to a fuel temperature of 111.1°K; the enthalpy base is that of reference 11. The inlet, combustor, and enclosed portion of the nozzle are assumed to be regeneratively cooled and therefore the heat removed by cooling these engine components is added to the fuel.

Engine parameters for $\phi \neq 1.0$.- The forebody flow field and inlet flow field are theoretically unaffected by fuel equivalence ratio and therefore values of pertinent performance parameters for the forebody and inlet discussed for $\phi = 1.0$ would be applicable to other fuel equivalence ratios. Combustor and nozzle heat-transfers, and to some extent friction losses, would be affected and therefore would have to be altered to account for a fuel equivalence ratio different from 1.0. Nozzle exit area and exit flow direction would also be affected along with nozzle plume drag. The effect of fuel equivalence ratio on these parameters was computed for the heat sink engine of reference 18. The results of these computations are presented in figures 17 through 20, nondimensionalized with respect to the value of the parameter being considered as computed for $\phi = 1.0$. Check computations for $\phi = 1.5$, $M_o = 7.0$ and $\omega = 3.6^0$ were made for the same parameters for the scramjet module of the present paper (for all except heat-transfer), and these results are also presented in figures 17 through 20. Based on the satisfactory comparison shown on these figures, it is assumed that at least for $\phi = 1.5$ realistic engine performance computations (possibly with the exception of heat-transfer) can be made using the curves of figures 17 through 20 and the value of the corresponding parameter for $\phi = 1.0$.

Predicted Thrust and Specific Impulse

The theoretically predicted performance of the Langley scramjet engine is presented in figures 21 through 23 in terms of force coefficients corresponding to engine forces A_A and A_B, thrust coefficient and specific impulse. These engine performance results are for the engine airframe integration configuration shown in figure 8. It is important to note that these theoretical results do not include three-dimensional effects in the afterbody flow, external cowl drag, or flow end effects on the two outboard engines. In the forebody computations the engine capture flow is penalized relative to friction and heat transfer losses at the free-stream pressure (Appendix). Physically these losses would occur at the forebody pressure and would result in a different entropy gain. A check into the effect of imposing the forebody friction and heat losses at the forebody pressure revealed an increase in predicted mass capture from 1.5 percent to 7 percent, and an increase in thrust coefficient of 1.9 percent to 10 percent for the range of forebody angles considered. Preliminary computations for the cowl drag indicate that the cowl drag is less than 4 percent to 6 percent of the predicted thrust; the order of magnitude of the three-dimensional effects and end effects are not known. The skin-friction drag and heat transfer of the vehicle afterbody portion of the nozzle are charged off to the aircraft. It was decided not to include the skin-friction drag and heat transfer of the vehicle afterbody portion of the vehicle in the engine performance computations due to the fact it is not known how and of what this afterbody portion of the nozzle is to be constructed. However, if it is assumed that the heat and friction losses of the vehicle afterbody portion of the nozzle are of the same order of magnitude (per unit area) as that of the internal portion of the nozzle, then for the configuration of figure 8, nozzle flow friction and heat losses would increase by about 60 percent and the effect on engine force A_A is theoretically predicted to be less than 3 percent. The theoretical predictions presented in figures 21 through 23 indicate that with the heat release schedule described by the combustor pressure integral parameter (reference 19) a thermal choke will occur for $M_o = 5.0$, $\phi = 1.0$ and a forebody surface angle between 9.6^o and 12.1^o. It must be noted that the thermal choking of the combustor predicted here one dimensionally is a result of assumptions made in reference 19 to obtain the wall pressure integral. This choking limit should not be interpreted as a general result and may not be a real limit. The components of the engine forces A_A and A_B (in the flight direction and in coefficient form) that make up the engine thrust are presented in figures 21(a) and 21(b). The predicted engine thrust as shown in figure 22 increases with an increase in vehicle forebody angle ω to an angle of 11^o to 12^o. The predicted specific impulse as shown in figure 23 decreases with an increase in vehicle forebody angle. These observations on predicted engine thrust and specific impulse indicate, from the view point of the Langley engine and the presently assumed vehicle-engine configuration, that the vehicle should be designed to cruise with vehicle forebody angles of about 10^o or less.

Sensitivity of Predicted Engine Force Parallel to Forebody Surface to Predicted and Assumed Engine Parameters

The performance predictions of a scramjet engine are influenced to various degrees by the predicted or assumed values for the engine parameters discussed in previous sections. The relative effects on predicted performance (through predicted engine force) of these engine parameters are discussed in terms of vehicle forebody parameters, engine inlet parameters, combustor parameters, and nozzle-plume parameters.

Vehicle forebody parameters.- The effect on predicted engine force A_A of increasing the forebody surface angle is demonstrated in figure 24 for $M_0 = 6.0$. The force A_A and mass flow captured are nondimensionalized by the predicted force A_A and mass flow captured for vehicle forebody angle of 4.6^0 and presented in figure 24 as a function of forebody angle ω. From the theoretical results presented in figure 24 for $M_0 = 6.0$, it is concluded that an increase in the forebody angle (or vehicle angle of attack) results in a increase in the predicted mass flow captured by the engine and a like increase in predicted force A_A.

The effects of forebody boundary-layer losses as well as the engine's internal boundary layer losses on engine thrust are introduced indirectly through the heat-transfer predicted to pass from the engine capture flow through the vehicle's forebody and engine's internal surfaces. The friction losses are then approximated using the form of Reynolds analogy presented by equation (2) of the Appendix. In order to evaluate separately and concurrently the sensitivity of predicted force A_A to assumed values for forebody friction and heat losses of the capture flow, three sets of computations were made for $M_0 = 6.0$ and the results are presented in figures 25 through 27. In figures 25 through 27 the force A_A, mass flow captured, heat losses, and friction losses are nondimensionalized with respect to the corresponding parameters predicted for the present engine at $M_0 = 6.0$.

The curves of figure 25 were predicted with friction losses held constant while allowing heat losses to vary from those predicted for $M_0 = 6.0$. The effects on predicted force A_A of increasing the engine's internal heat losses (with the forebody heat loss held constant) are shown in figure 25(a) to be quite small; less than 1 percent for 50 percent increase in engine internal heat losses. Of particular note is that the capture mass flow remains constant. The forebody, inlet, combustor and nozzle flow heat losses assumed for the generation of the curves of figure 25(a) are related in the following manner to the $M_0 = 6.0$ values of figure 1:

$$\Delta H_f = (\Delta H_f)_{PE}$$

$$\Delta H_I = \chi(\Delta H_I)_{PE}$$

$$\Delta H_{comb} = \chi(\Delta H_{comb})_{PE} \qquad (6)$$

$$\Delta H_N = \chi(\Delta H_N)_{PE}$$

The effects on engine force Λ_A and mass flow captured of increasing the forebody heat transfer (possibly by decreasing the forebody surface temperature) are illustrated in figures 25(b) and 25(c). The forebody, inlet, combustor, and nozzle flow heat losses assumed for the generation of the curves of figures 25(b) and 25(c) are related in the following manner to the values for $M_o = 6.0$ of figure 1:

$$\Delta H_f = \zeta(\Delta H_f)_{PE}$$

$$\Delta H_I = \zeta(\Delta H_I)_{PE}$$

$$\Delta H_{comb} = \zeta(\Delta H_{comb})_{PE} \qquad (7)$$

$$\Delta H_N = \zeta(\Delta H_N)_{PE}$$

An increase in forebody heat-transfer is shown to result in an increase in engine force Λ_A and mass flow captured. A 23 percent increase in forebody heat-transfer (change in forebody surface temperature from 666.7^oK to 111.1^oK) results in a 4.7 percent to 6.6 percent increase in engine force Λ_A and a 3.8 percent to 5.2 percent increase in mass flow captured. The predicted increase in engine mass flow coincides with the fact that cooling the boundary layer flow reduces the displacement thickness and therefore the mass flow difference of the boundary layer due to friction losses.

The curves of figure 26 were predicted with heat losses held constant while allowing friction losses to vary from those predicted at $M_o = 6.0$. The effects on engine force Λ_A of varying the engine's internal friction losses (with the forebody friction losses held constant) are indicated in figure 26(a) to be small. A 50 percent increase or decrease in engine internal friction losses results, respectively, in a 2.25 percent to 3.35 percent decrease or a 2.45 percent to 3.52 percent increase in the engine's predicted force Λ_A while capture mass flow remains constant. The forebody, inlet, combustor and nozzle flow friction losses used to generate the curves of figure 26(a) are related in the following manner to the values for $M_o = 6.0$:

$$
\begin{aligned}
(\Delta F_f) &= (\Delta F_f)_{PE} \\
(\Delta F_I) &= \sigma(\Delta F_I)_{PE} \\
(\Delta F_{comb}) &= \sigma(\Delta F_{comb})_{PE} \\
(\Delta F_N) &= \sigma(\Delta F_N)_{PE}
\end{aligned}
\tag{8}
$$

The effects of varying the vehicle forebody friction losses on predicted values of engine force A_A and mass flow captured are illustrated in figures 26(b) and 26(c). The forebody, inlet, combustor, and nozzle flow friction losses assumed in the generation of the curves of figures 25(b) and 25(c) are related in the following manner to the values for $M_o = 6.0$:

$$
\begin{aligned}
\Delta F_f &= \xi(\Delta F_f)_{PE} \\
\Delta F_I &= \xi(\Delta F_I)_{PE} \\
\Delta F_{comb} &= \xi(\Delta F_{comb})_{PE} \\
\Delta F_N &= \xi(\Delta F_N)_{PE}
\end{aligned}
\tag{9}
$$

A 50 percent increase in forebody friction loss results in a 19.5 percent to 22.7 percent decrease in the engine force A_A with a corresponding 17.2 percent to 21.5 percent decrease in engine mass flow. The engine capture mass flow without any boundary layer would be between 13 percent to 18 percent greater than the present case. Therefore, there is a limit to the amount the friction can be reduced relative to the heat loss and still be physically realistic. Therefore, no conclusions will be drawn from the reduction in friction portion of the curves of figures 26(b) and 26(c).

The curves of figure 27 were predicted assuming engine heat losses and friction losses vary by the same factor from those predicted at $M_o = 6.0$. This is the more realistic relationship to assume relative to possible errors in predicted values. Equations (7) and (9) present the manner the forebody, inlet, combustor, and nozzle flow heat and friction losses (assumed to generate figure 27) are related to the corresponding values for $M_o = 6.0$. The variations of engine mass flow are presented in figure 27(a) and the variations of predicted values for engine force A_A are presented in figure 27(b). The curves of figure 27 indicate that the beneficial effects of increased forebody heat transfer can be realized only by not increasing the friction losses in the same proportion, otherwise they will be more than offset by the corresponding increase in forebody friction losses.

The theoretical results presented in figures 24 through 27 were obtained by varying simultaneously and separately various vehicle forebody (forebody angle, friction and heat losses) and engine internal (friction and heat losses) flow characteristics. From these theoretical results it is concluded that the engine's predicted capture mass flow and therefore the engine's predicted force A_A are strongly influenced by any changes in forebody flow characteristics. Therefore, it is confirmed that knowing the quantity and physical characteristics of the mass flow captured by the engine is of primary importance for predicting engine performance. The theoretical results of figures 24 through 27 also suggest some possible forebody design considerations which would improve engine capture mass flow as well as thrust. For example, a conical forebody and forebody surface cooling (forebody surface washed by engine capture flow) would decrease the boundary layer thickness at the engine inlet face as well as decrease the boundary layer mass flow deficiency. Both of these forebody characteristics would increase engine capture flows and therefore thrust.

Engine inlet parameters.- There are five engine inlet parameters for which engine performance sensitivities are known or are evaluated and the results presented. Two of these, the friction and heat losses, were evaluated and the results discussed along with the forebody flow friction and heat loss results. A third is the mass flow spilled. Previous results already presented (figures 24 through 27) indicate that engine force A_A values are approximately proportional to engine mass flow captured. The three remaining engine inlet parameters are the additive drag, inlet aerodynamic contraction ratio and inlet inviscid kinetic energy efficiency. The additive drag, and spillage mass flow could possibly be a function of inlet contraction ratio but at the present time the relationship is not known. The lowest value computed for the inlet inviscid kinetic energy efficiency is .994 (for $(M_1)_{Inv.} = 6$) and is assumed for all calculations.

The additive drag given by $D_A \cos \omega$ nondimensionalized by the predicted engine force A_A is presented for $M_0 = 6.0$ in figure 28 (plume drag is also presented) as a function of forebody angle (ω). The additive drag distribution of figure 28 was generated in the manner discussed in a previous section. At forebody angles of about 14^0 a 50 percent change in the predicted additive drag can result in a 7.9 percent change (in the opposite direction) in predicted engine force A_A. This sensitivity of predicted force A_A to the additive drag indicates the importance of an accurate prediction of additive drag.

The effects on engine force A_A of varying the inlet aerodynamic contraction ratio from those determined experimentally is illustrated for $M_0 = 6.0$ in figure 29. The engine force A_A predicted by varying the inlet aerodynamic contraction ratio is presented as a function of the aerodynamic contraction ratio A_1/A_2 with both predicted force A_A and aerodynamic contraction ratio divided by the corresponding value assumed for $M_0 = 6.0$. A 20 percent change

in inlet aerodynamic contraction ratio is shown in figure 29 to result in a 3 percent to 4 percent change in predicted engine force A_A.

Engine combustor parameters.- There are seven engine combustor parameters for which predicted engine performance sensitivities are known or are evaluated and the results presented and discussed. These combustor parameters are the heat and friction losses, the combustor wall pressure integral factor, size of the combustor exit area, injected fuel temperature, combustion chemical efficiency and the fuel equivalence ratio.

Predicted engine force A_A sensitivities to friction and heat losses are discussed in a previous section. The combustor wall pressure integral factor is the integral of the actual combustor wall pressure area distribution ratioed to a wall pressure area value corresponding to the assumption that the mean combustor pressure is an arithmetic average of the combustor entrance and exit values. If the arithmetic average of entrance and exit combustor pressures are used instead of the integral, possible errors in predicted engine force A_A values at $M_0 = 8.0$ are shown in reference 19 to be as large as 20 percent. Therefore, a correlation for the combustor wall pressure integral factor developed in reference 19 is utilized in the present computations. The size of the combustor exit area for the Langley scramjet engine is fixed to be 64 percent of the cowl area and therefore the sensitivity of predicted engine force A_A values to the size of the combustor exit area is not considered. Theoretical computations of engine force revealed a 5.6 percent increase in A_A with an increase in injected fuel temperature (non-regenerative) from $300^{\circ}K$ to $1000^{\circ}K$; the feasibility of fuel temperatures of $1000^{\circ}K$ is questionable. Theoretical computations of engine force A_A as a function of combustion efficiency were made for the heat sink engine of reference 18. These theoretical computations which were for $M_0 = 7$ and $\phi = 1.0$ revealed a decrease of combustion efficiency from 1.0 to 0.85 resulted in a 14.1 percent decrease in engine force A_A.

The effects of the fuel equivalence ratio on engine force A_A are illustrated in figure 30 for $M_0 = 6.0$. The ratio of predicted engine force A_A to that predicted for $\phi = 1.0$ is presented as a function of fuel equivalence ratio ϕ. Also presented in figure 30 is the corresponding engine force A_A distribution computed for the heat sink engine of reference 18 but for $M_0 = 7$, $q_0 \approx 19{,}496\ N/m^2$ and combustion efficiency $\eta_{comb} = 0.95$. The combustion efficiencies for the Langley scramjet engine computations are assumed to be 0.95 for $\phi = 1.0$ and 1.0 for $\phi = 0.5$ and 1.5. The conclusion can be drawn from figure 30 that predicted engine force A_A values are a strong function of the fuel equivalence ratio. For fuel equivalence ratios between 1.0 and 0.5 the decrease in engine force A_A is predicted to be 41 percent to 45.5 percent depending on the vehicle forebody angle. For fuel equivalence ratios between

1.0 and 1.5 the increase in predicted engine force Λ_A is 18.2 percent to 19.5 percent depending on the vehicle forebody angle. The conclusion can be drawn from the theoretical curves of figure 30 that the increase in engine force Λ_A appears to level off above $\phi = 1.5$ which is consistent with other calculations.

Engine nozzle parameters.- There are five engine nozzle parameters for which engine performance sensitivities are known or are to be evaluated and the results presented. These nozzle parameters are the nozzle flow heat and friction losses, the average nozzle exit flow angle relative to the vehicle forebody, the nozzle plume drag, and the size of the nozzle exit area A_4 relative to the inlet capture area A_1.

Predicted engine force Λ_A sensitivities to nozzle flow heat and friction losses are discussed in a previous section. The average nozzle exit flow angle (β) relative to the vehicle forebody is shown to be between 0^o and -8^o (figure 12) which influences engine force Λ_A prediction through multiplication of cos β times (smallest value of cosine β is greater than 0.99) the nozzle exit momentum. As the engine thrust is a small difference between two large numbers, the nozzle exit flow momentum and the inlet entrance flow momentum, this correction on the nozzle exit momentum can result in significant percentage changes in predicted engine force Λ_A. For example, computations for the heat sink engine (of reference 18) for $M_o = 7.0$ and $\phi = 1.0$ for $\beta = 0^o$ and -6^o revealed 3.8 percent reduction in predicted engine force Λ_A. The nozzle plume drag given by $D_E \cos \omega$ nondimensionalized by the predicted engine force Λ_A is presented for $M_o = 6.0$ in figure 28 as a function of the forebody flow angle (ω). The plume drag distribution of figure 28 was generated in the manner discussed in a previous section. A 50 percent change in the predicted plume drag can result in a 3 percent change in predicted engine force Λ_A.

The effects of reducing the size of the nozzle exit area on predicted engine force Λ_A are illustrated for $M_o = 6.0$ in figure 31. This reduction in size of the nozzle exit area was affected by the reduction of the length of the vehicle afterbody portion of the nozzle while keeping the same vehicle afterbody surface angle. For $M_o = 6.0$ and the present engine-vehicle configuration, a 49.5 percent reduction in nozzle length results in a 39 percent reduction in size of the nozzle exit area and a 13 percent to 15.2 percent reduction in predicted engine force Λ_A.

CONCLUSIONS

A one-dimensional theoretical method is presented for the prediction of a scramjet engine's internal performance. This method of solution consists of

combining a one-dimensional flow model and real gas equilibrium thermodynamics with the control volume concept. Using this one-dimensional theoretical method, the evaluation of the effects of vehicle forebody flow parameters and characteristics on predicted thrust values for the Langley scramjet engine indicate that the engine's predicted capture mass flow, and thus the predicted thrust, is strongly influenced. It is confirmed that knowledge of the quantity and physical characteristics of the mass flow captured by the engine is shown to be of primary importance for predicting engine performance. Also some vehicle forebody design considerations such as high surface cooling and shaping the forebody are suggested as they would decrease the boundary layer mass defect and thus increase engine mass flow. The theoretical evaluation of the effects of any changes in the engine's internal parameters on predicted thrust values indicate changes in some internal parameters such as additive drag, fuel equivalence ratio, nozzle length or nozzle exit area and combustor pressure integral cause significant changes in values of predicted internal thrust. Changes in other internal engine parameters such as heat and friction losses and plume drag result in less significant changes in the predicted values of thrust.

Theoretical internal engine performance predictions in terms of thrust coefficient and specific impulse are presented for free-stream Mach numbers of 5, 6, and 7, free-stream dynamic pressure of 23,940 N/m^2, forebody surface angles from 4.6^o through 14.6^o and a fuel equivalence ratio of 1.0. These engine performance predictions indicate combustor thermal choking at free-stream Mach number of 5.0 and a vehicle forebody angle between 9.6^o and 12.1^o; this thermal choking as predicted one dimensionally is a function of the combustor exit size and wall pressure integral assumed. From the viewpoint of the predicted internal thrust and specific impulse, the vehicle should be designed to cruise with vehicle forebody angles of less than 10^o.

APPENDIX

Performance Analysis and Solution Technique

The method of calculating engine performance consists of combining a one-dimensional fluid flow model with real gas equilibrium thermodynamic properties and the control volume concept illustrated in figure 2. The capture mass flow passes from the free stream, through the vehicle bow shock, along the forebody surface, through the inlet (spilling flow through the bottom of the inlet), through the combustor and out through the nozzle exit. The changes in the flow properties through the engine are computed by means of the one-dimensional conservation equations for mass, momentum, and energy. Calculations for the capture flow are made separately for the vehicle forebody flow field, inlet, combustor, and nozzle. These one-dimensional computations account approximately for the shock losses, friction losses, and heat losses that occur in each component of the engine. Details of the analysis of each component flow process and the methods used to obtain a solution are presented in the following sections.

Free-Stream Flow

The free-stream conditions ahead of the forebody shock (station "o") are computed based on the 1962 Standard Atmosphere Tables (reference 20). In order to accomplish the computations of the free-stream conditions using reference 20, values for the flight altitude and Mach number are required. Initial guesses for free-stream capture area (A_o) and total momentum of the capture flow ($p_oA_o + W_oV_o$) are then computed from these conditions using an initial guess for the capture mass flow (W_o). These free-stream flow quantities are modified in the portion of the forebody flow field computations in which the actual capture mass flow is computed.

Forebody Flow

The change in flow properties from the free stream across the forebody flow field to a station on the surface just in front of the inlet (station 1) is computed using a form of the one-dimensional momentum and energy equations. These equations account for forebody flow friction and heat losses as well as inlet mass flow spillage. A method is also included which approximately accounts for forebody shock losses. The pressure ratio p_1/p_o across the bow shock, the inviscid kinetic energy efficiency $(\eta_K)_f$ across the bow shock, inlet mass flow spillage to free-stream capture flow excluding spillage $\frac{(W_o - W_1)}{W_o}$

are specified. The forebody inviscid kinetic energy efficiency $(\eta_K)_f$ is given by,

$$(\eta_K)_f = \frac{V_{1,\,S}^2}{(V'_{1,\,S})^2} \tag{A1}$$

The subscript "S" means these parameters correspond to the expansion of station "1" flow isentropically to the pressure at the preceding flow station (which in this case is station 0). The prime means no forebody shock losses are included in this quantity. The forebody friction losses are computed using the form of Reynolds analogy as given by,

$$\Delta H_f = \frac{(C_{F_{AV}})_f \quad (\rho V)_{AV_f} \quad (h_{t,\,o} - h_{W,\,f}) \quad (A_W)_f}{2\ Pr^{\frac{2}{3}}} \tag{A2}$$

The momentum relationship assumed for the one-dimensional forebody flow is given by,

$$W_1\ (V'_{1,\,S}) + A'_{1,\,S}\ p'_{1,\,S} = p_o\ A_o + W_1\ V_o - \left(\frac{\rho V^2}{2}\right)_{AV}\ (A_W)_f\ (C_{F_{AV}})_f$$

$$-(A_o - A'_{1,\,S})\ F\ (p_o,\ p'_{1,\,S}) \tag{A3}$$

or,

$$V'_{1,\,S} = \frac{p_o A_o}{W_1} + V_o - \left(\frac{\rho V^2}{2}\right)_{AV_f}\ \left(\frac{A_W}{W_1}\right)_f\ (C_{F_{AV}})_f$$

$$-\left(\frac{A_o - A'_{1,\,S}}{W_1}\right) F\ (p_o, p'_{1,\,S}) - \frac{A'_{1,\,S}\ p'_{1,\,S}}{W_1} \tag{A4}$$

The momentum relationship of equations (3) and (4) include no forebody shock losses. For $p'_{1,\,S}$ equal p_o,

$$F\ (p_o,\ p'_{1,\,S}) = p_o \tag{A5}$$

and, combining equations (4) and (5) gives,

$$V'_{1,\,S} = V_o - \frac{(\rho V^2)}{2}_{AV_f} \left(\frac{A_W}{W_1}\right)_f (C_{F_{AV}})_f \tag{A6}$$

Utilizing the form of Reynolds analogy as put forth in equation (2) gives,

$$(\rho \frac{V^2}{2})_{AV_f} \left(\frac{A_W}{W_1}\right)_f (C_{F_{AV}})_f = \frac{Pr^{\frac{2}{3}} \Delta H_f (V_{AV})_f}{(h_{t,o} - h_{w,f})W_1} \tag{A7}$$

combining equations (6) and (7) gives,

$$V'_{1,\,S} = V_o - \frac{Pr^{\frac{2}{3}} \Delta H_f (V_{AV})_f}{(h_{t,o} - h_{w,f})W_1} \tag{A8}$$

Accounting the forebody shock losses on $V'_{1,\,S}$ through use of the forebody shock kinetic energy efficiency gives,

$$V_{1,\,S} = V'_{1,\,S} \; (\eta_K)_f^{\frac{1}{2}} \tag{A9}$$

The energy relationship assumed for the one-dimensional forebody flow is given by,

$$h_o + \frac{V_o^2}{2} = h_{1,\,S} + \frac{V_{1,\,S}^2}{2} + \frac{\Delta H_f}{W_1} \tag{A10}$$

or

$$h_{1,\,S} = h_o + \frac{V_o^2}{2} - \frac{V_{1,\,S}^2}{2} - \frac{\Delta H_f}{W_1} \tag{A11}$$

with $h_{1,\,S}$ and $p_{1,\,S}$ known ($p_{1,\,S} = p_o$) an iteration on the temperature is performed. The first guess for $T_{1,\,S}$ is that it is equal to T_o and succeeding guesses are computed using,

$$T_{1,S} = (T_{1,S} - \Delta T) + 2\Delta T \left(\frac{h_{1,S} - h^-}{h^+ - h^-} \right) \tag{A12}$$

Thermodynamic property data are then used to find the values of h^- for $(T_{1,S} - \Delta T)$ and h^+ for $(T_{1,S} + \Delta T)$, respectively, and the iteration is continued until succeeding guesses of $T_{1,S}$ differ by less than one degree. The thermodynamic property data that are used in the present calculations consist of values for enthalpy, entropy, specific heat, and molecular weight of each species included in the equilibrium calculations. The data are taken from reference 12 and the enthalpy base is adjusted to match that of reference 13.

The station 1 flow conditions are then determined using the isentropic flow relations and the station 1 isentropically expanded flow conditions defined in equations (1) through (12). The isentropic flow relationship between station 1 areas A_1 and $A_{1,S}$ is given by,

$$\frac{A_1}{A_{1,S}} = \frac{\rho_{1,S} V_{1,S} A_o \left(1 - \frac{W_o - W_1}{W_o} \right)}{\left(\frac{A_o}{A_{1,J}} \right) W_1} \tag{A13}$$

where $A_{1,J}$ is the area at station 1 that mass flow W_o (no spillage) would occupy with station 1 velocity and density (including boundary layer losses). The area $A_{1,J}$ would be equal to the cowl area if there were no forebody friction and heat losses and no inlet spillage. In order to find station 1 flow conditions, an isentropic compression process from the station 1 isentropically expanded flow (subscript 1, S) to station 1 flow is computed using equation (13) in conjunction with a double iteration process. This double iteration process consists of assuming a capture mass flow W_1 and iterating on $A_o/A_{1,J}$ until a value of $A_1/A_{1,S}$ is obtained which when substituted into the isentropic relations produces a value of p_1/p_o within 0.001 of the value specified initially. The isentropic relations and the method of solution are as follows:

Isentropic Relations

$$F_1 = (F_1 - 1)^{E_{1,S}} \left[\left(\frac{2}{K_{1,S} - 1} \right)^{E_{1,S}} \left(\frac{A_1}{A_{1,S} M_{1,S}} \right)^{2E_{1,S}} F_{1,S} \right] \tag{A14}$$

$$F = 1 + \frac{K - 1}{2} M^2 \tag{A15}$$

$$E = \frac{K - 1}{K + 1} \tag{A16}$$

A trial value of $F_1 = F_{1,S}$ is assumed initially and successive values of F_1 are computed until the new F_1 changes by less than 0.001. Initial guesses for the values of p_1 and T_1 are obtained from:

$$p_1 = p_{1,S} \left(\frac{F_{1,S}}{F_1} \right)^{\frac{K_{1,S}}{K_{1,S} - 1}} \tag{A17}$$

$$T_1 = T_{1,S} \left(\frac{F_{1,S}}{F_1} \right) \tag{A18}$$

The thermodynamic property data are then used along with $(p_1, T_1 + \Delta T)$ and (p_1, T_1) to obtain entropy values of S_1^+ and S_1, respectively. The value of the temperature is improved by the equation

$$T_1 = T_1 \left(\frac{T_1}{T_1 + \Delta T} \right)^{\frac{S_{1,S} - S_1}{S_1 - S_1^+}} \tag{A19}$$

Where S_1 and S_1^+ are the entropies for the states corresponding to (p_1, T_1) and $(p_1, T_1 + \Delta T)$, respectively. Successive values of T_1 are computed until the new value of T_1 computed differs from the old value by one degree. The

value of the capture mass flow W_1 is then computed from

$$W_1 = \rho_1 V_1 A_c \left(1 - \frac{W_o - W_1}{W_o}\right) \tag{A20}$$

and compared with the assumed value for W_1. If the ratio of the new value of W_1 to the assumed value differs from 1.0 by more than 0.001 the entire iteration procedure is repeated using the new value of W_1 as the assumed value. This iteration is required because $(\Delta H)_f$ is independent of W_1. When the ratio of the new value of W_1 to the assumed value differs by 0.001 or less, the free-stream capture mass flow and capture area (both excluding inlet spillage), and the free-stream momentum of the capture mass flow W_1 are computed by

$$W_o = W_1 \Big/ \left(1 - \frac{W_o - W_1}{W_o}\right) \tag{A21}$$

$$A_o = W_o/\rho_o V_o \tag{A22}$$

$$\Omega_o = (p_o A_o + W_o V_o) \left(1 - \frac{W_o - W_1}{W_o}\right) \tag{A23}$$

In the present forebody computations the engine capture flow is penalized relative to friction and heat-transfer losses at the free-stream pressure. Physically these losses would occur at the forebody pressure and would result in a different entropy gain. A check into the effect of imposing the forebody friction and heat losses at the forebody pressure revealed an increase in predicted mass capture from 1.5 percent to 7 percent and an increase in thrust coefficient of 1.9 percent to 10 percent for the range of forebody angles considered.

Inlet Flow

The change in flow properties from the forebody or (or inlet entrance) station 1 to the inlet throat or station 2 is computed in a similar manner to that of the forebody flow. A form of the one-dimensional momentum and energy equations is used which accounts for inlet friction and heat losses as well as inlet mass flow spillage and a similar method is utilized to approximately account for inlet flow shock losses. The area ratio A_1/A_2 from inlet

entrance to inlet throat, the ratio of the inlet inviscid kinetic energy efficiency $(\eta_K)_I$ (assumed to be equal to .994) through the inlet shocks, the ratio of inlet mass flow spillage to free-stream capture flow excluding spillage $\frac{(W_o - W_1)}{W_o}$ and the inlet flow heat loss (ΔH_I) are specified. The inlet kinetic energy efficiency is given by

$$(\eta_K)_I = \frac{(V_{2,\,s})^2}{(V'_{2,\,s})^2} \tag{A24}$$

which differs from the normal kinetic energy efficiency definition in that only the inviscid inlet shock losses are included. The friction losses are estimated through the Reynolds analogy expression given in the following relationships.

$$\Delta H_I = \frac{(C_{F_{AV}})_I \quad (\rho V)_{AV,\,I} \quad (h_{t,\,o} - h_{W,\,I}) \quad A_{W,\,I}}{2\ Pr^{\frac{2}{3}}} \tag{A25}$$

This method of consideration of friction losses with heat losses is felt to be preferable to that of using adiabatic experimental kinetic energy efficiencies. The use of $h_{t,\,o}$ in the Reynolds analogy expression throughout the inlet combustor and nozzle is justifiable through the fact that sensitivity studies on varying friction losses revealed large changes in an engine's internal friction losses result in small changes in engine performance. The remaining governing equations for inlet flow are

$$W_1 V'_{2,\,s} + p'_{2,\,s} A'_{2,\,s} = p_1 A_1 + W_1 V_1 - \frac{(\rho V^2)_{AV,\,I}}{2} A_{W,I} (C_{F_{AV}})_I$$
$$- (A_1 - A'_{2,\,s})\ F\ (p_1,\ p'_{2,\,s}) \tag{A26}$$

$$V'_{2,\,s} = \frac{p_1 A_1}{W_1} + V_1 - \frac{(\rho V^2)_{AV,\,I}}{2} \frac{A_{W,\,I}}{W_1} (C_{F_{AV}})_I - \frac{(A_1 - A'_{2,\,s})}{W_I} F\ (p_1,\ p'_{2,\,s})$$
$$- \frac{p'_{2,\,s} A'_{2,\,s}}{W_1} \tag{A27}$$

$$F(p_1,\ p'_{2,\,s}) = p_1 \tag{A28}$$

$$V'_{1,\,S} = V_1 - \frac{(\rho V^2)_{AV,\,I}}{2}\,\frac{A_{W,\,I}}{W_1}\left(C_{F_{AV\ I}}\right) \tag{A29}$$

$$\frac{(\rho V^2)_{AV,\,I}}{2}\,\frac{A_{W,\,I}}{W_1}\,\left(C_{F_{AV}}\right)_I = \frac{Pr^{\frac{2}{3}}\,\Delta H_I\,V_{AV,\,I}}{(h_{t,\,o} - h_{W,\,I})W_I} \tag{A30}$$

$$V'_{2,\,S} = V_1 - \frac{Pr^{\frac{2}{3}}\,\Delta H_I\,V_{AV,\,I}}{(h_{t,\,o} - h_{W,\,I})W_1} \tag{A31}$$

$$V_{2,\,S} = V'_{2,\,S}\,(\eta_K)_I^{\frac{1}{2}} \tag{A32}$$

$$h_1 + \frac{V_1^2}{2} = h_{2,\,S} + \frac{V_{2,\,S}^2}{2} + \Delta H_I \tag{A33}$$

$$h_{2,\,S} = h_1 + \frac{V_1^2}{2} - \frac{V_{2,\,S}^2}{2} - \Delta H_I \tag{A34}$$

$$T_{2,\,S} = (T_{2,\,S} - \Delta T) + 2\Delta T\left(\frac{h_{2,\,S} - h^-}{h^+ - h^-}\right) \tag{A35}$$

$$\frac{A_2}{A_{2,\,S}} = \frac{\rho_{2,\,S}\,V_{2,\,S}\,A_1}{W_1\left(\frac{A_1}{A_2}\right)} \tag{A36}$$

Isentropic Relations

$$F_2 = (F_2 - 1)^{E_{2,\,S}}\left[\left(\frac{2}{K_{2,\,S} - 1}\right)^{E_{2,\,S}}\left(\frac{A_2}{A_{2,\,S}\,M_{2,\,S}}\right)^{2E_{2,\,S}}\,F_{2,\,S}\right] \tag{A37}$$

$$F = 1 + \frac{K - 1}{2} M^2 \tag{A38}$$

$$E = \frac{K - 1}{K + 1} \tag{A39}$$

Guessed values of pressure and temperature are computed from:

$$p_2 = p_{2,\,S} \left(\frac{F_{2,\,S}}{F_2} \right)^{\frac{K_{2,\,S}}{K_{2,\,S} - 1}} \tag{A40}$$

$$T_2 = T_{2,\,S} \left(\frac{F_{2,\,S}}{F_2} \right) \tag{A41}$$

As for the forebody flow computations, the thermodynamic property data of references 12 and 13 are used along with $(p_2, T_2 + \Delta T)$ and (p_2, T_2). The value of the temperature is improved by the equation

$$T_2 = T_2 \left(\frac{T_2}{T_2 + \Delta T} \right)^{\frac{S_{2,\,S} - S_2}{S_2 - S_2^+}} \tag{A42}$$

where S_2 and S_2^+ are the entropies for the states corresponding to (p_2, T_2) and $(p_2, T_2 + \Delta T)$, respectively. When successive values of T_2 differ by less than 1^o, the area ratio $\frac{A_2}{A_{2,\,S}}$ is computed from the relation

$$\frac{A_2}{A_{2,\,S}} = \frac{\rho_{2,\,S} V_{2,\,S}}{\rho_2 \left[2 \left(h_{t,\,2} - h_2 \right) \right]} \frac{1}{2} \tag{A43}$$

and compared with the value computed by equation (36). If the value of $A_2/A_{2,\,S}$ computed by equation (43) is not within 0.00001 of the value computed by equation (36) the new station 2 flow values are input into equation (37) for the isentropic expanded flow parameters and the iteration beginning with equation (37) is repeated.

Combustor Flow

The change in flow properties from the inlet throat or combustor entrance (station 2) to the combustor exit station (station 3) is computed utilizing a form of the one-dimensional momentum and energy equations. The one-dimensional flow equations as utilized in the combustor analysis are generated through application of the control volume concept on the combustor as indicated in figure 3. The fuel equivalence ratio ϕ, combuscion efficiency η_{comb}, the combustor heat loss ΔH_{comb}, the area ratio across the combustor A_3/A_2, heat added (J/Kg) to the combustor per kilogram of fuel $(h_t)_{fuel}$, and the total heat added to fuel ΔH_{fuel} through the engine cooling cycle are specified.

The one-dimensional momentum equation as obtained through application of the control volume concept to the combustor is given by,

$$W_1V_2 + p_2A_2 = V_3W_1\left(1 + \frac{W_{fuel}}{W_1}\right) + p_3A_3 + \frac{(\rho V^2)_{AV,\ comb.}}{2} A_{W,\ comb} (C_{f_{AV}})_{comb} - \int_{"2"}^{"3"} p_W dA \tag{A44}$$

The wall pressure integral is given by,

$$\int_{"2"}^{"3"} p_W dA = (A_3 - A_2)\ (p_3 + p_2)\ \frac{B_p}{2} \tag{A45}$$

The parameter B_p is the combustor wall pressure integral factor of reference 19 which relates the wall pressure integral with the value for the integral assuming the wall pressure distribution can be approximated by the arithmetic average of the combustor entrance (station "2") and exit (station "3") pressures. The form of Reynolds analogy assumed is given by,

$$\Delta H_{comb} = \frac{(C_{F_{AV}})_{comb} (\rho V)_{AV,\ comb} (h_{t,\ o} - h_{W,\ comb})\ A_{W,\ comb}}{2Pr^{\frac{2}{3}}} \tag{A46}$$

$$\frac{(\rho V^2)_{AV,\ comb}}{2} A_{W,\ comb.} (C_{F_{AV}})_{comb} = \frac{Pr^{\frac{2}{3}}\ \Delta H_{comb}\ V_{AV,\ comb}}{(h_{t,\ o} - h_{W,\ comb})} \tag{A47}$$

Substituting equation (47) into equation (44) and rearranging gives

$$V_3 = \frac{\left[W_1 V_2 + p_2 A_2 - p_3 A_3 - \frac{Pr^{\frac{2}{3}} \Delta H_{comb} V_{AV,\,comb}}{(h_{t,\,o} - h_{W,\,comb})} + \int_{"2"}^{"3"} p_W dA \right]}{\left[W_1 \left(1 + \frac{W_{fuel}}{W_1} \right) \right]} \tag{A48}$$

The one-dimensional energy equation as obtained through application of the control volume concept on the combustor is given by

$$h_{t,\,3} = \left[h_2 + \frac{V_2^2}{2} - \frac{\Delta H_{comb}}{W_1} + \frac{\Delta H_{fuel}}{W_1} + (h_t)_{fuel} \left(\frac{W_{fuel}}{W_1} \right) - (1 - \eta_{comb}) (h)_{fuel} \frac{W_{fuel}}{W_1} \right] \Bigg/ \left[1 + \frac{W_{fuel}}{} \right] \tag{A49}$$

The use of the combustion efficiency in the manner shown in equation (49) accounts for the reduction in heat release corresponding to the portion of the fuel not burned. The one-dimensional energy relation for the combustor exit (station 3) gives

$$h_3 = h_{t,\,3} - \frac{V_3^2}{2} \tag{A50}$$

The method of solution for the flow conditions at the combustor exit (station 3) consists of making a first guess for the pressure p_3 and temperature T_3, computing a first guess for the velocity V_3 from equation (48) and computing a first guess for the enthalpy h_3 from equations (49) and (50). Thermodynamic property data are then used to obtain first guess values for the remaining combustor exit conditions. The first guess for the combustor exit mass flow is then computed from

$$(W_3)_G = \rho_3 V_3 A_c \tag{A51}$$

and compared with the known combustor exit mass flow given by

$$W_3 = W_1 \left[1 + \frac{W_{fuel}}{W_1}\right] \tag{A52}$$

The combustor exit static pressure is then corrected by

$$p_3 = (p_3)_G \frac{W_3}{(W_3)_G} \tag{A53}$$

This iteration procedure is repeated until the ratio of the computed (or guessed) mass flow from equation (51) to the known mass flow of equation (52) differs from 1.0 by 0.0001.

Nozzle Flow

The change in flow properties from combustor exit (or nozzle entrance) station 3 to the nozzle exit station 4 is computed using a form of the one-dimensional momentum and energy equations assuming equilibrium chemistry. The form of these equations also accounts for nozzle flow friction and heat losses. The area ratio A_4/A_1 from the nozzle exit to the inlet entrance and the nozzle heat losses are specified.

For a well designed nozzle (no strong shock waves) the flow is essentially isentropic in nature and therefore the method of computation consists of first expanding the flow from the combustor exit (station 3) to the nozzle exit (station 4) isentropically corresponding to the area ratio given by

$$\frac{A_4}{A_3} = \frac{\frac{A_4}{A_1}}{\frac{A_3}{A_1}} \tag{A54}$$

The total enthalpy at station 4 is given by

$$h_{t,4} = h_{t,3} - \frac{\Delta H_{loss}}{W_3} \tag{A55}$$

The method of solution and the isentropic relations are as follows.

Isentropic Relations

$$F_{4,\,A} = \left(F_{4,\,A} - 1\right)^{E_3}\left[\left(\frac{2}{K_3 - 1}\right)^{E_3}\left(\frac{A_4}{A_3 M_3}\right)^{2E_3} F_3\right] \tag{A56}$$

$$F = 1 + \frac{K - 1}{2} M^2 \tag{A57}$$

$$E = \frac{K - 1}{K + 1} \tag{A58}$$

Guessed values of pressure and temperature are computed from

$$p_{4,\,A} = p_3 \left(\frac{F_3}{F_{4,\,A}}\right)^{\frac{K_3}{K_3 - 1}} \tag{A59}$$

$$T_{4,\,A} = T_3 \left(\frac{F_3}{F_{4,\,A}}\right) \tag{A60}$$

As was for the forebody flow computations, the thermodynamic property data are then used along with $(p_{4,\,A},\ T_{4,\,A} + \Delta T)$, and $(p_{4,\,A},\ T_{4,\,A})$ to obtain values of S_1^+ and S_1. The guessed value of the temperature is improved by

$$T_{4,\,A} = T_{4,\,A}\left[\frac{T_{4,\,A}}{T_{4,\,A} - \Delta T}\right]^{\frac{S_3 - S_{4,\,A}}{S_{4,\,A} - S^+_{4,\,A}}} \tag{A61}$$

where $S_{4,\,A}$ and $S^+_{4,\,A}$ are the entropies for the states corresponding to $(p_{4,\,A},\ T_{4,\,A})$ and $(p_{4,\,A},\ + \Delta T)$, respectively. When successive values of $T_{4,\,A}$ differ by less than 1° the area ratio A_4/A_3 is computed from the relation

$$\frac{A_4}{A_3} = \frac{\rho_3 V_3}{\rho_{4,A}\left[2\left(h_{t,4} - h_{4,A}\right)\right]^{\frac{1}{2}}} \tag{A62}$$

and compared with the value computed by equation (54). If the value of A_4/A_3 computed by equation (62) is not within 0.00001 of the value computed by equation (54), the new flow values corresponding to the subscript (4, A) are input into equation (56) for the station 3 parameters and the iteration beginning with equation (56) is repeated.

The momentum relationship assumed for the one-dimensional nozzle flow is given by

$$V_4 = V_{4,A} - \frac{Pr^{\frac{2}{3}}\ \Delta H_N\ V_{AV,N}}{(h_{t,o} - h_{W,N})W_3} \tag{A63}$$

and the one-dimensional energy equation assumed is given by

$$h_4 = h_3 + \frac{V_3^2}{2} - \frac{V_4^2}{2} - \frac{\Delta H_N}{W_3} \tag{A64}$$

The first guess of the nozzle exit static pressure and temperature is made using the relations of adiabatic flow of a perfect gas in a constant area channel with friction. The Mach number is computed by iterating for the Mach number M_4 using the relation

$$M_4 = \frac{V_4}{V_{4,A}} M_{4,A}\left(\frac{F_4}{F_{4,A}}\right)^{\frac{1}{2}} \tag{A65}$$

where,

$$F = 1 + \frac{K-1}{2} M^2 \tag{A66}$$

and K_4 is assumed equal to $K_{4,A}$. The value of $M_{4,A}$ is used as the first guess for M_4 (in F_4 on right-hand side of equation (65)) and the iteration is

repeated until successive values of M_4 differ by less than 0.001. When this tolerance is satisfied the first guess static pressure and temperature are computed using

$$p_4 = p_{4,\,A} \frac{M_{4,\,A}}{M_4} \left(\frac{F_{4,\,A}}{F_4} \right)^{\frac{1}{2}} \tag{A67}$$

$$T_4 = T_{4,\,A} \left(\frac{F_4}{F_{4,\,A}} \right) \tag{A68}$$

With a guess for p_4 (equation (67)) and the value for h_4 computed by equation (64), an iteration on the temperature is performed using as a first guess the value of T_4 computed by equation (68). Succeeding guesses for T_4 are computed from

$$T_4 = (T_4 - \Delta T) + 2\Delta T \left(\frac{h_4 - h^-}{h^+ - h^-} \right) \tag{A69}$$

Thermodynamic property data of references 12 and 13 are used to find the values of h^- for $(T_4 - \Delta T)$ and h^+ for $(T_4 + \Delta T)$, respectively, and the iteration is repeated until succeeding guesses for T_4 differ by less than 1°. The area A_4 is computed from the relation

$$A_4 = \frac{W_3}{\rho_4 V_4} \tag{A70}$$

The area A_4 as computed by equation (70) is compared with the value of A_4 as computed from

$$A_4 = \frac{A_4}{A_1} A_1 \tag{A71}$$

If the nozzle exit area computed by equation (70) is not within 0.01 percent of the value computed by equation (71) a new guess for the value of p_4 is made using

$$p_4 = \frac{p_4}{\rho_4 V_4} \left[\frac{W_3}{\left(\frac{A_4}{A_1}\right) A_1} \right] \qquad \text{(A72)}$$

The iteration is then repeated beginning with equation (69) until the two values of the nozzle exit area A_4 agree within 0.01 percent.

REFERENCES

1. Johnston, P. J.; Cubbage, J. M.; Weidner, J. P.: Studies of Engine-Airframe Integration on Hypersonic Aircraft. AIAA Atmospheric Flight Mechanics Conference, Tullahoma, Tennessee, May 13-15, 1970.

2. Williams, L. J.; Wilcox, D. E.: Scramjet Vehicle Engine-Airframe Integration Effects. Conference on Hypersonic Aircraft Technology, NASA SP-148, 1967.

3. Gregory, T. J.; Wilcox, D. E.; Williams, L. J.: The Effects of Propulsion System-Airframe Interactions on the Performance of Hypersonic Aircraft. AIAA Paper No. 67-493, 1967.

4. Trexler, Carl A.; Souders, Sue W.: Design and Performance at a Local Mach Number of 6 of an Inlet for an Integrated Scramjet Concept. NASA TN D-7944, August 1975.

5. Mueller, James N.; Trexler, Carl A.; Souders, Sue W.: Wind Tunnel Tests on a 3-Dimensional Fixed-Geometry Scramjet Inlet at M = 2.30 to 4.60. NASA TM X-73933, March 1977.

6. Trexler, Carl A.: Inlet Performance of the Integrated Langley Scramjet Module (M = 2.3 to 7.6). AIAA/SAE 11th Propulsion Conference, Anaheim, California, September 29 - October 1, 1975.

7. Henry, John R.; Anderson, Griffin Y.: Design Considerations for the Airframe-Integrated Scramjet. NASA TM X-2895, 1973.

8. Becker, John V.: New Approaches to Hypersonic Aircraft. Seventh Congress of International Council of the Aeronautical Sciences ICAS: Rome, Italy, September 14-18, 1970.

9. Craig, R. R.; Ortwerth, P. J.: An IBM 7090 Program for Calculating the Theoretical Performance of a Supersonic-Combustion Engine. ASRMPR Technical Memorandum 62-16, April 1962.

10. Groffman, L.; Lieberman, E.: Engine Performance Program with Equilibrium Chemistry. GASL Technical Report 567, November 1965.

11. Jackson, Robert J.; Wang, Tennyson T.: Computer Program Description Ramjet and Scramjet Cycle Performance. AiResearch Manufacturing Company Report Number AP-1001-1, September 1966.

12. Browne, W. G.; Warlick, D. L.: Properties of Combustion Gases System; H_2-Air. General Electric Company, R62FPD-366, September 1964.

13. Huff, Vearl N.; Gordon, Sanford; Morell, Virginia E.: General Method and Thermodynamic Tables for Computation of Equilibrium Composition and Temperature of Chemical Reactions. NACA Report 1037, 1951.

14. Edwards, C. L. W.: A Forebody Design Technique for Highly Integrated Bottom-Mounted Scramjets with Application to a Hypersonic Research Airplane. NASA TN D-8369, December 1976.

15. Moretti, G.: Thoughts and Afterthoughts About Shock Computations. Polytechnic Institute of New York, PIBAL Report No. 72-37, Dec. 1972.

16. Salas, Manuel D.: The Anatomy of Floating Shock Fitting. AIAA Second Computational Fluid Dynamics Conference, Hartford, Connecticut, June 19-20, 1975.

17. Pinckney, S. Z.: Turbulent Heat-Transfer Prediction Method for Application to Scramjet Engines. NASA TN D-7810, November, 1974.

18. Boatright, W. B.; Sabol, A. P.; Sebacher, D. I.; Pinckney, S. Z.; Guy, R. W.: Langley Facility for Tests at Mach 7 Subscale, Hydrogen-Burning Airframe-Integrated, Scramjet Models. AIAA Paper No. 76-11, AIAA 14 Aerospace Science Meeting, Washington, D. C., Jan. 26-28, 1976.

19. Anderson, Griffin Y.: An Examination of Injector/Combustor Design Effects on Scramjet Performance. 2nd International Symposium on Air Breathing Engines, Sheffield, England, March 25-29, 1974.

20. U. S. Standard Atmosphere, 1962; Prepared under the sponsorship of National Aeronautics and Space Administration, United States Air Force, and the United States Weather Bureau.

TABLE I

Parameters Needed for Engine Performance Computations

Free Stream

1. Altitude (meters)
2. Free-stream Mach number, M_o
3. $(h_{t,\,o} - h_w)$ (Joules/Kg)
4. Guessed capture mass flow (Kg/sec)
5. Spillage flow parameter $\frac{A_c - A_1}{A_c}$

Forebody Flow

1. Pressure ratio across forebody shock, p_1/p_o
2. Inviscid forebody flow Mach number, $M_{1,\,Inv.}$
3. Kinetic energy efficiency across forebody shock, $(\eta_K)_f$
4. Loss of heat by capture flow to forebody, $(\Delta H)_f$ (Joules/sec)
5. Cowl area
6. Forebody angle to flight direction, ω (deg)

Inlet Flow

1. Inlet contraction ratio, A_1/A_2
2. Kinetic energy efficiency across inlet shocks, $(\eta_K)_I$
3. Loss of heat by capture flow to inlet surfaces, $(\Delta H)_I$ (Joules/sec)

Combustor Flow

1. Fuel Equivalence ratio, ϕ
2. Combustion efficiency, $(\eta)_{comb}$
3. Combustor exit area to combustor entrance area, A_3/A_2 $(A_3/A_c = 0.64)$
4. Combustor wall pressure integral parameter, B_p
5. Loss of heat by capture flow to combustor surfaces, $(\Delta H)_{comb}$ (Joules/sec)
6. Heat added to the combustor per kilogram of fuel, $(h_t)_{fuel}$ (Joules/Kg)
7. Heat added to fuel due to regenerative cooling of engine, $(\Delta H)_{fuel}$ (Joules/sec)

TABLE I.- Continued

Nozzle Flow

1. Equilibrium flow is assumed
2. Area ratio across nozzle, A_4/A_3
3. Nozzle kinetic energy efficiency, $(\eta_K)_N$
4. Loss of heat by capture flow to nozzle surfaces, $(\Delta H)_N$ (Joules/sec)
5. Nozzle exit flow angle with forebody surface, β (deg)

Stream Tube Force Parameters

1. Pressure force on the capture flow stream tube over the spillage area and normal to forebody surface, A_I (N)
2. Pressure force on the lower surface of the plume normal to forebody surface, A_p (N)
3. Inlet additive drag, D_A (N)
4. Nozzle plume drag, D_E (N)

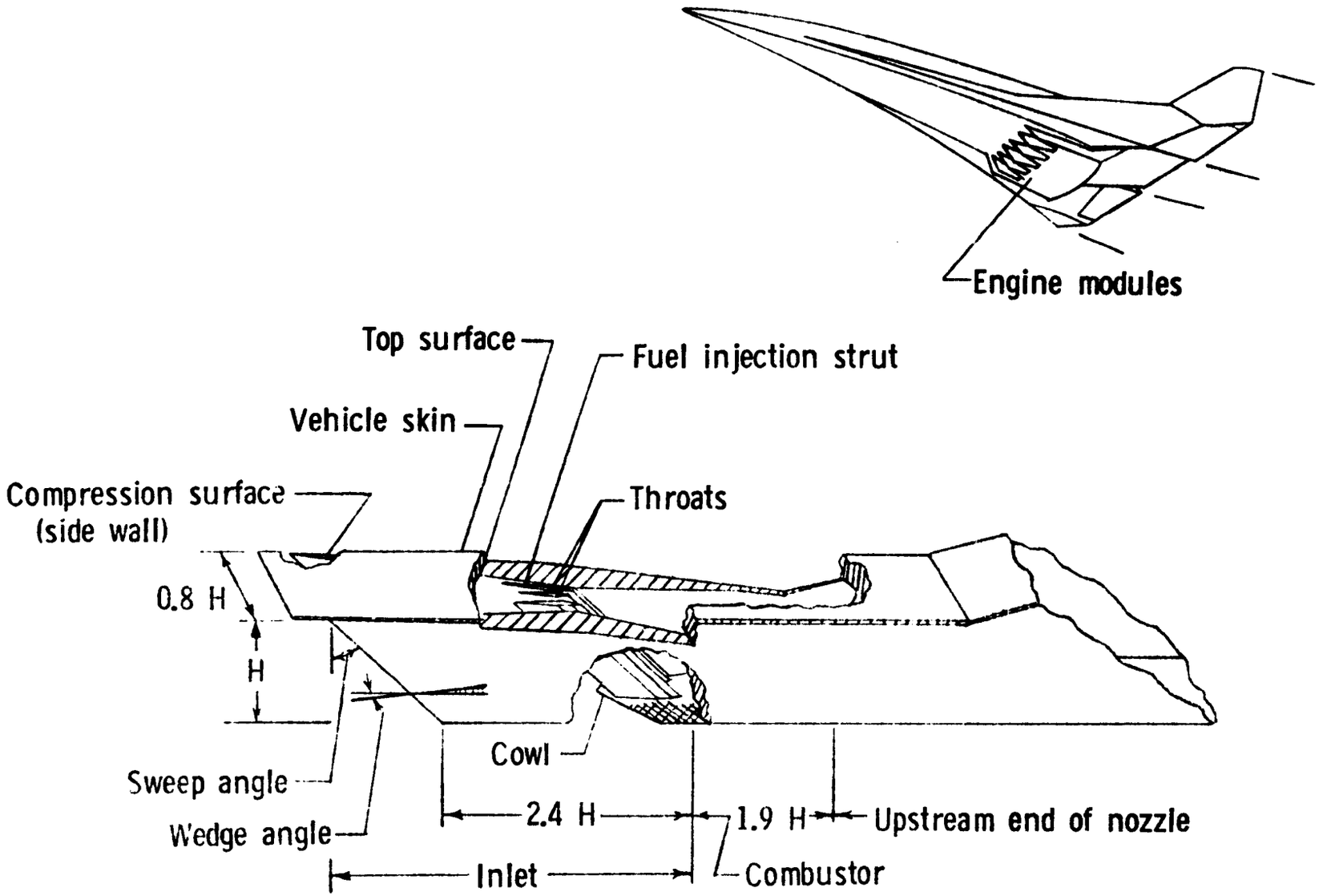

Figure 1.- Inner module of scramjet engine concept; H = 0.46 meters and sweep angle equals 48 degrees in the present engine.

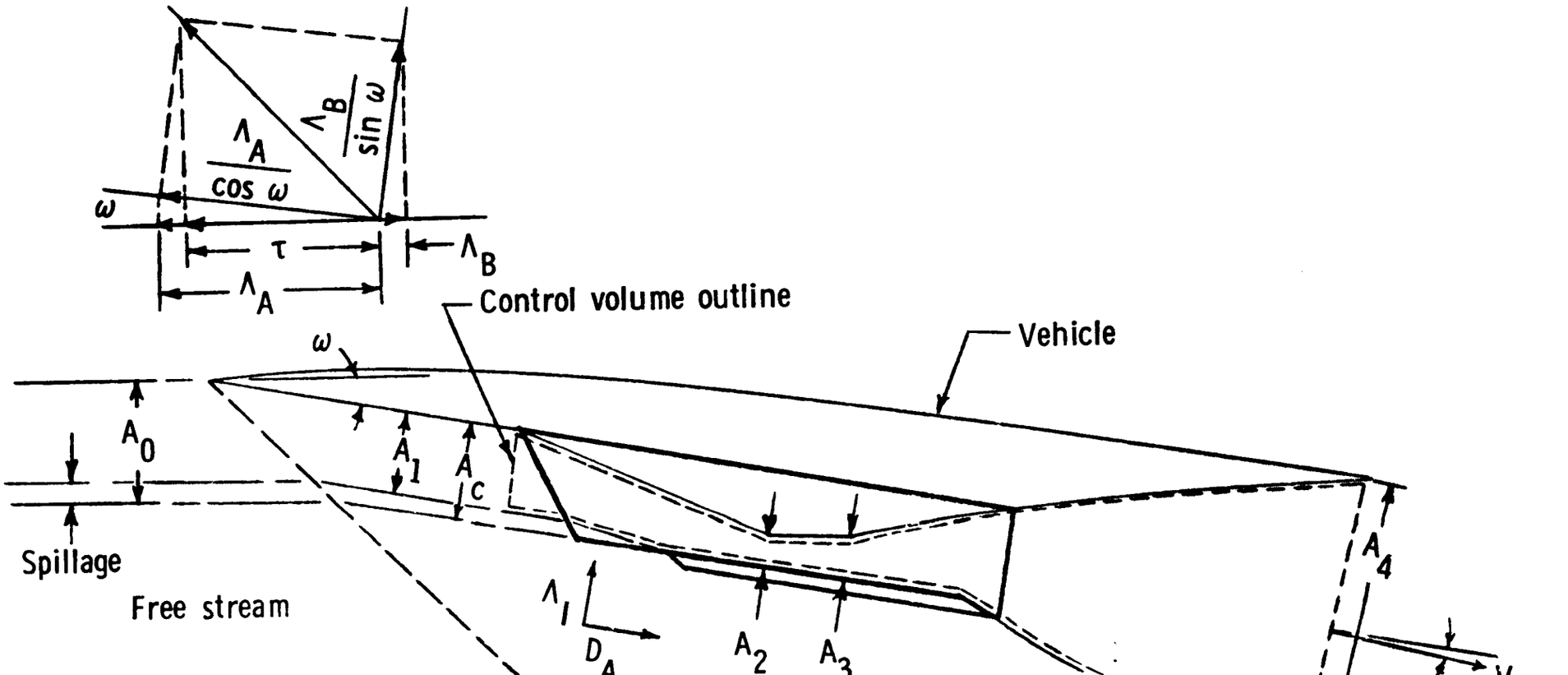

Figure 2.- One-dimensional flow model, control volume, and vectoral relationship between engine forces Λ_A and Λ_B.

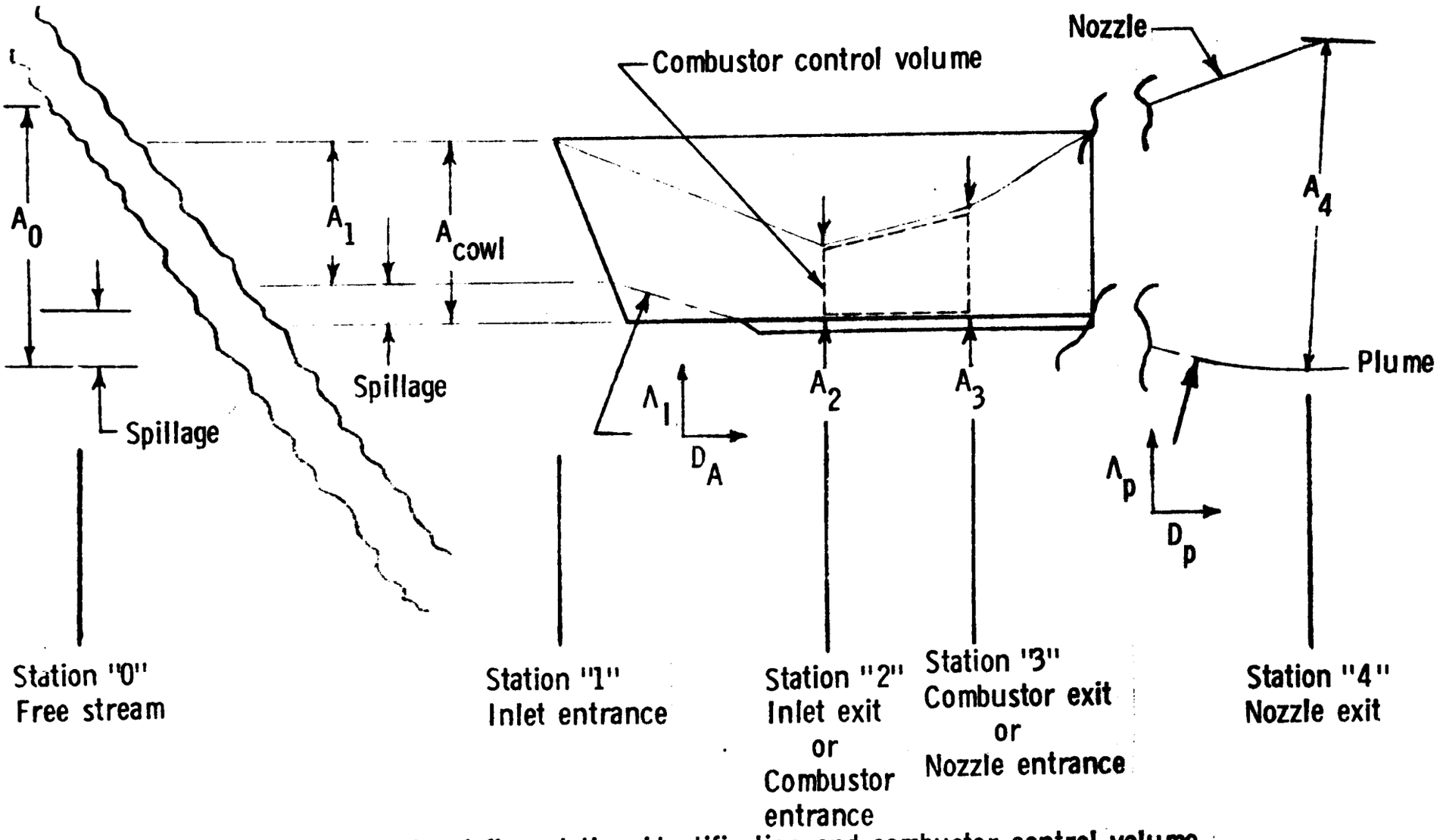

Figure 3.- One-dimensional flow station identification and combustor control volume.

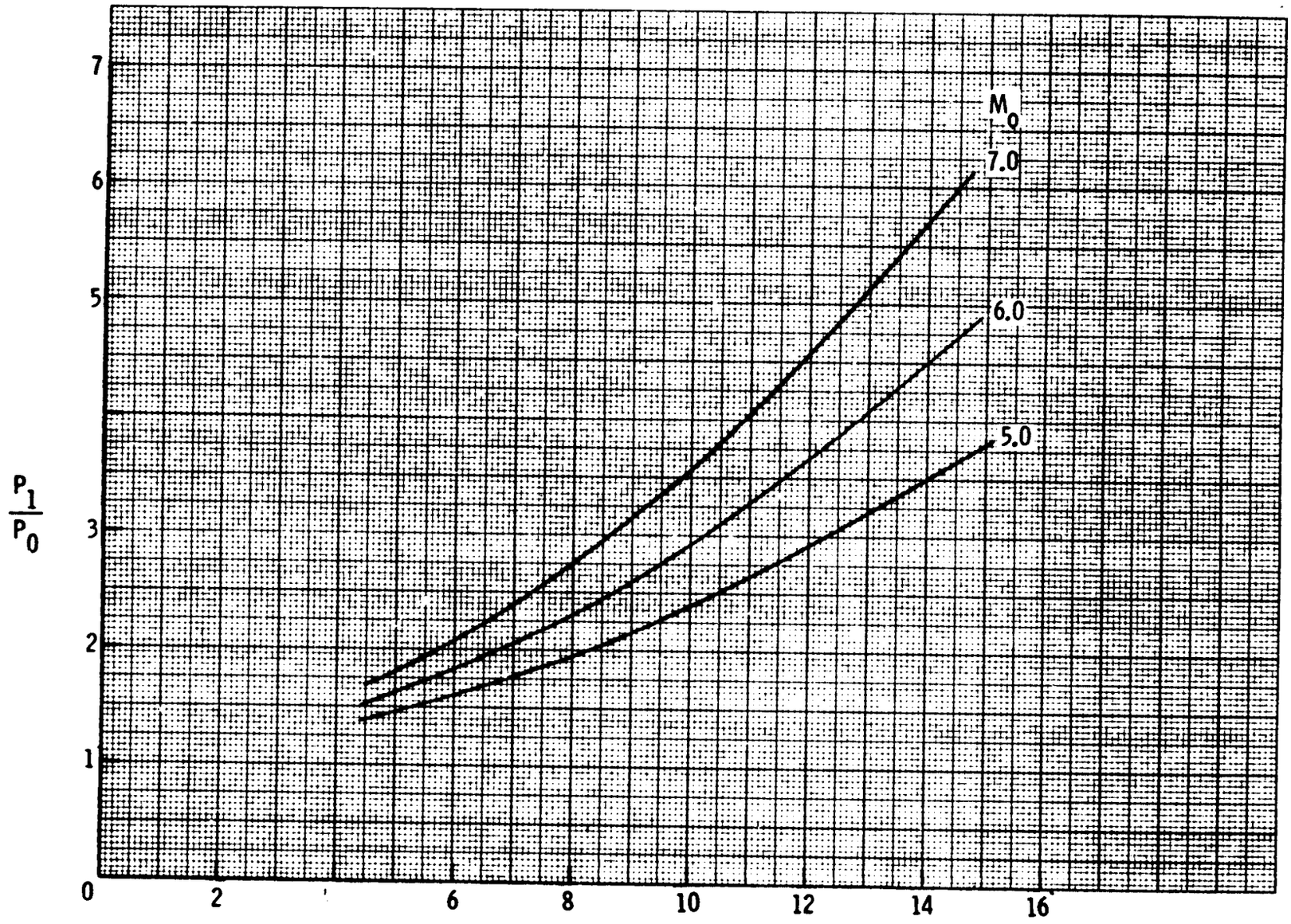

(a) Pressure ratio across vehicle forebody shock.

Figure 4.- Nonviscous forebody flow.

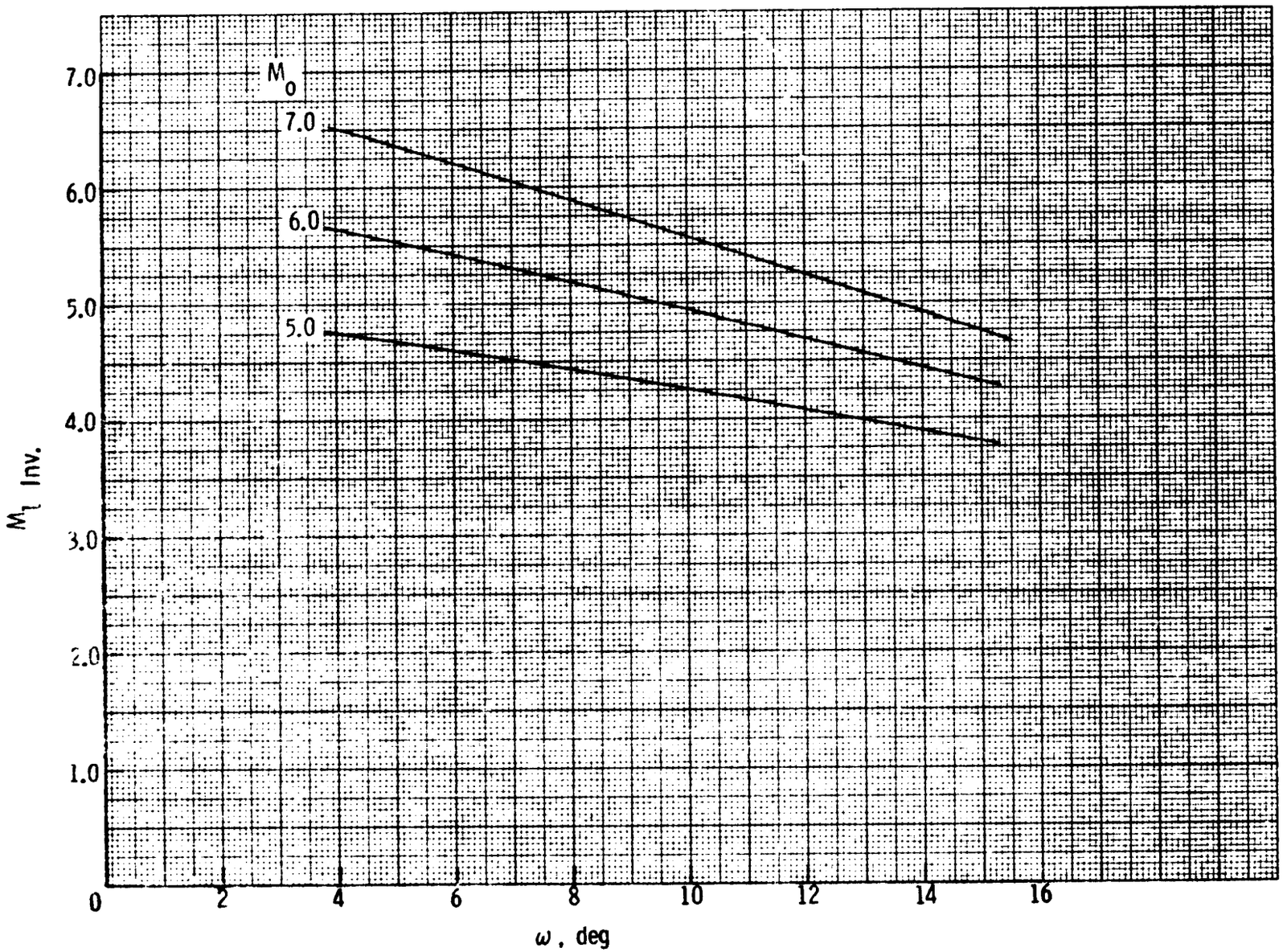

(b) Inviscid forebody Mach number.

Figure 4.- Continued.

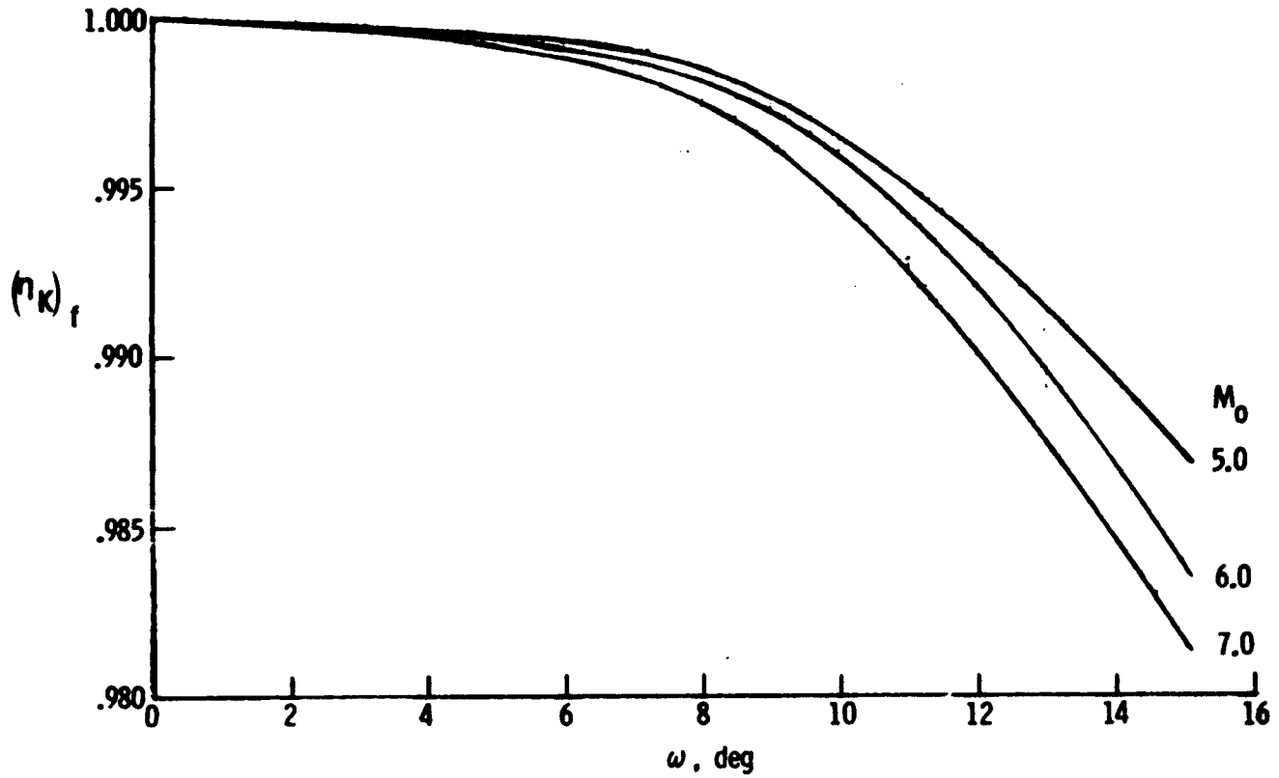

(c) Invisid kinetic energy efficiency across the vehicle forebody shock.

Figure 4.- Concluded.

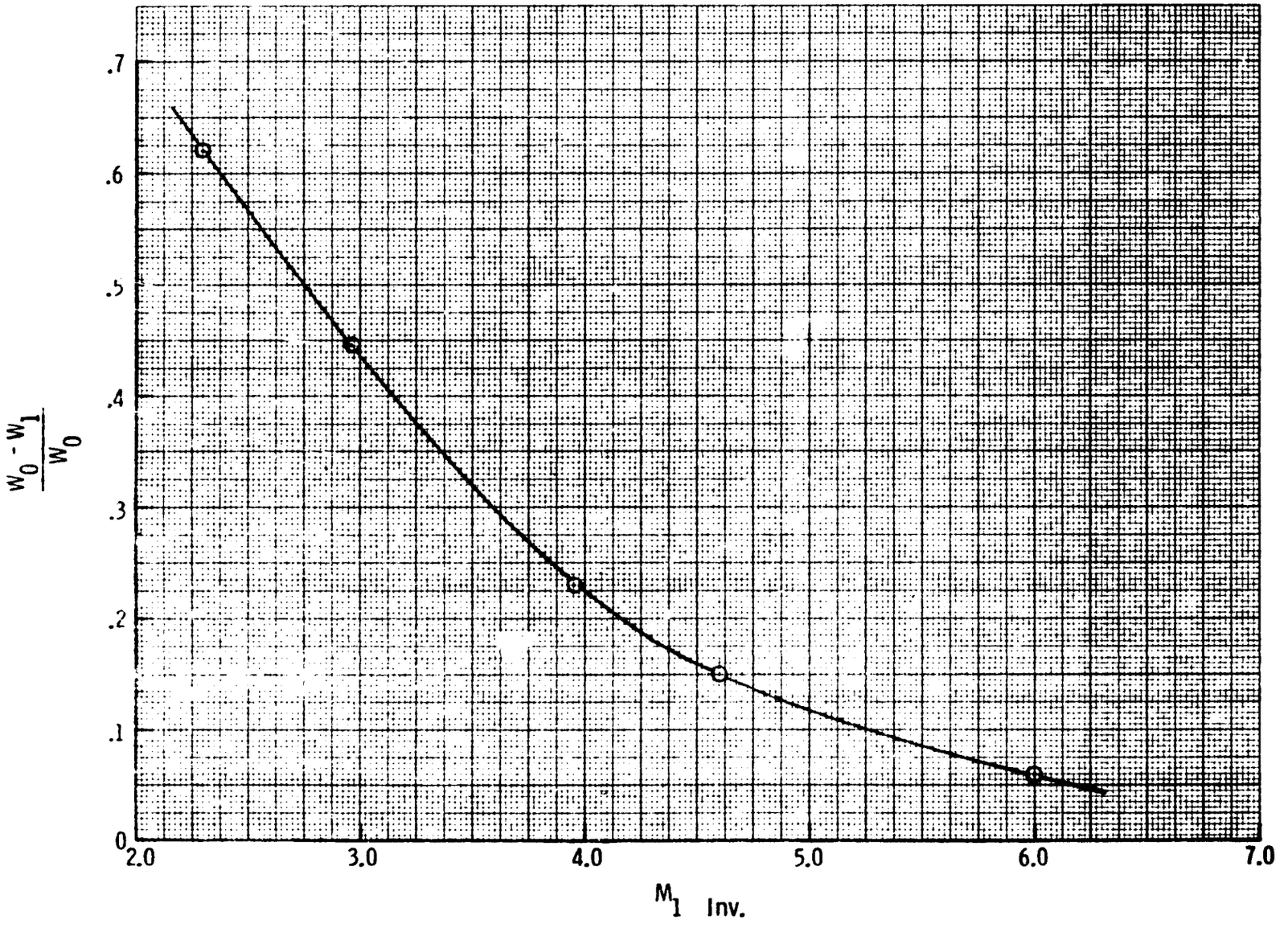

(a) Inlet mass flow spillage (experimental).

Figure 5.- Engine mass flow.

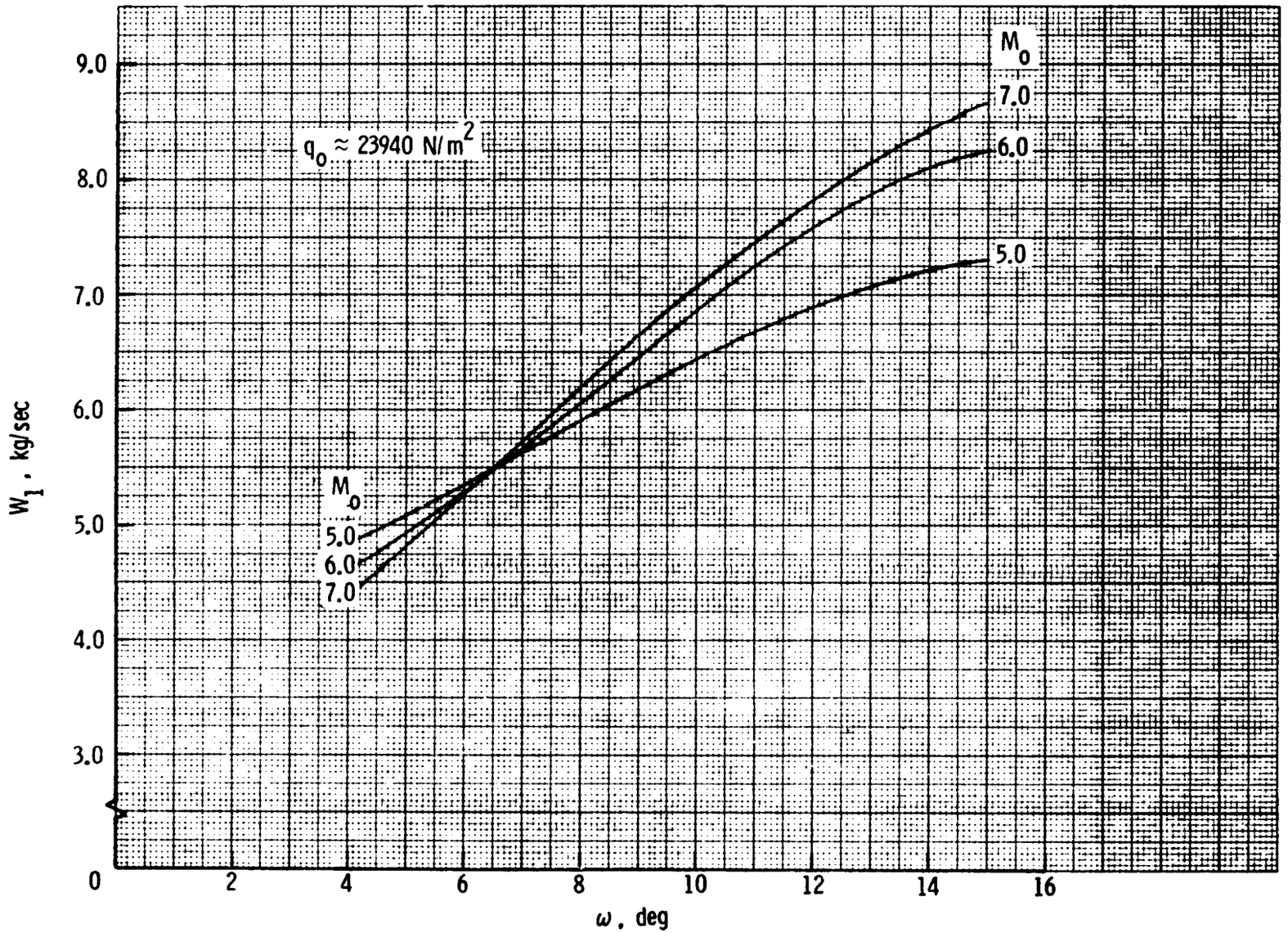

(b) Engine module capture flow.

Figure 5.- Concluded.

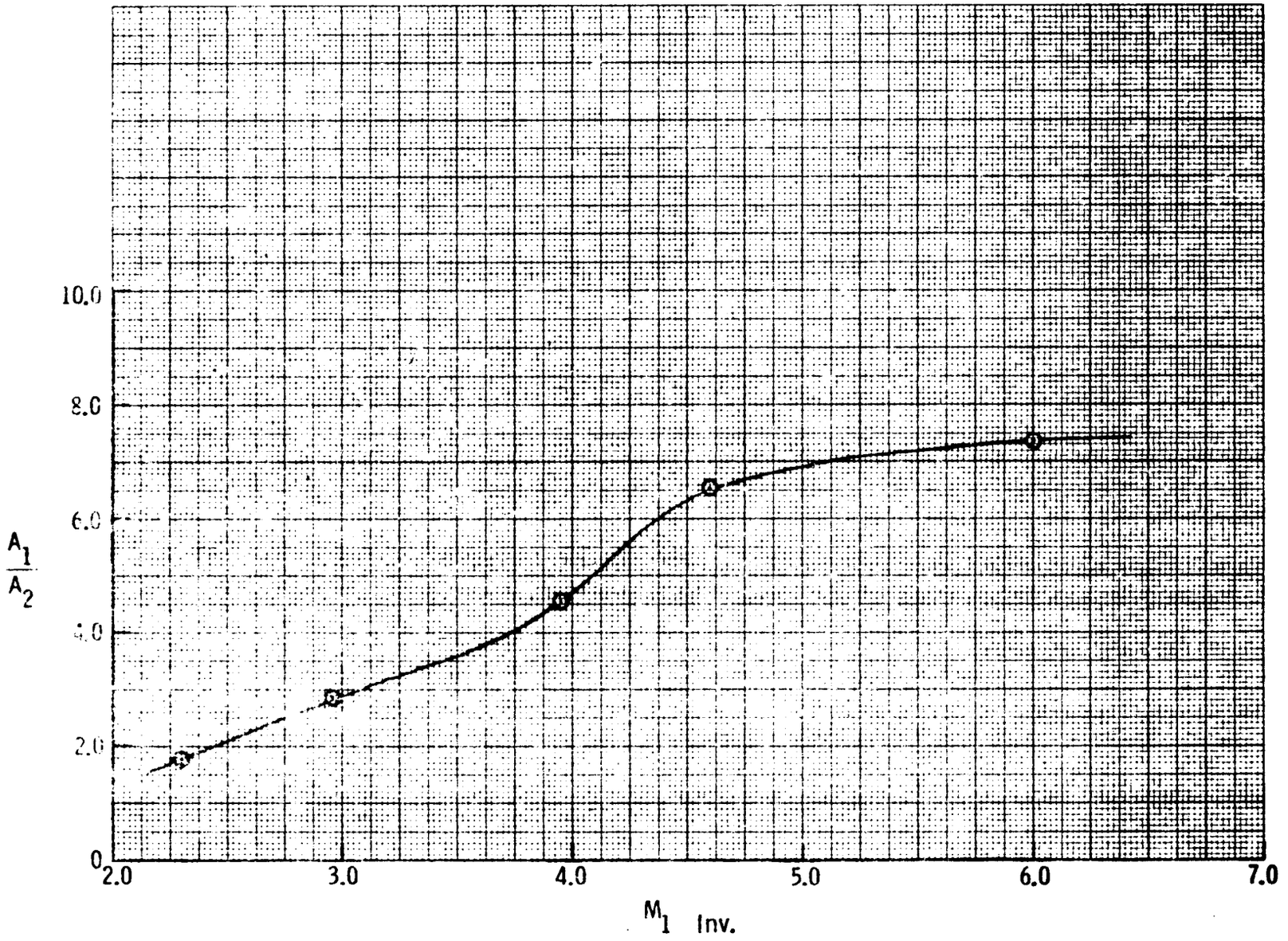

Figure 6.- Inlet aerodynamic contraction ratio (experimental).

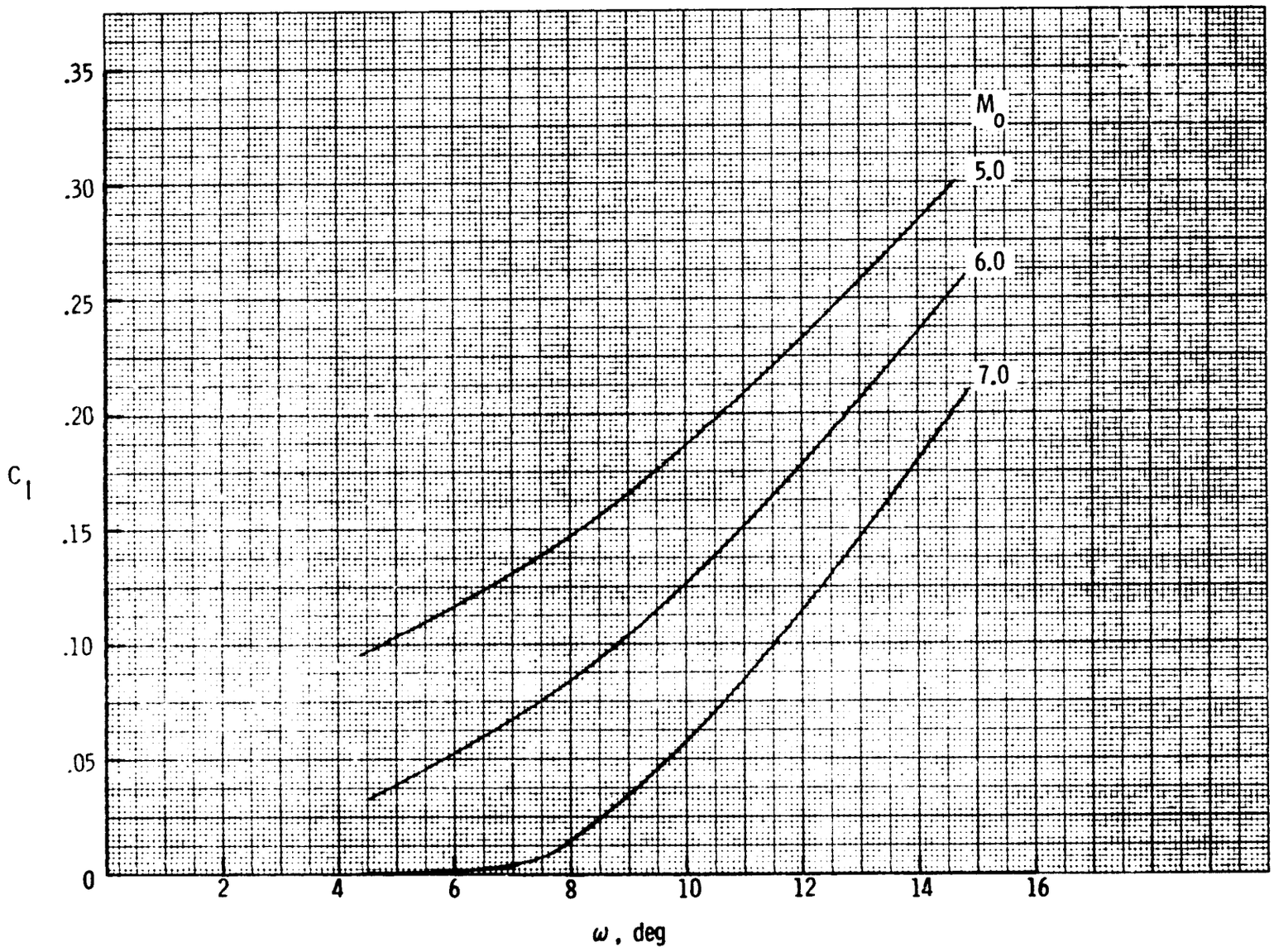

Figure 7.- Additive drag coefficient.

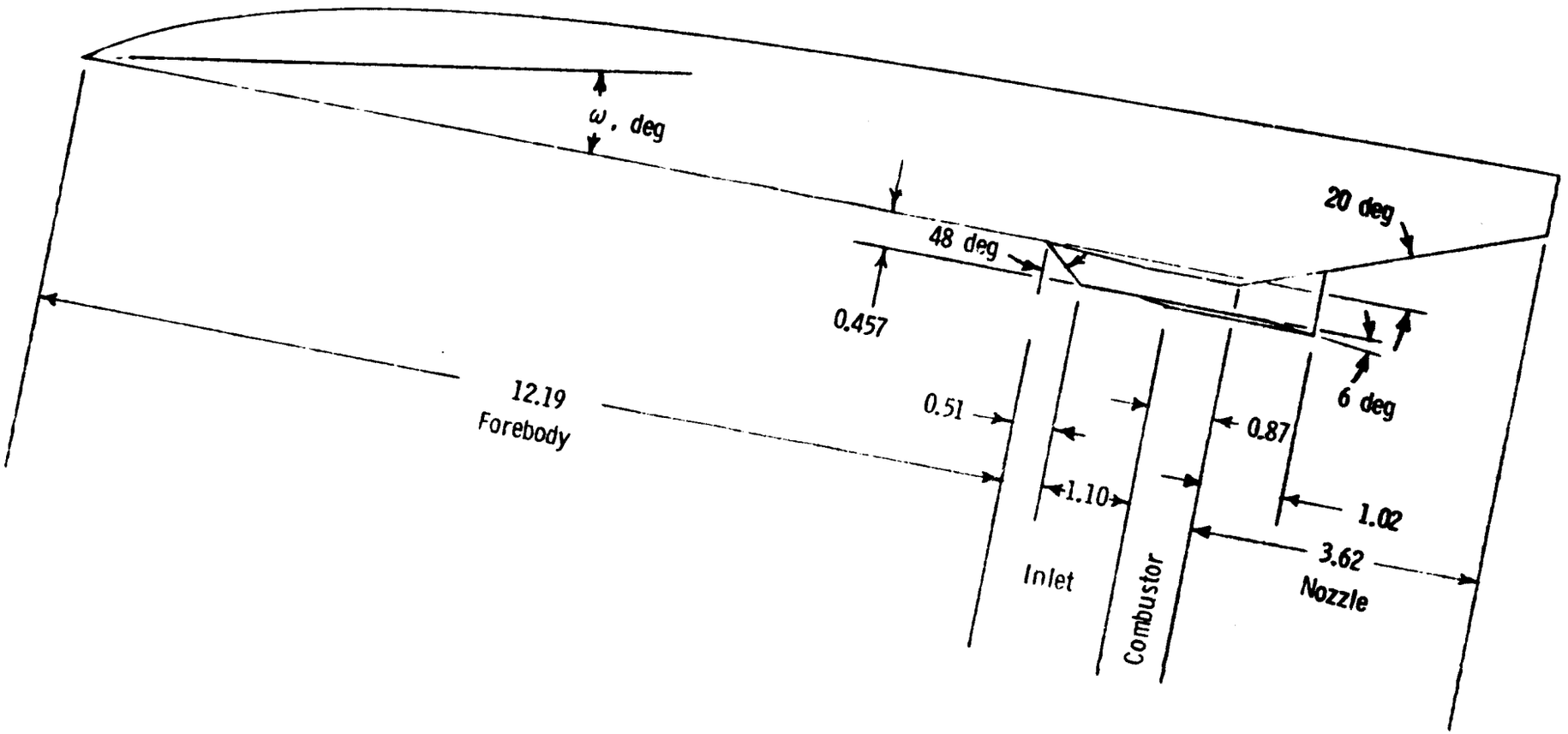

Figure 8.- Relationship of present engine with vehicle assumed (for engine performance computations) including nozzle-vehicle afterbody relationship (dimensions in meters). Cowl external surface is inclined 3^0 to forebody surface.

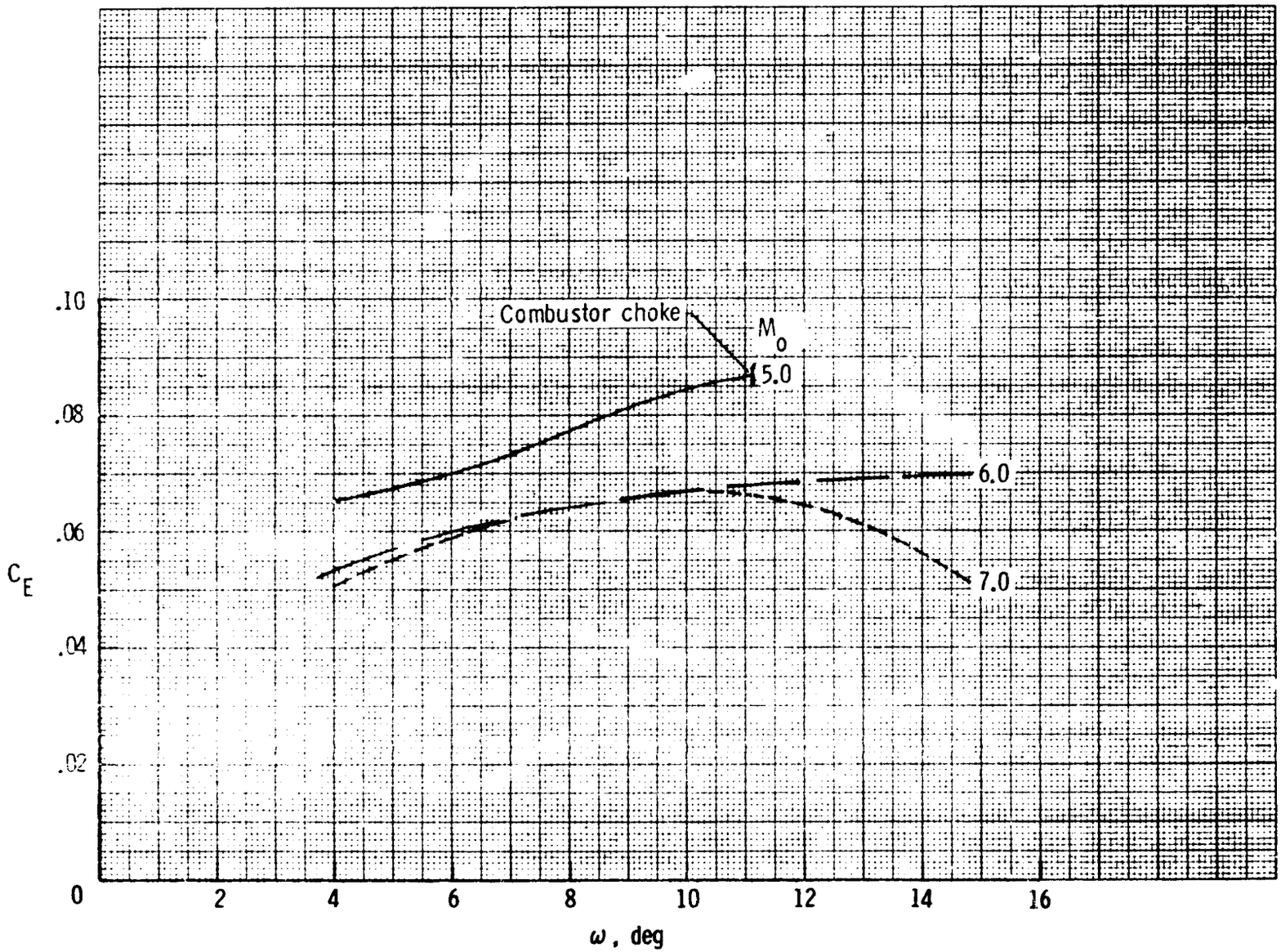

Figure 9.- Plume drag coefficient.

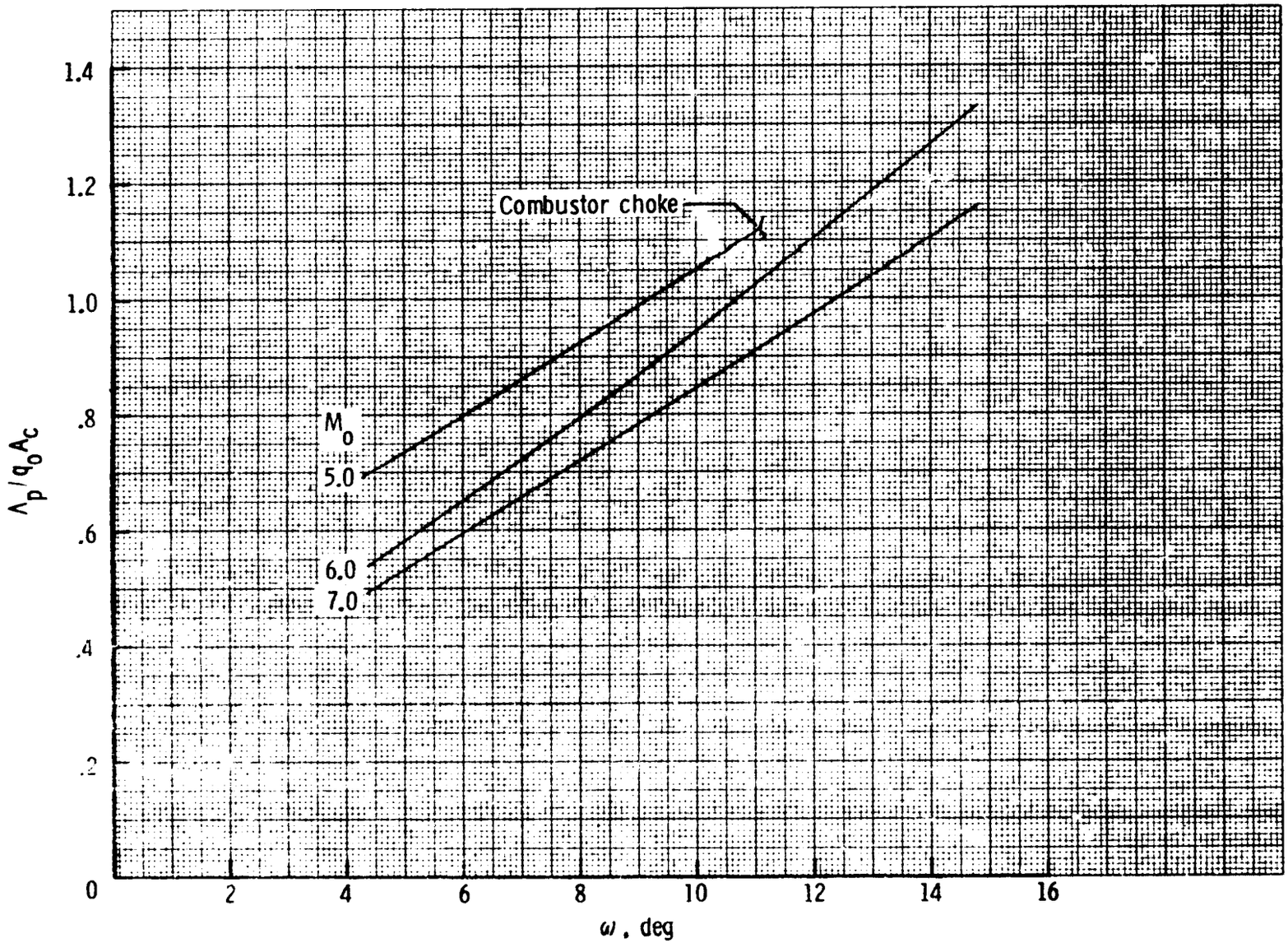

Figure 10.- Plume force coefficient normal to forebody surface.

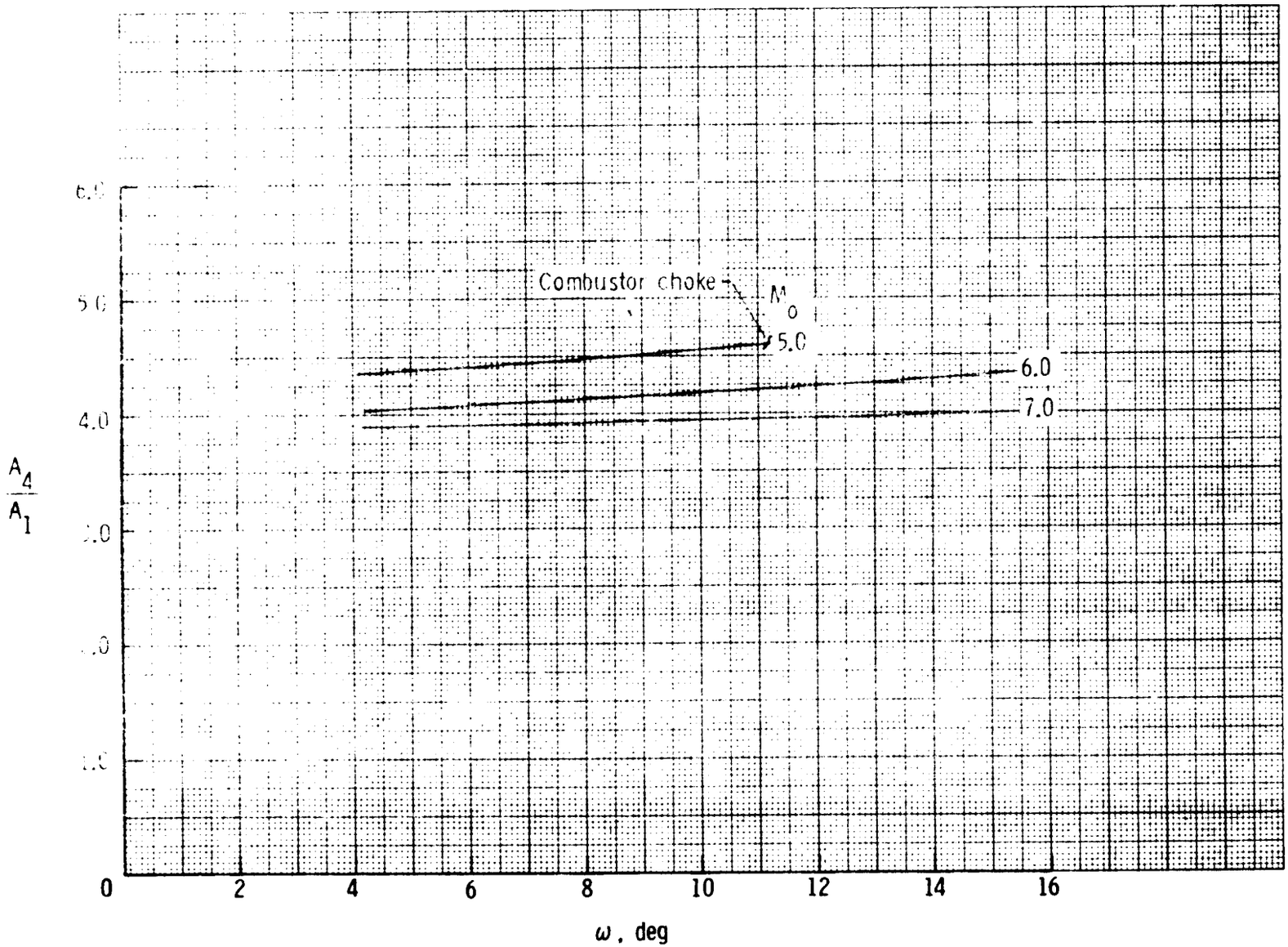

(a) In terms of area A_1.

Figure 11.- Nozzle exit area.

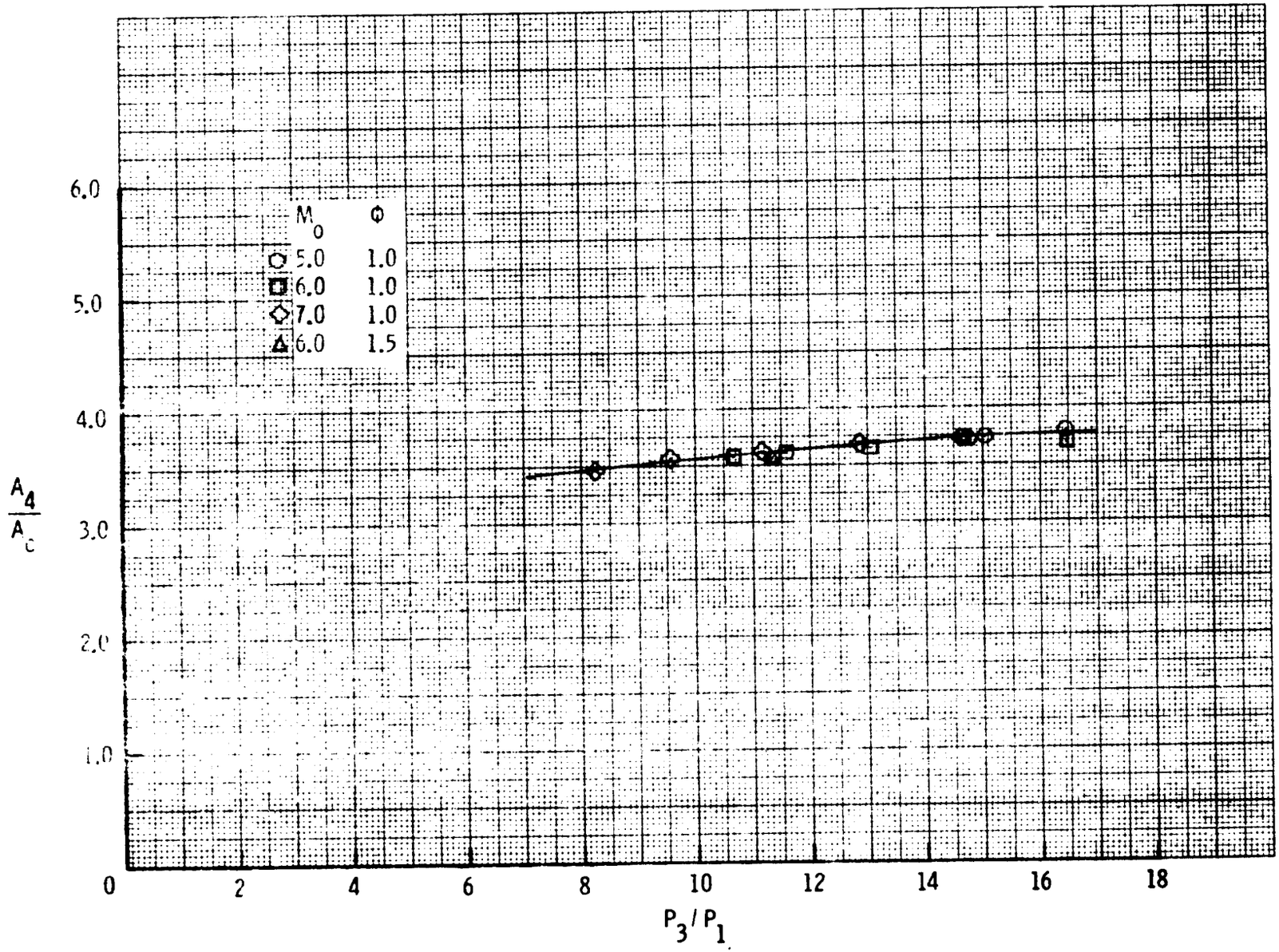

(b) In terms of cowl area, A_c.

Figure 11.- Concluded.

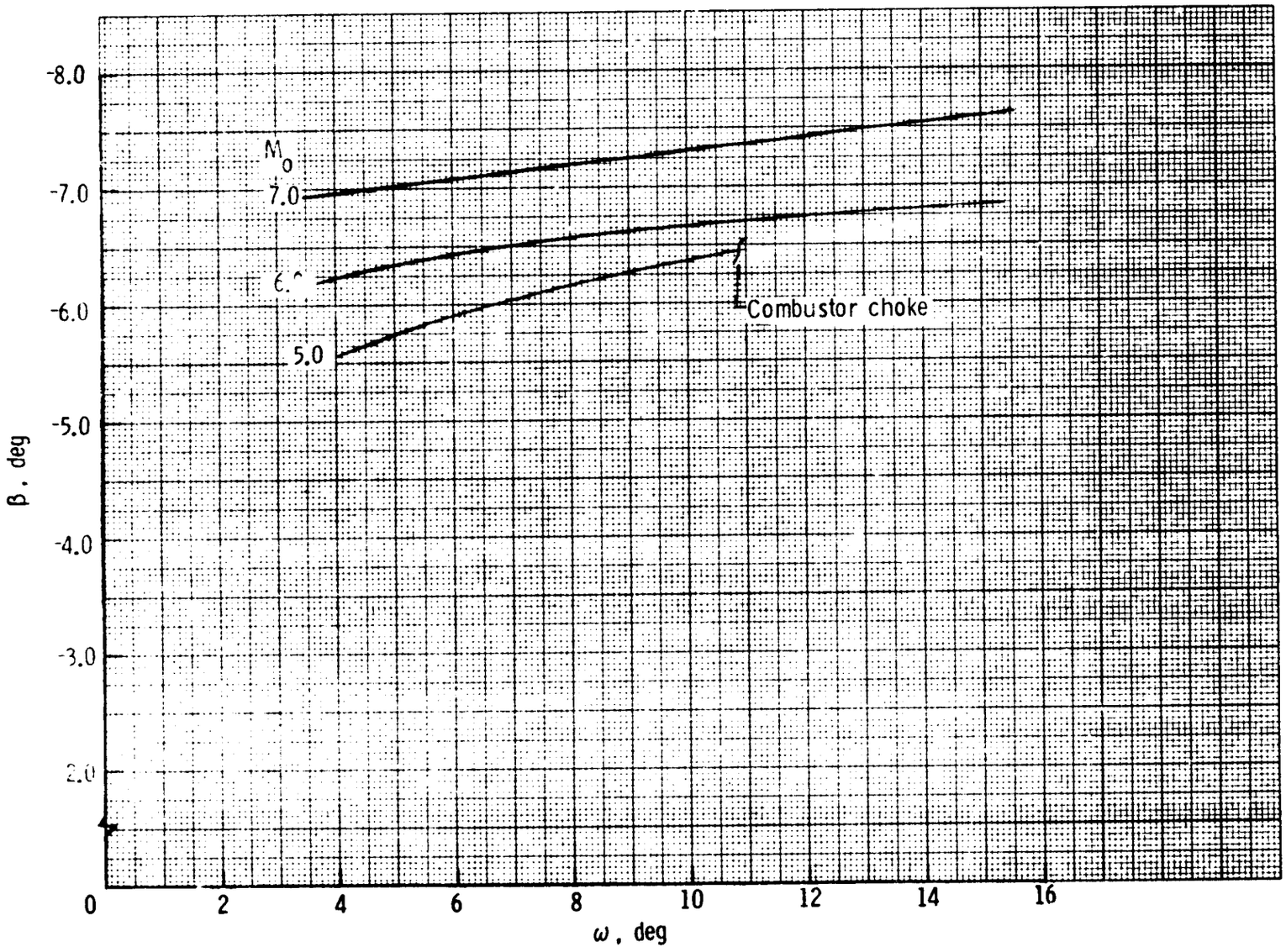

Figure 12.- Mass weighted average nozzle exit flow angle β relative to the forebody surface.

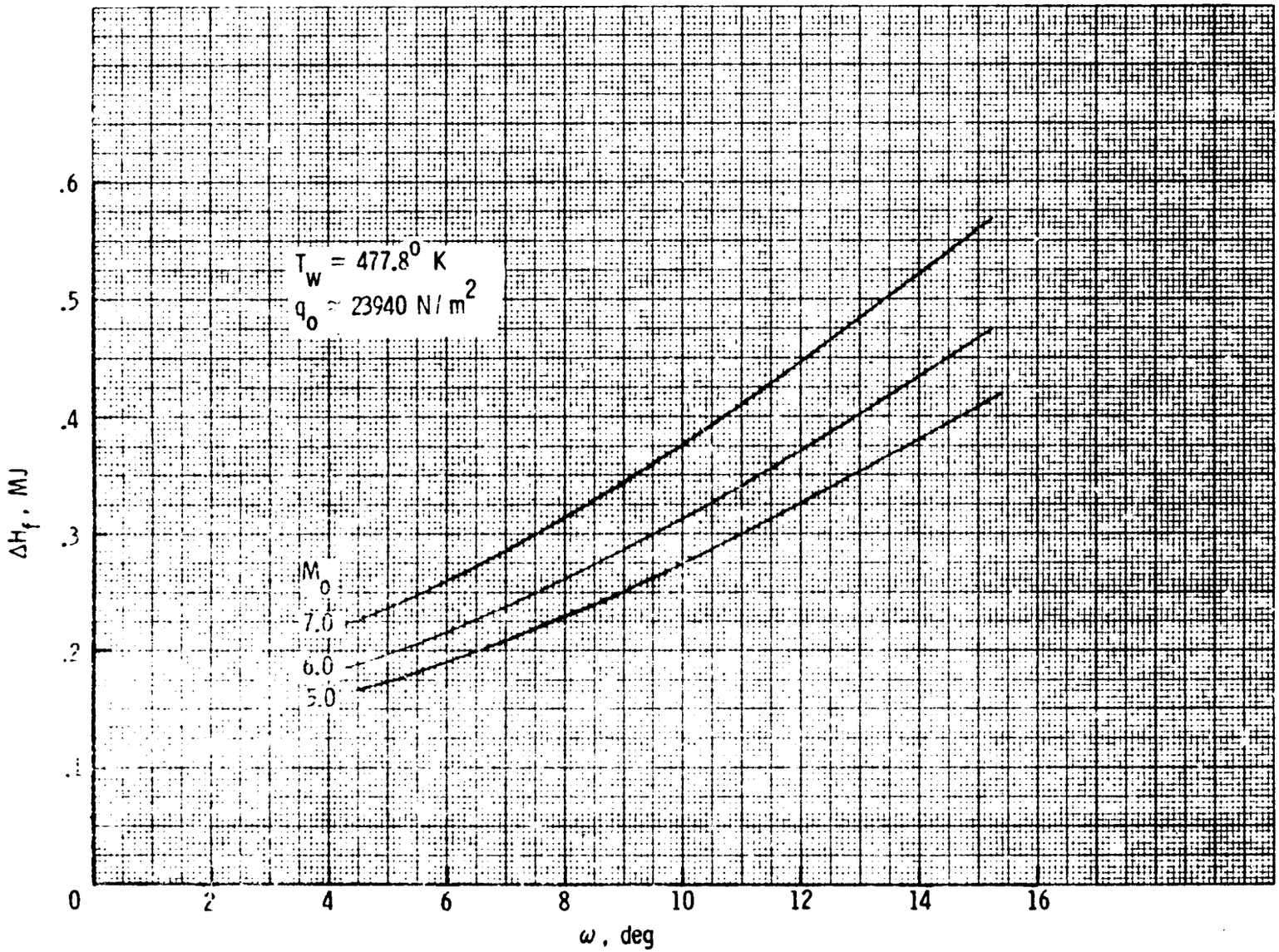

Figure 13.- Capture flow heat loss to vehicle forebody.

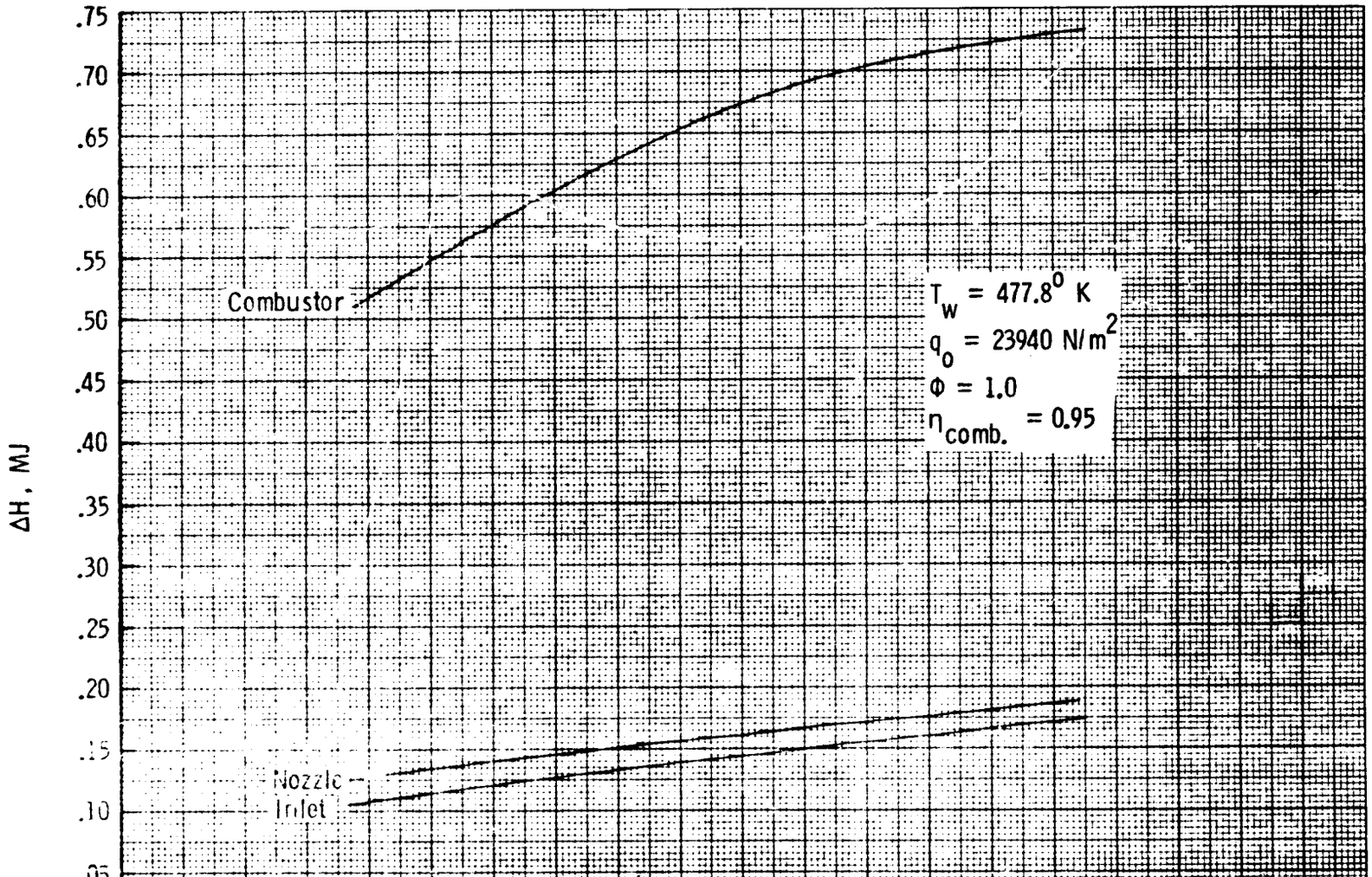

Figure 14.- Capture flow heat losses for M_0 = 6.0.

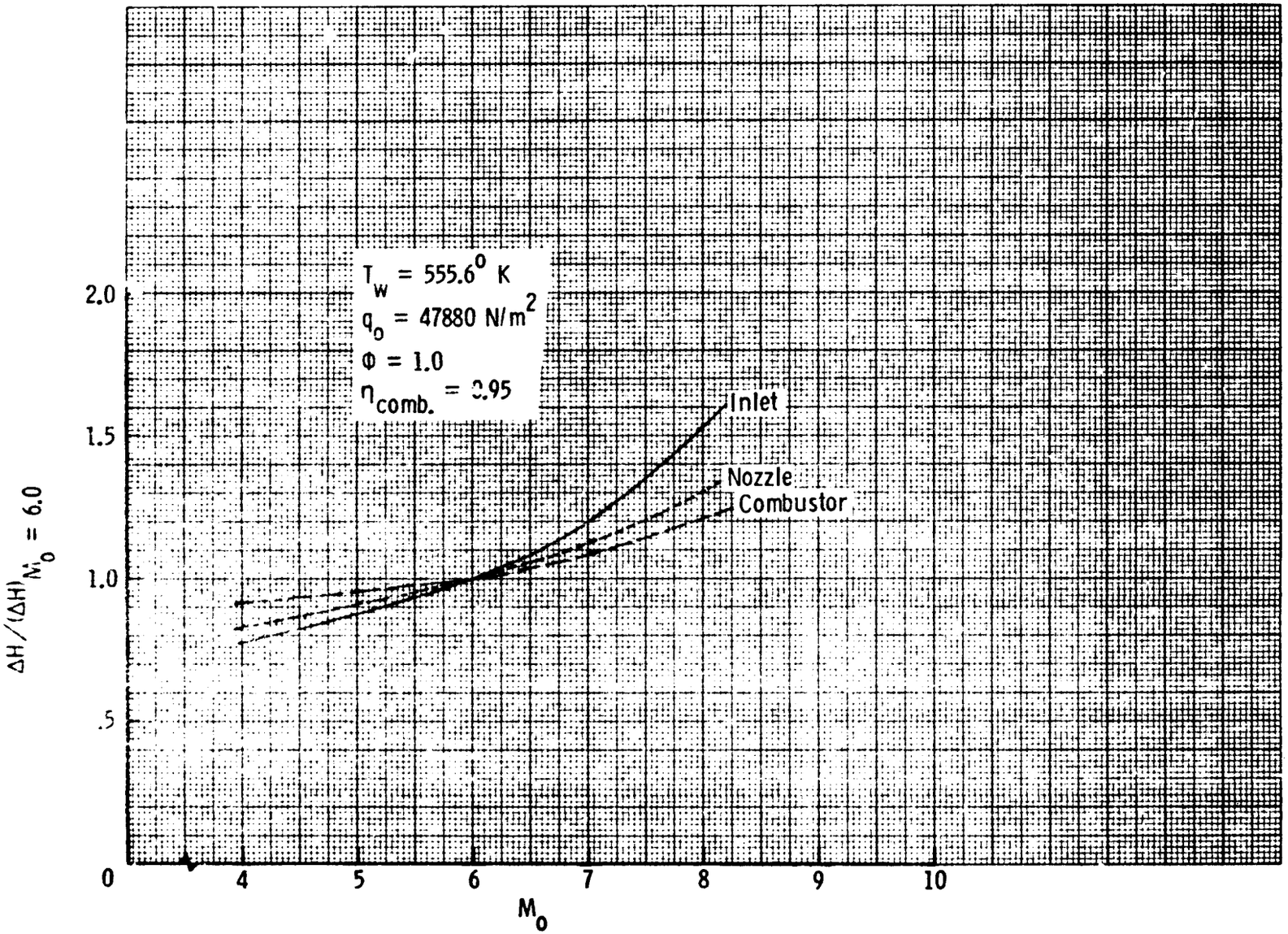

Figure 15.- Heat transfer ratioed to heat transfer for $M_0 = 6.0$ as inferred from reference 5.

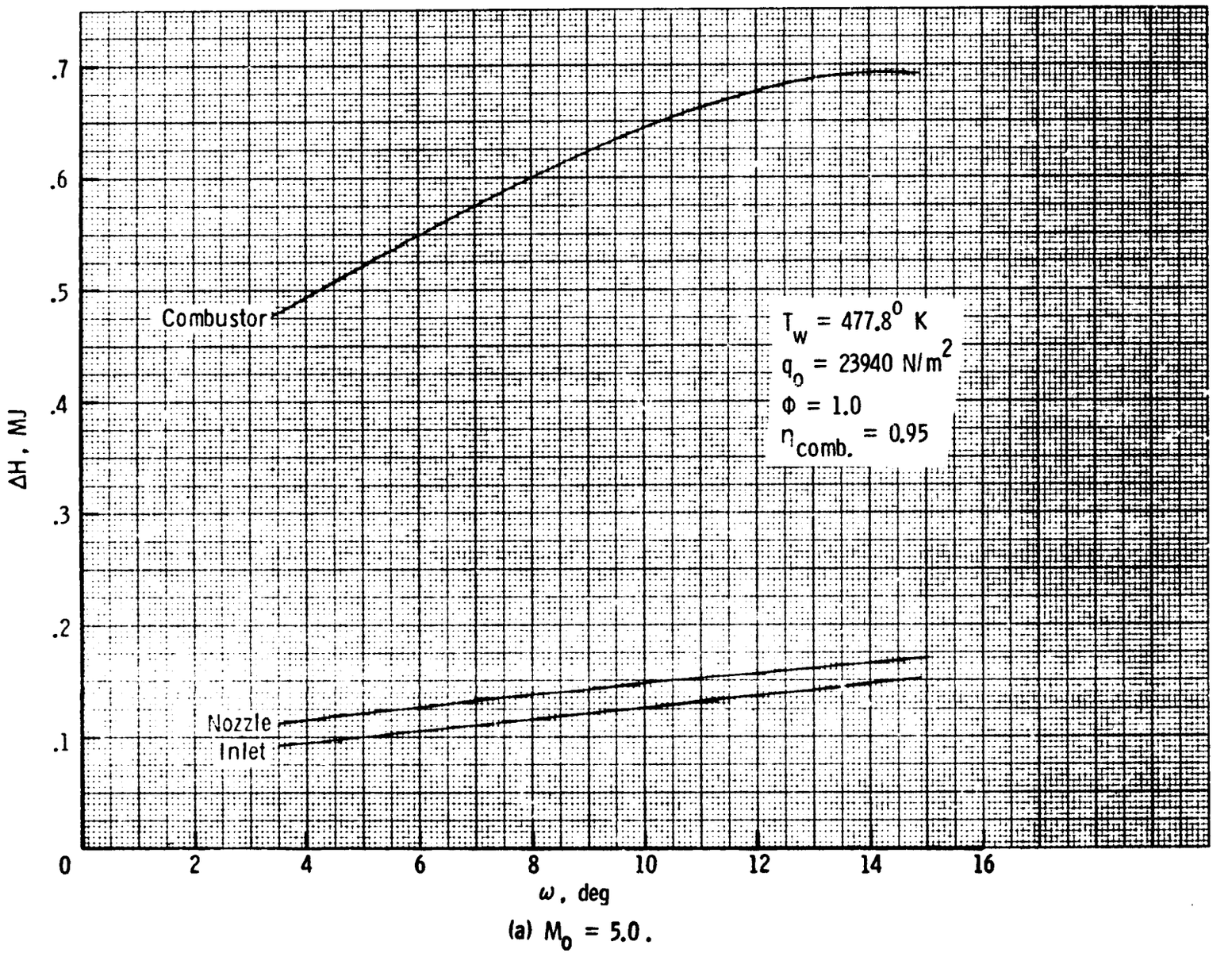

(a) $M_0 = 5.0$.

Figure 16.- Capture flow heat losses.

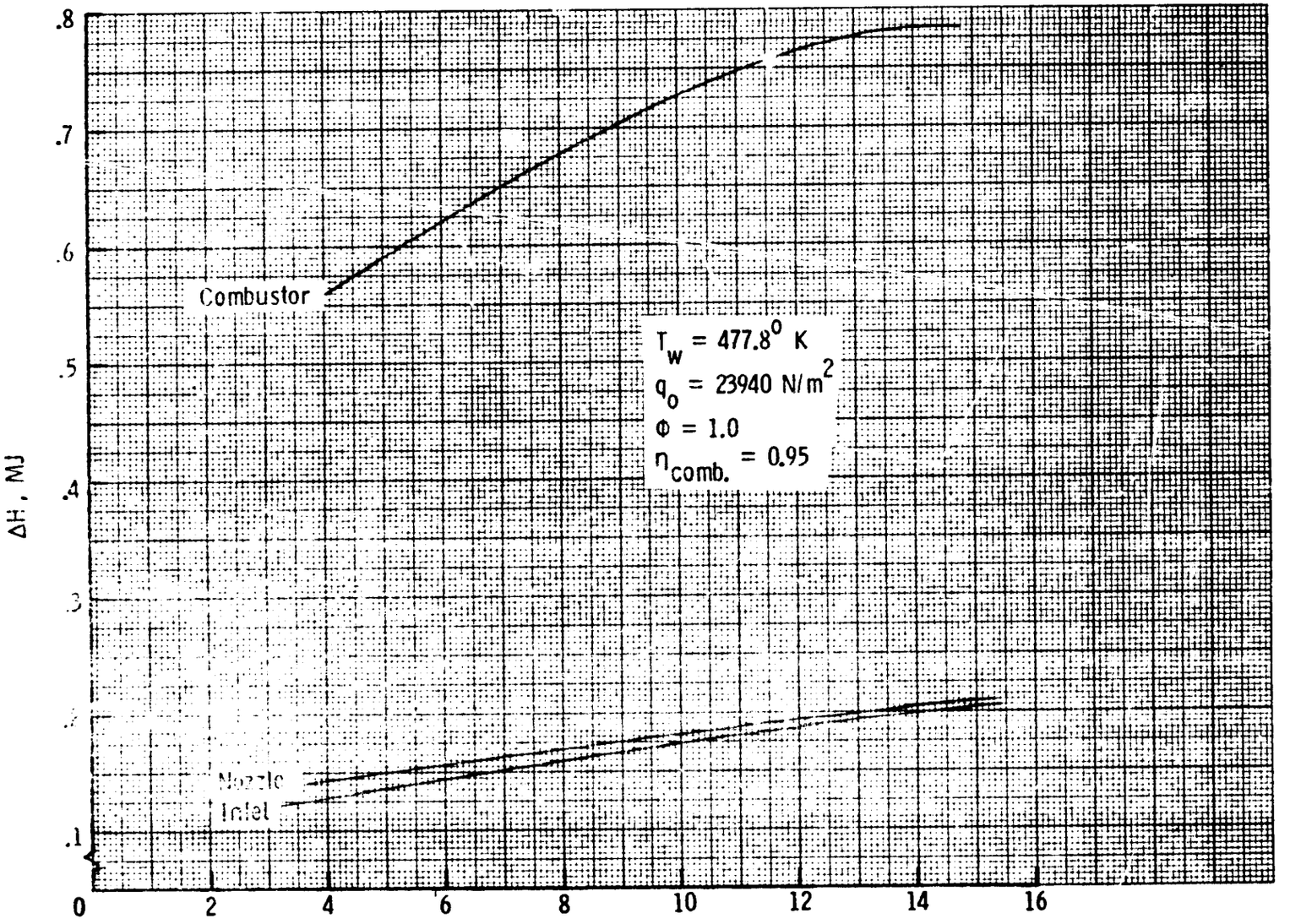

(b) $M_0 = 7.0$.

Figure 16.- Concluded.

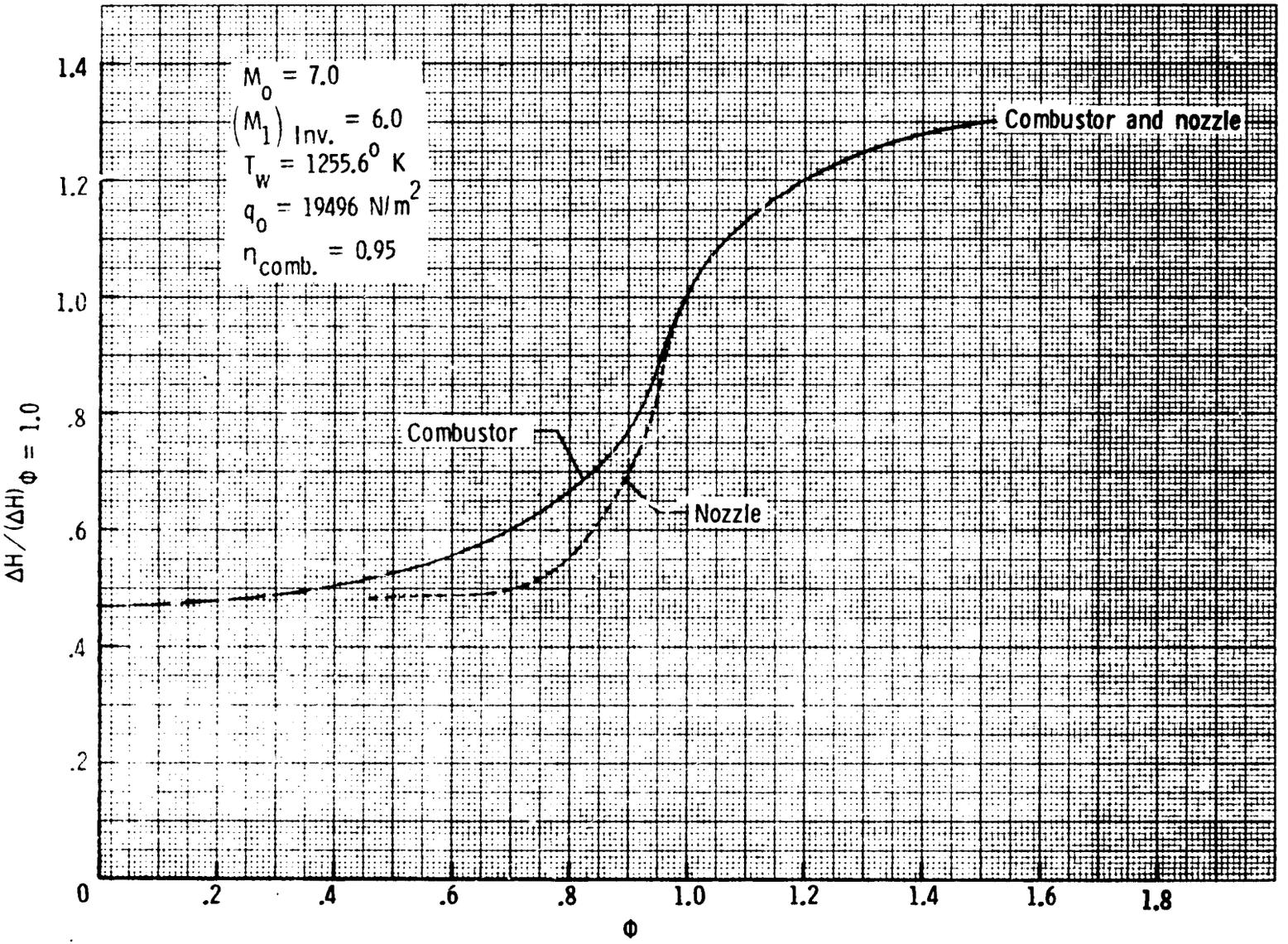

Figure 17.- Heat transfer for the heat sink engine of reference 18 ratioed to the heat transfer for $\Phi = 1.0$.

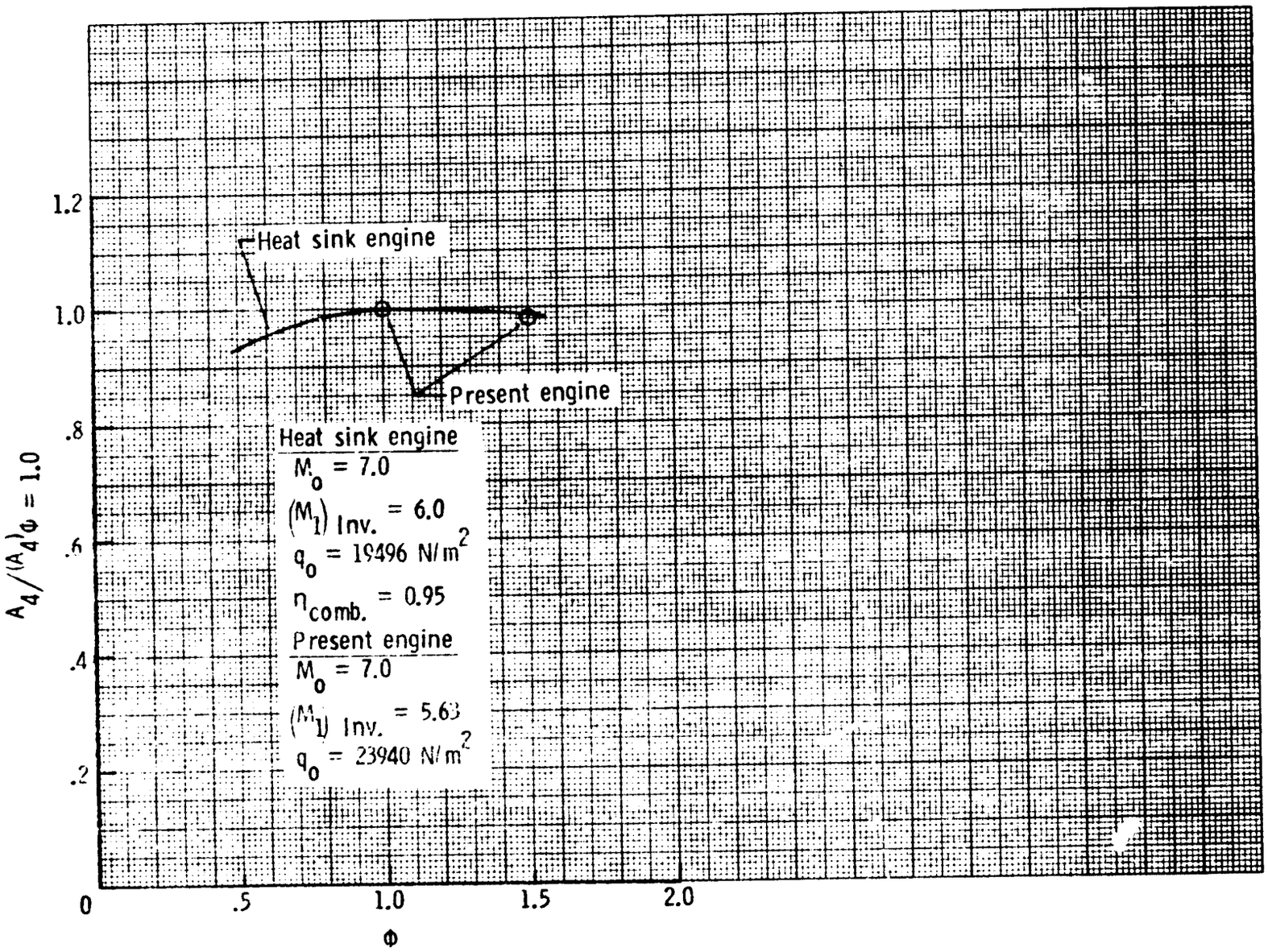

Figure 18.- Theoretical nozzle exit flow area for the heat sink engine of reference 18 ratioed to the nozzle exit flow area for Φ = 1.0 as compared with the same parameter of the present engine.

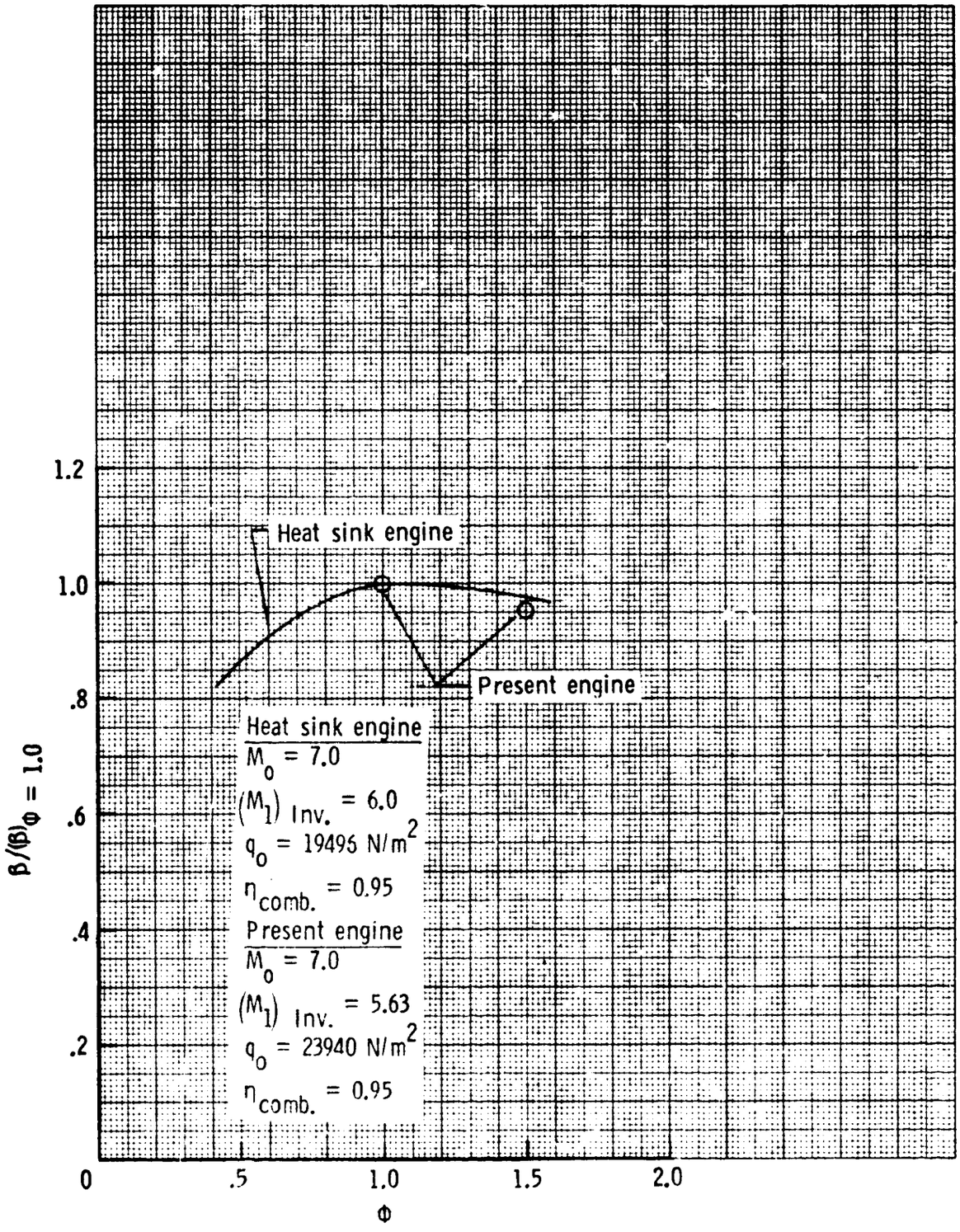

Figure 19.- Theoretical mass weighted nozzle exit flow angle for the heat sink engine of reference 18 ratioed to the nozzle exit flow angle for $\Phi = 1.0$ as compared with the same parameter for the present engine.

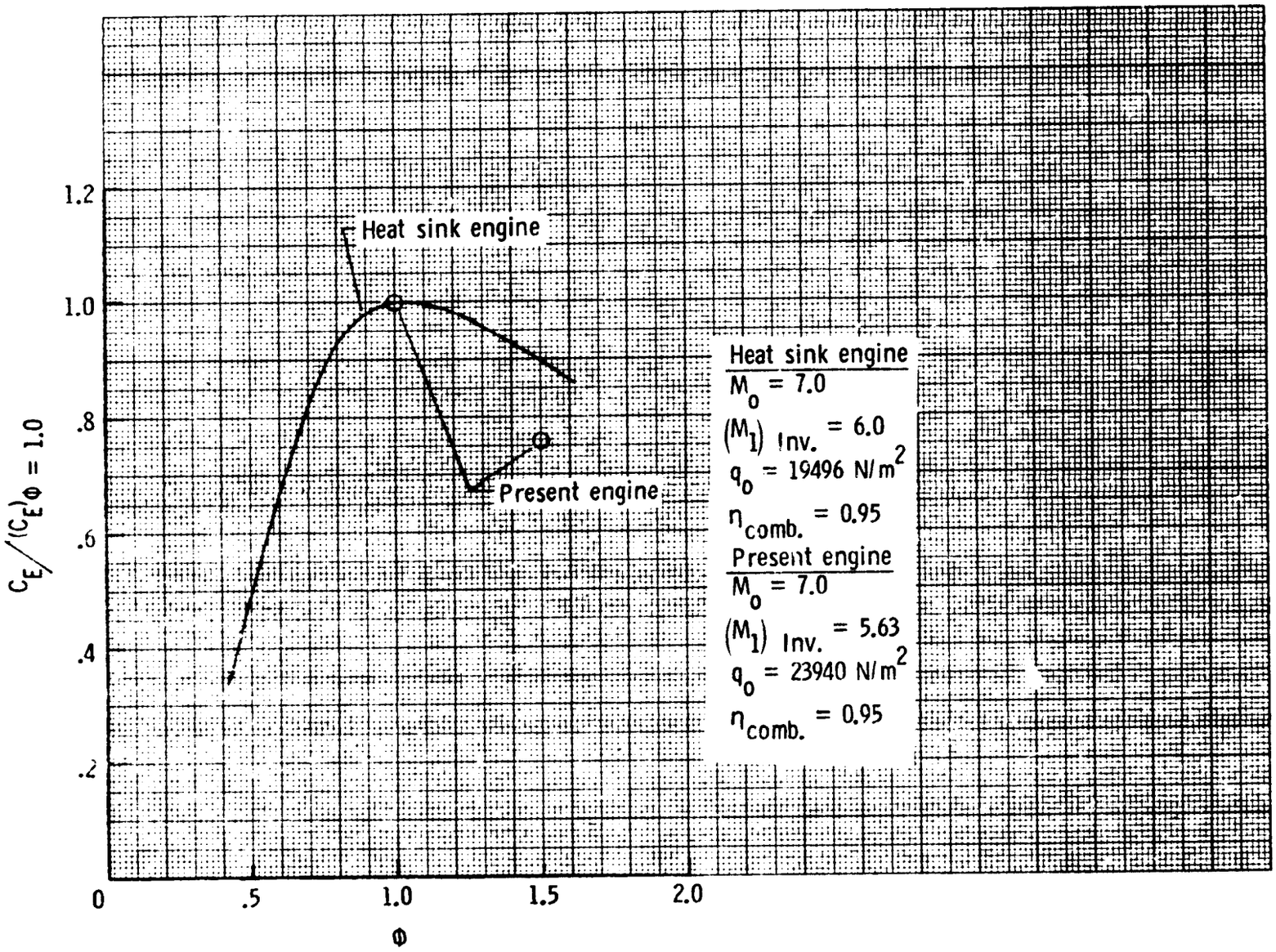

Figure 20.- Theoretical plume drag coefficient for heat sink engine of reference 18 ratioed to the plume drag coefficient for $\Phi = 1.0$ as compared with the same parameter for the present engine.

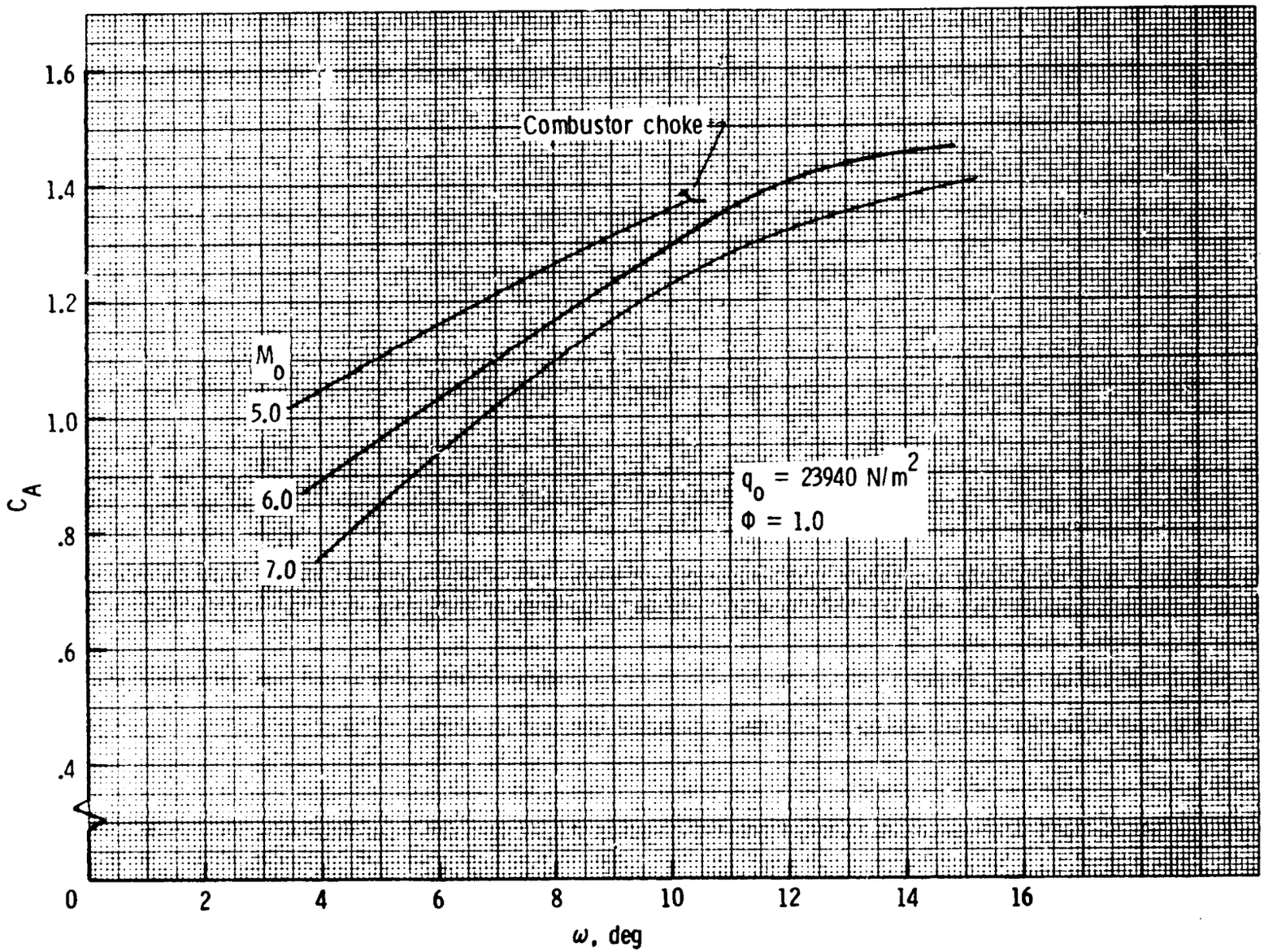

(a) Thrust component corresponding to engine force A_A which is in the flight direction.

Figure 21.- Langley scramjet engine's components of thrust in coefficient form.

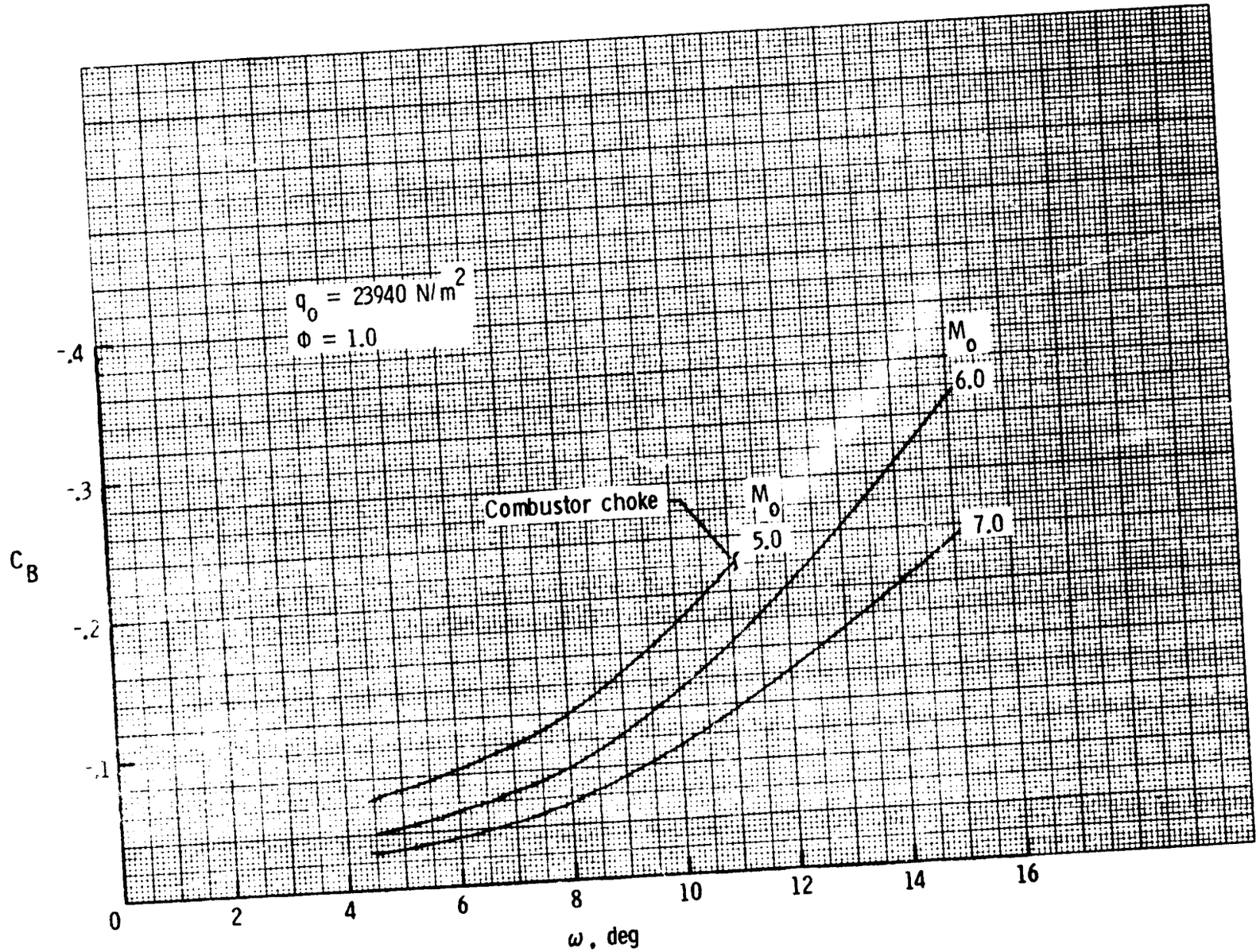

(b) Thrust component corresponding tc engine force A_B which is in the flight direction.

Figure 21.- Concluded.

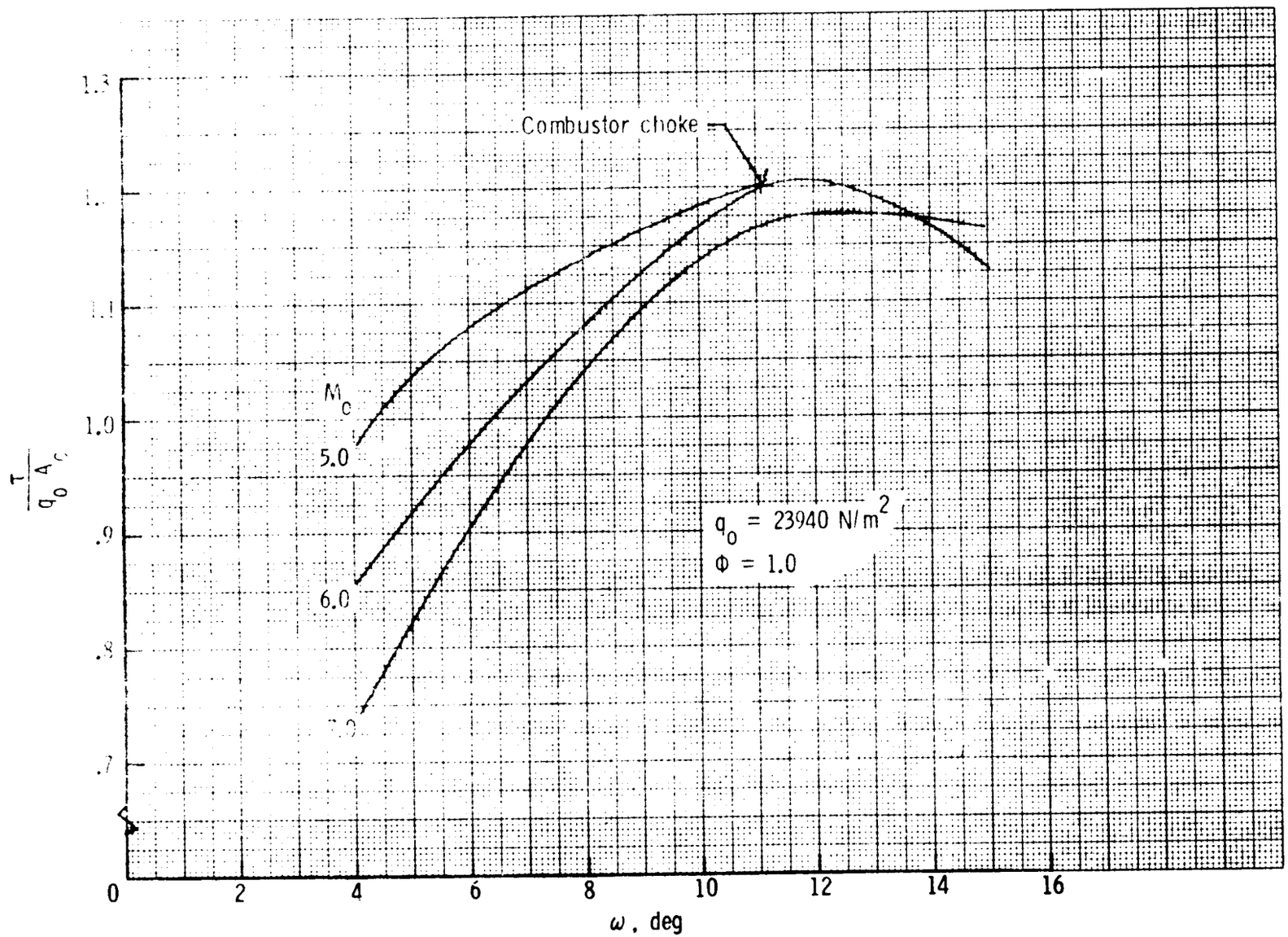

Figure 22. - Thrust coefficient of Langley scramjet engine.

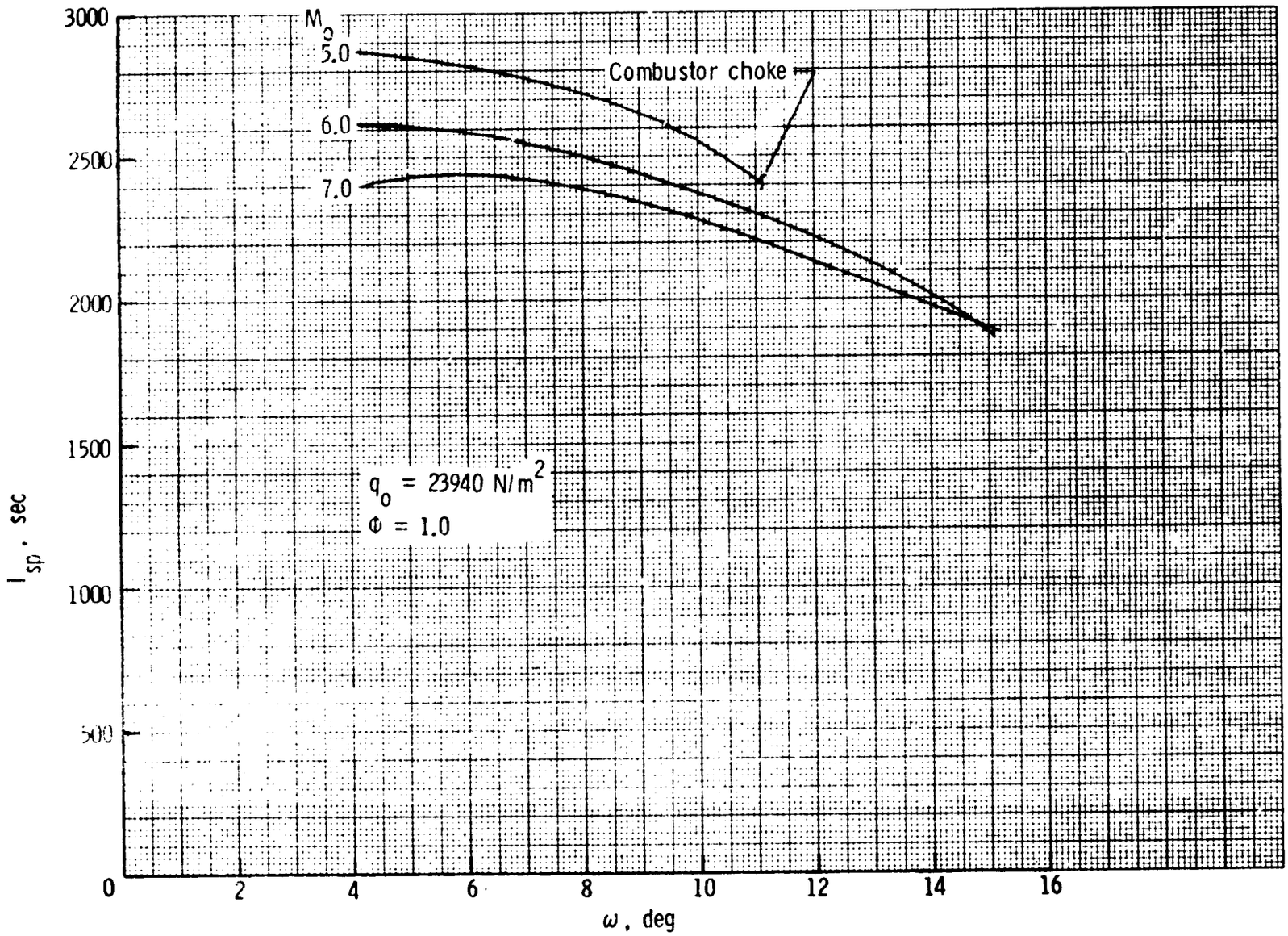

Figure 23. - Specific impulse of Langley scramjet engine.

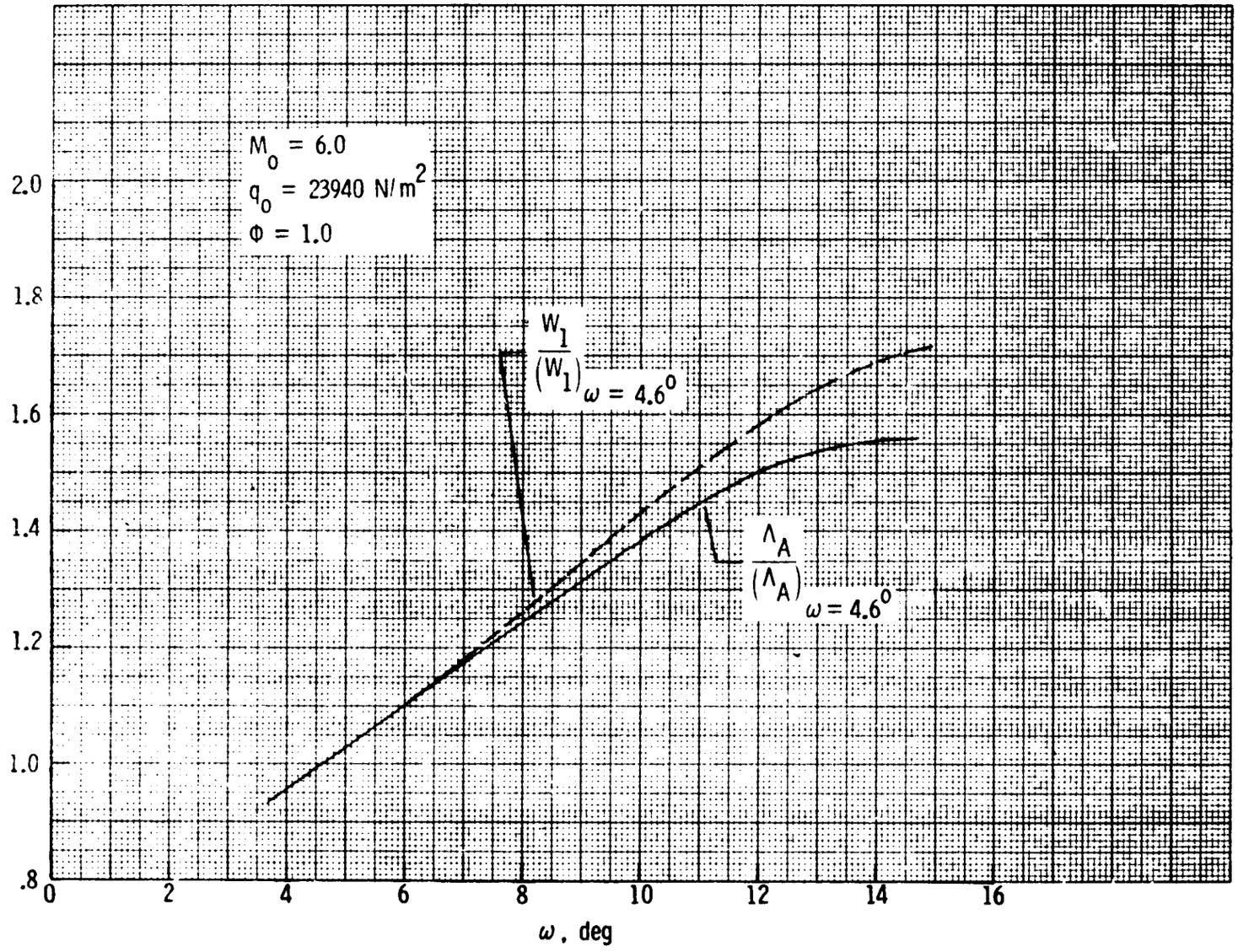

Figure 24.- Effect of vehicle forebody angle on mass capture and force Λ_A.

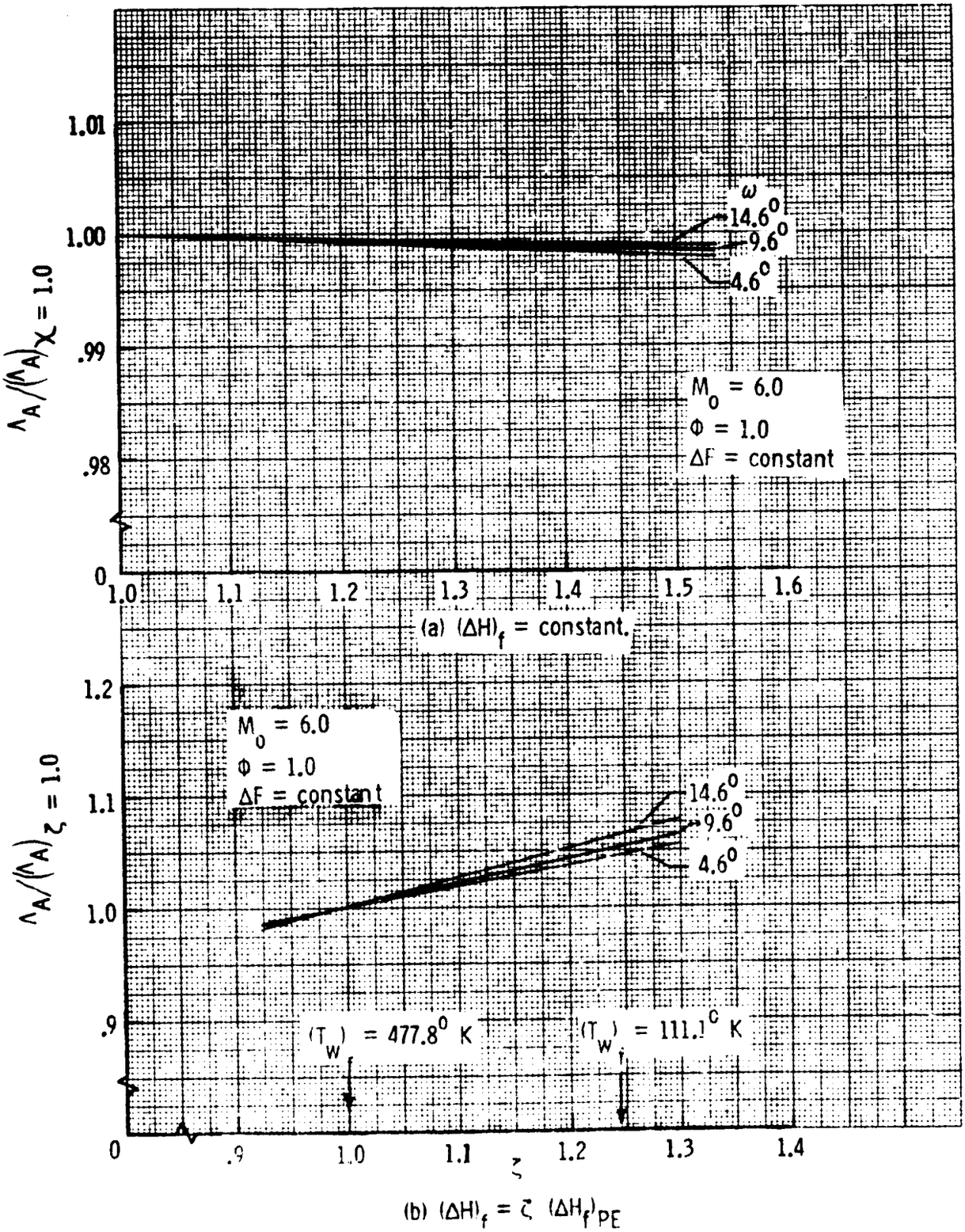

Figure 25.- Effects of engine capture mass flow heat losses with engine friction losses held constant.

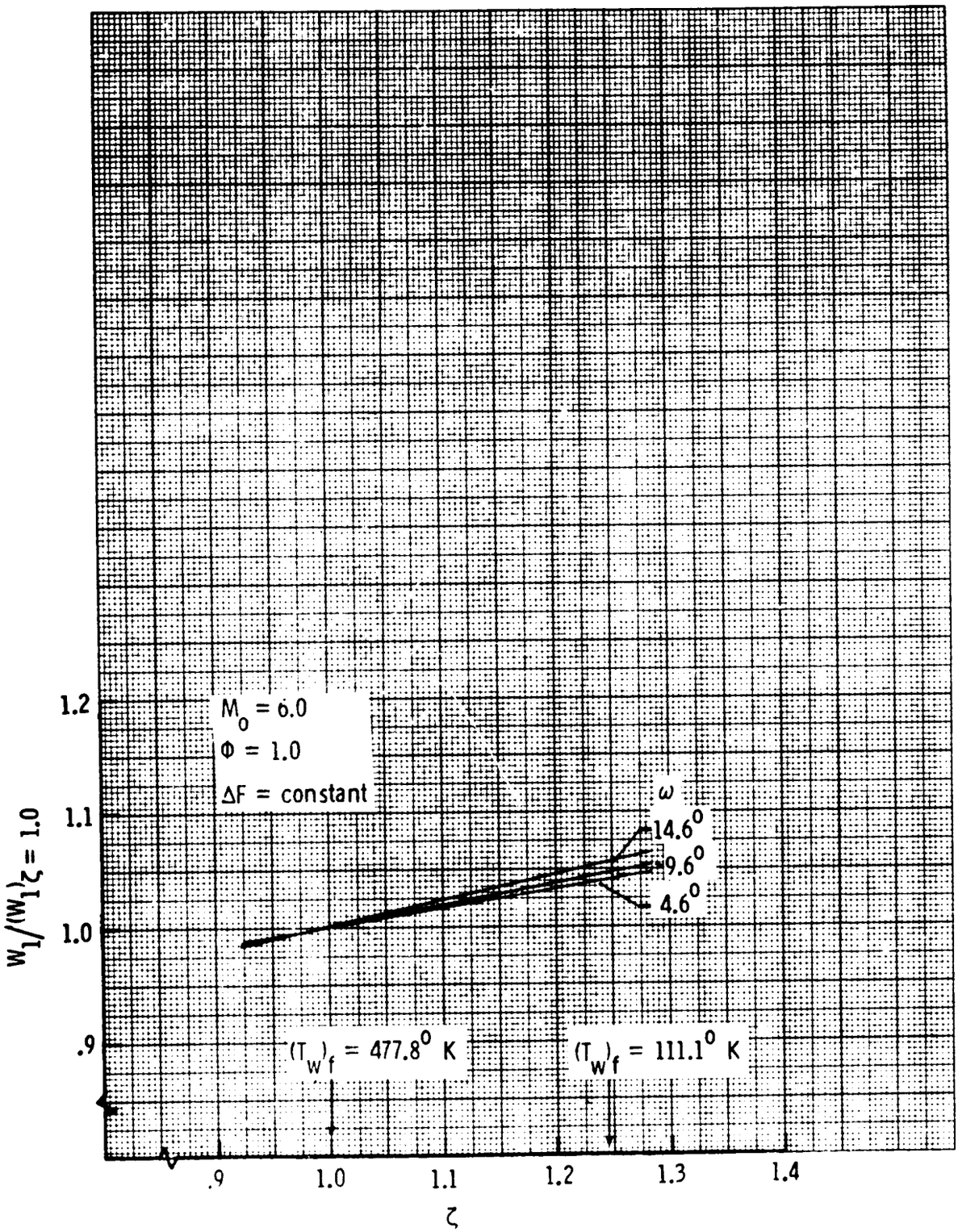

(c) Engine mass flow captured for $(\Delta H)_f = \zeta\,(\Delta H_f)_{PE}$.

Figure 25.- Concluded.

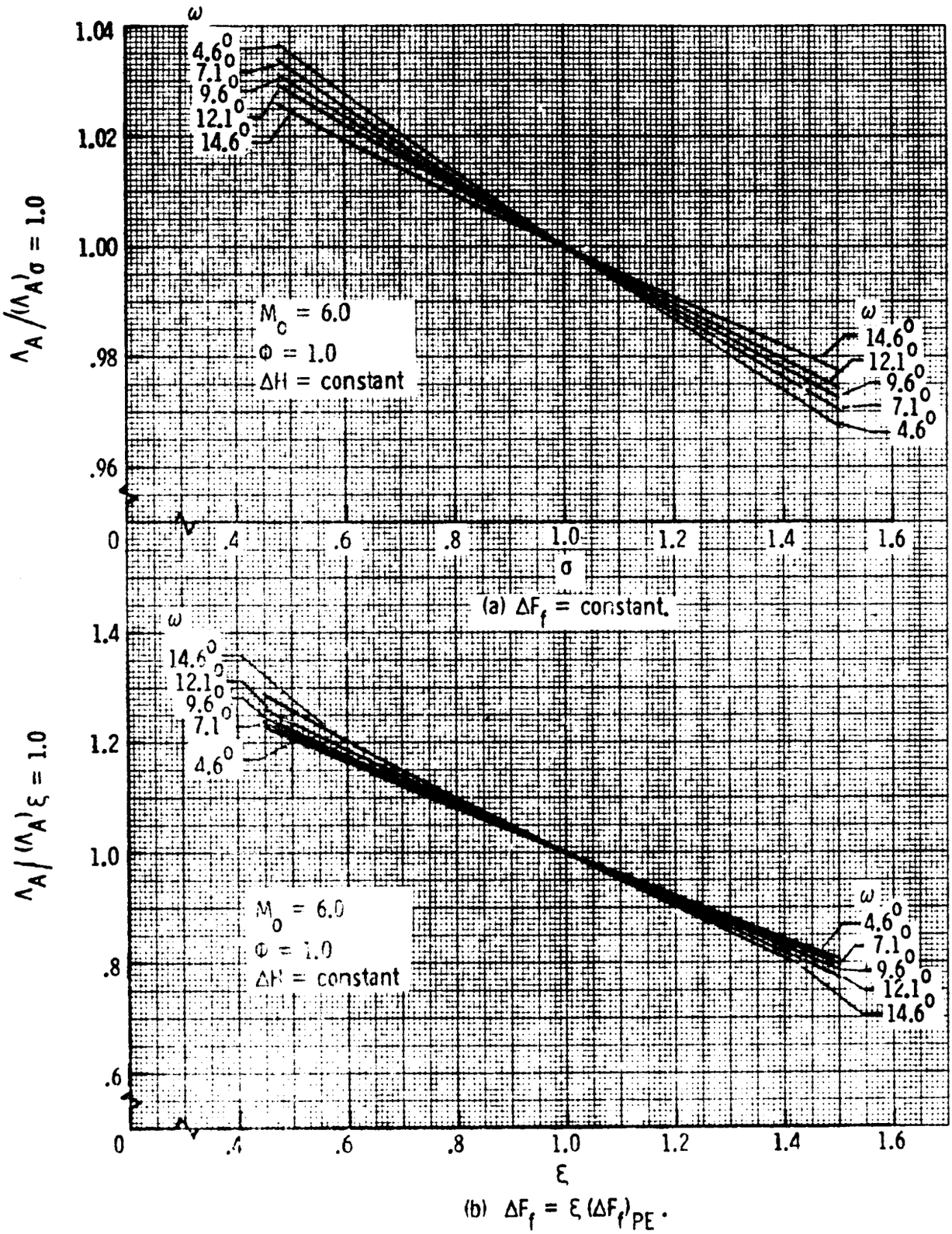

Figure 25 - Effects of engine capture flow friction losses with engine heat losses held constant.

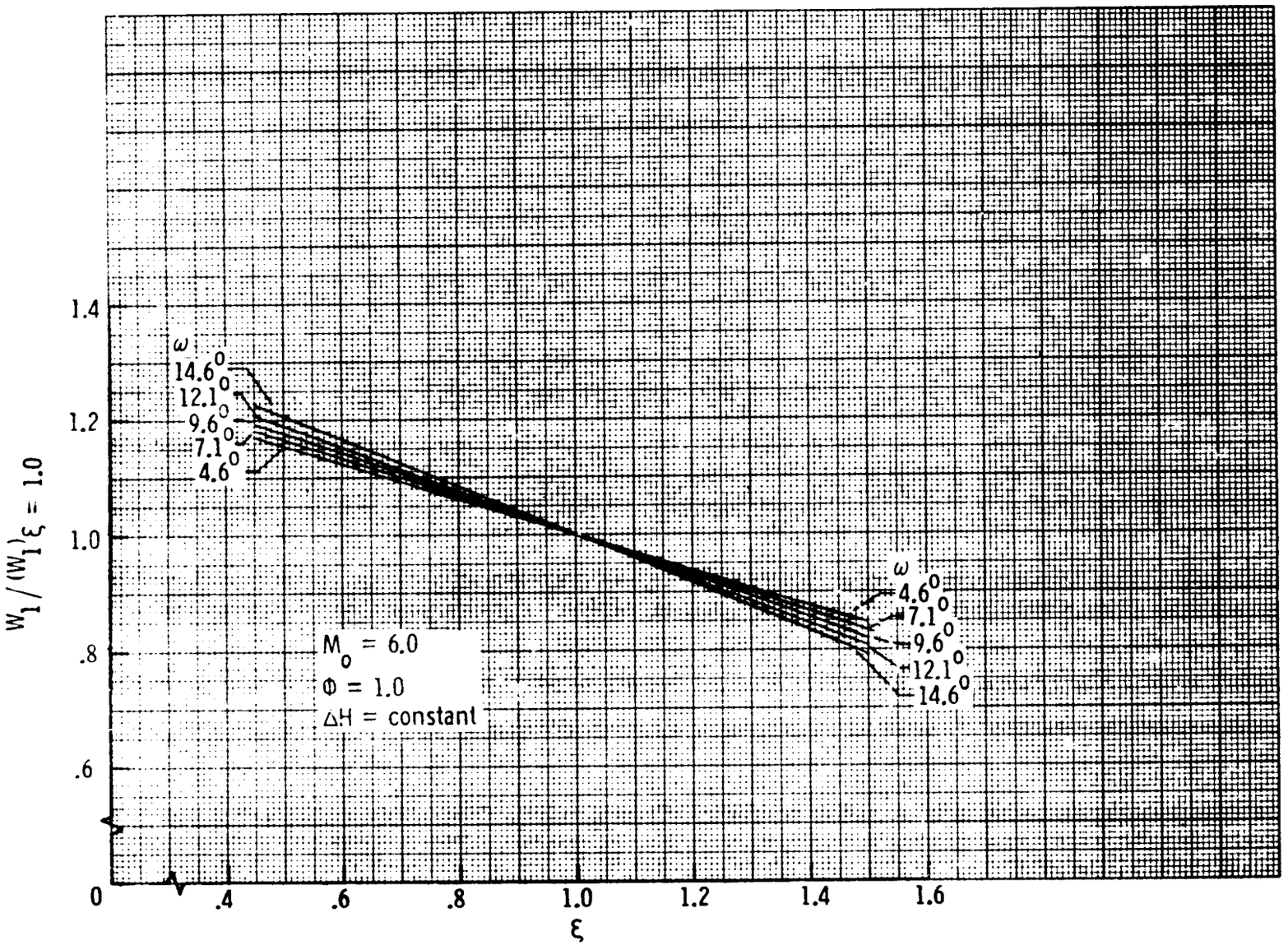

(c) Engine mass flow captured for $\Delta F_f = \xi(\Delta F_f)_{PE}$.

Figure 26. Concluded.

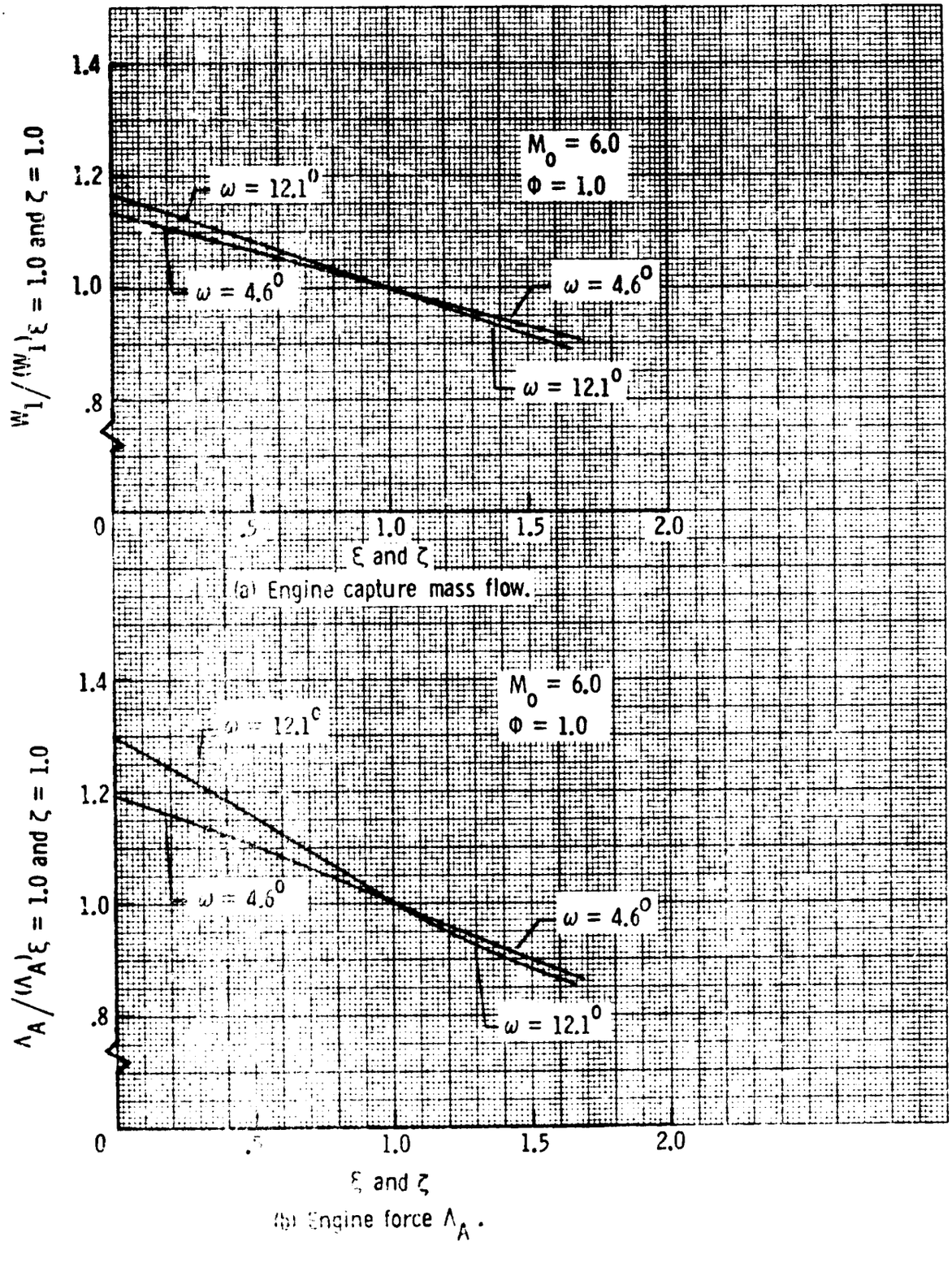

Figure 27.- Effects of engine capture mass flow friction and heat losses.

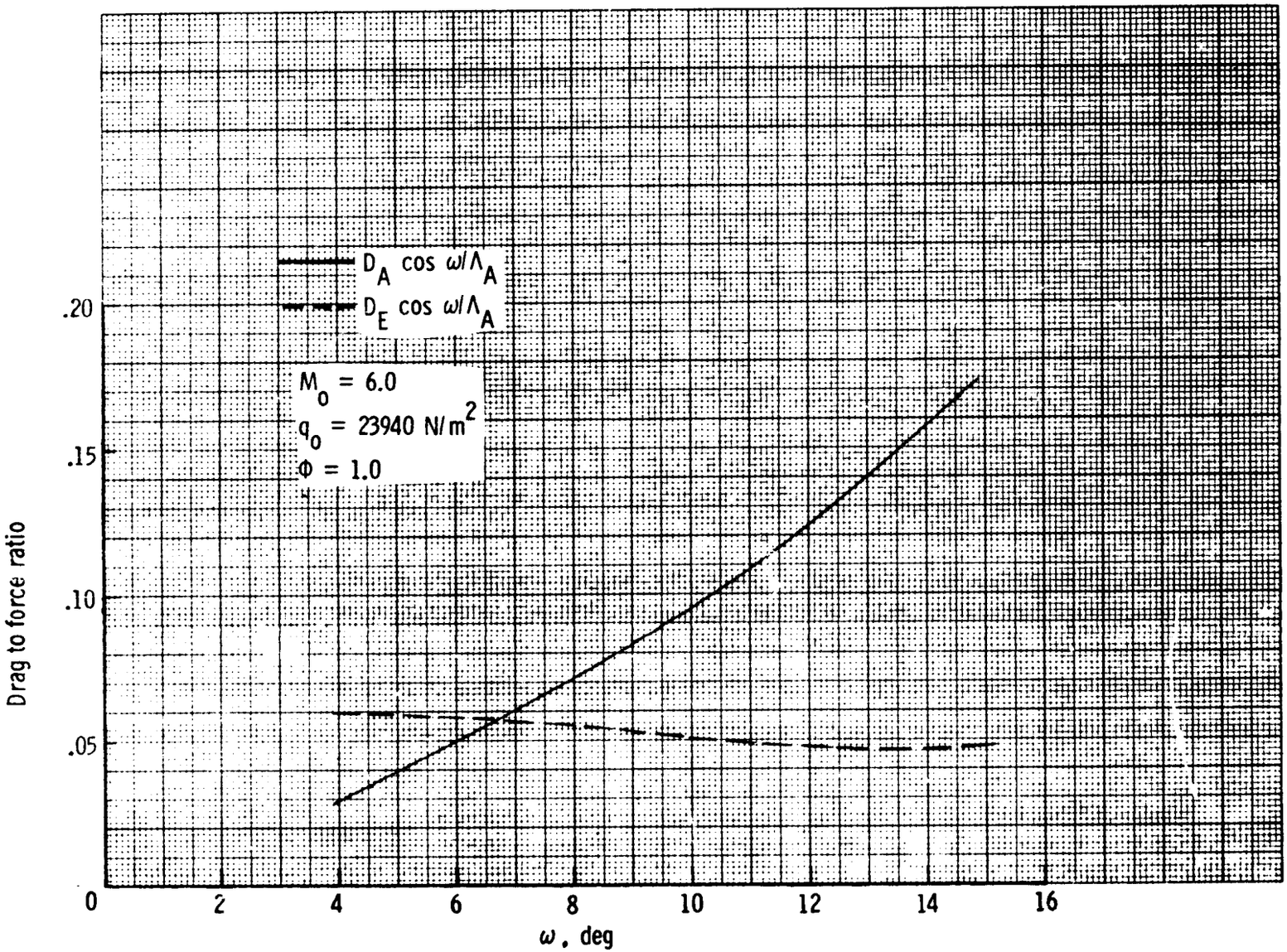

Figure 28.- Additive drag, D_A, and nozzle plume drag, D_E, ratioed to engine force Λ_A

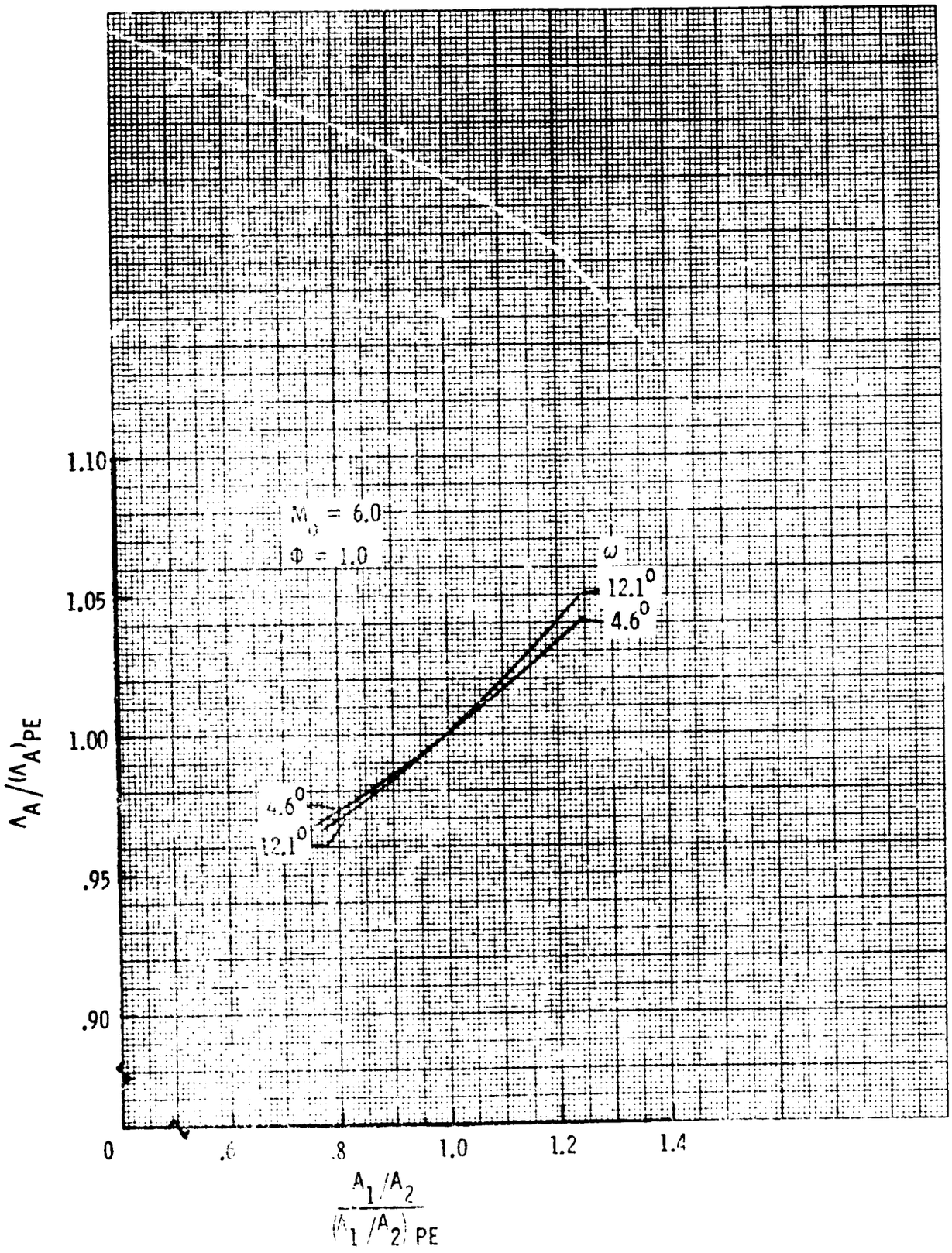

Figure 29.- Effect of aerodynamic contraction ratio on engine force Λ_A.

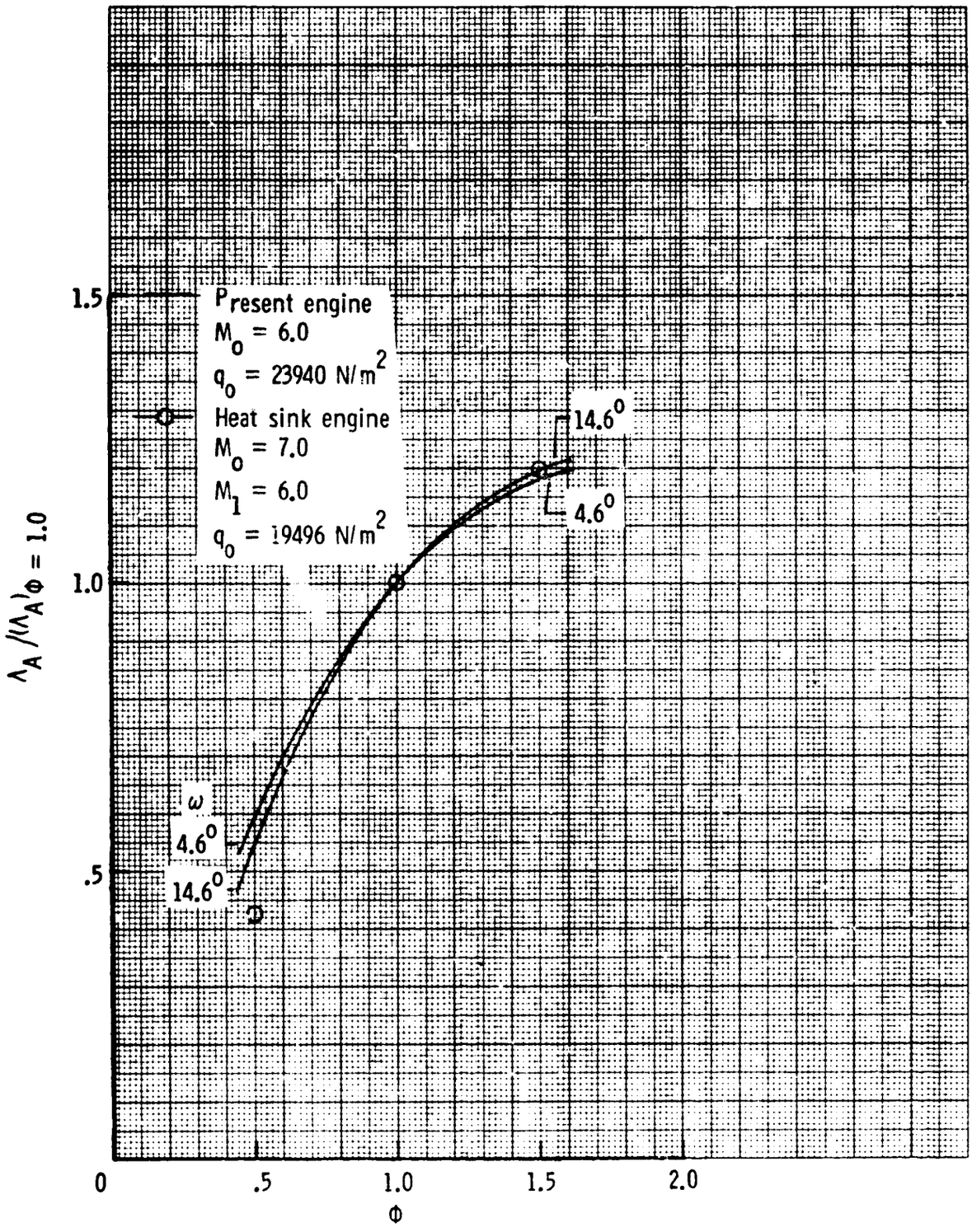

Figure 30.- Effect of fuel equivalence ratio on engine force Λ_A.

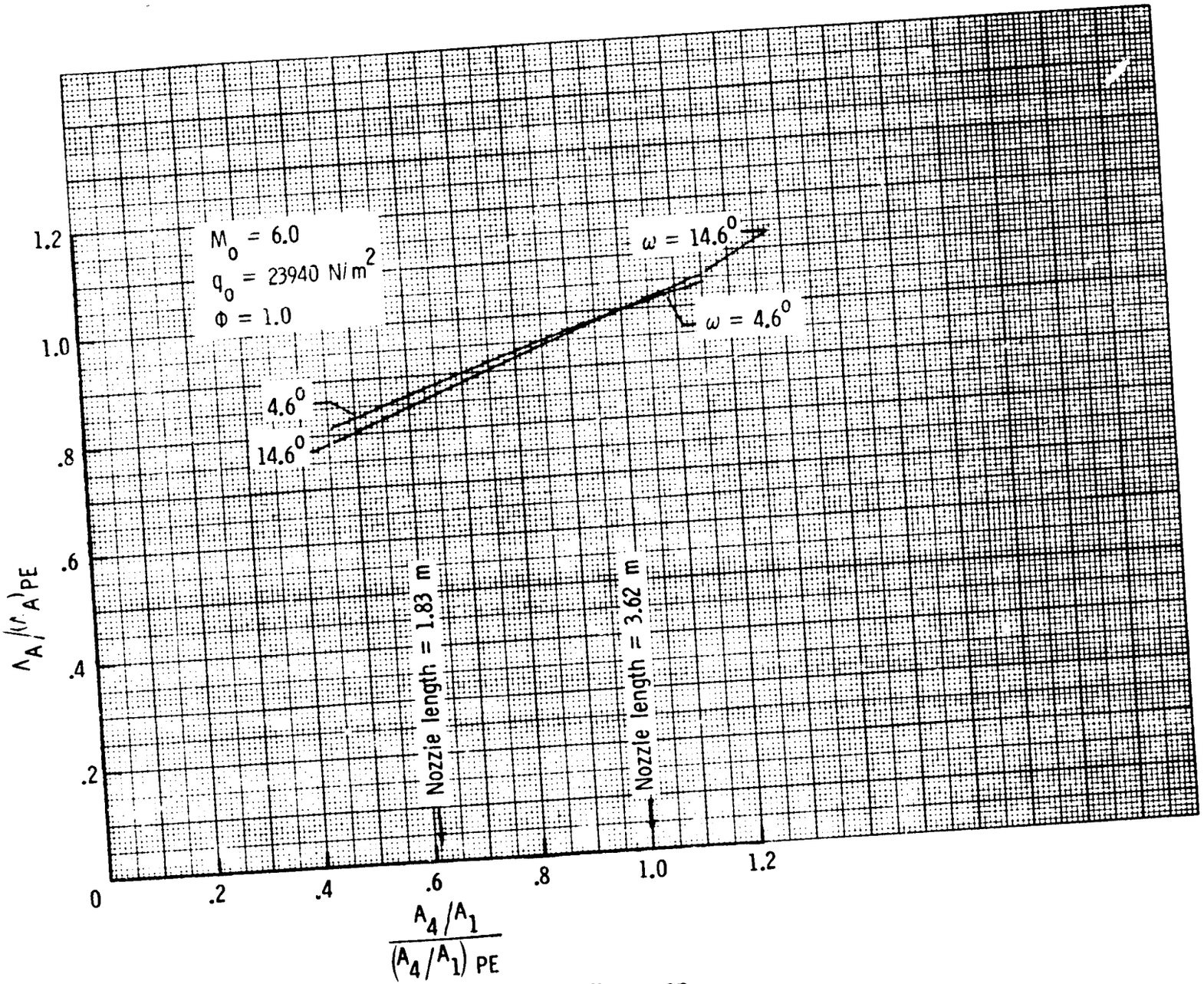

Figure 31.- Effect of size of nozzle exit area on engine force Λ_A.

1. Report No.	2. Government Accession No.	3. Recipient's Catalog No.
NASA TM X-74038		

4. Title and Subtitle	5. Report Date
INTERNAL PERFORMANCE PREDICTIONS FOR LANGLEY SCRAMJET ENGINE MODULE	January 1978
	6. Performing Organization Code 3740
7. Author(s) S. Z. Pinckney	8. Performing Organization Report No.
	10. Work Unit No. 505-05-41-08
9. Performing Organization Name and Address NASA Langley Research Center Hampton, VA 23665	11. Contract or Grant No.
	13. Type of Report and Period Covered Technical Memorandum
12. Sponsoring Agency Name and Address National Aeronautics and Space Administration Washington, D.C. 20546	14. Sponsoring Agency Code

15. Supplementary Notes
This is the final release of special information not suitable for formal publication which serves the following need: present scramjet performance information in a form suitable for distribution and referencing.

16. Abstract

A one-dimensional theoretical method for the prediction of the internal performance of a scramjet engine is presented. Using this method, the effects of changes in vehicle forebody flow parameters and characteristics on predicted thrust for the Langley scramjet engine are evaluated and the results presented. A theoretical evaluation of the effects of changes in the Langley scramjet engine's internal parameters is also presented. Theoretical internal performance predictions, in terms of thrust coefficient and specific impulse, are presented for the Langley scramjet engine for free-stream Mach numbers of 5, 6, and 7, free-stream dynamic pressure of 23,940 N/m^2, forebody surface angles of 4.6° to 14.6°, and fuel equivalence ratio of 1.0.

17. Key Words (Suggested by Author(s))	18. Distribution Statement
Integrated Scramjet Performance Hypersonic Propulsion Internal Performance Sensitivity Cycle Analysis	Unclassified - Unlimited

19. Security Classif. (of this report)	20. Security Classif. (of this page)	21. No. of Pages	22. Price*
Unclassified	Unclassified	80	$5.00

* For sale by the National Technical Information Service, Springfield, Virginia 22161

END

DATE

FILMED

APR 12 1978